Leveraging TCR signaling for the design of sensitive bispecific receptors for cancer therapy

Grace Bugos

A dissertation

submitted in partial fulfillment of the

requirements for the degree of

Doctor of Philosophy

University of Washington

2024

Reading Committee:

Stanley Riddell, Chair

Evan Newell

Jarrod Dudakov

Program Authorized to Offer Degree:

Immunology

University of Washington

Abstract

Leveraging TCR signaling for the design of sensitive bispecific receptors for cancer therapy

Grace Bugos

Chair of Supervisory Committee:

Stanley Riddell

Department of Immunology

Abstract

Immune-based therapies have revolutionized the treatment of cancer by improving the immune system's capacity to target and kill cancer cells. These advances were built on foundational research in immunology, underscoring that continued immunology research is critical to the improvement of human health. Adoptive T cell therapies, particularly chimeric antigen receptors (CAR) T cell therapies exemplify the direct impact of fundamental immunology on treatment innovations. Chimeric Antigen Receptors (CARs) are engineered by combining and extracellular binding domain with signaling molecules essential T cell activation into one molecule, enabling specific activation of T cells to target tumor cells expressing the ligand for the extracellular binder. Research in T cell biology, particularly the T cell receptor (TCR) enabled the design of CARs by identifying essential TCR activation signals that were incorporated in the CAR architecture. Thousands of

patients have been treated with CAR T cell therapies, with remarkable success, particularly in therapy of B cell malignancies and multiple myeloma. However, further advances are required to overcome the escape of tumor cells that express low levels or lack the target antigen improve the durability of responses and expand the application T cell therapies.

This thesis presents the development a novel class of receptors for adoptive T cell therapy, termed chimeric T cell receptors (ChTCRs)that provide improved sensitivity and specificity over traditional CAR T cell therapies. Our receptor design leverages an understanding of TCR signaling to more closely mimic native TCR signaling, and improves receptor sensitivity. This approach led to the development of two novel receptors: the monospecific 'Full ChTCR,' which has superior antigen sensitivity and tumor control in pre-clinical mouse models relative to existing CARs and other ChTCR variants, and the dual-antigen targeting 'Bi-ChTCR,' which has enhanced sensitivity and efficacy in to targeting heterogenous tumors compared to monospecific and bispecific CARs.

Additionally, I developed a mass cytometry tool to determine similarities and differences in proximal receptor signaling in engineered T cells and understand how improved signaling may impact cell differentiation and function. Collectively this work demonstrates the value of TCR signaling research in guiding novel receptor design for adoptive T cell therapies. It introduces a tool to study signaling dynamics and reports an adaptable receptor architecture for sensitive targeting of tumor antigen.

Table of Contents

List of Figures

List of Tables

Acknowledgements

There are so many people who supported me during my PhD that I would like to thank. First, I would like to thank my advisor, Stan Riddell. I came to UW Immunology with the intention of studying cancer immunotherapies at the Hutch. I consider myself incredibly fortunate to have been able to train with Stan. I have benefited so much from Stan's expertise and perspective. I am grateful for the opportunity listen and learn, enjoying frequent chats in the desk area, talking about a new paper, discussing a talk, or some fresh new data. Stan can keep a level head, talking us through times of peak frustration, keeping us on track to get done what needs to be done. He cares for 'his people.' Advising them on next steps, and continuing support trainees even after they have left the lab. As I finish grad school, I feel a level of safety a security knowing Stan has my back. Lastly, I would like to officially thank Stan for taking me on as a graduate student, even as he was beginning to plan for his retirement. I may have contributed to that being drawn out a bit, so thank you!

My time as a graduate student have benefit more than I can really say from working with Sylvain Simon. I met Sylvain at the same time I met Stan, we all bumped elbows in late February 2020, days before the world shut down, and chatted about TCR signaling and making "TCR-CARs." Ever since that meeting Sylvain and I have worked together as a team. Collaboration, and eventual co-authorship could be a recipe for disaster. Instead, it was the fundamental to our success. I am so thankful for Sylvain's generosity and support as we built the story of ChTCRs together. Sylvain is someone I can bounce half-baked idea off of and someone to commiserate with in times of stress and frustration. In addition to the scientific knowledge I have gained working with Sylvain, I have been able to witness how to 'be' a scientist. He demonstrates a belief in scientific collaboration; if you have figured out how to do something, share your protocol, share your reagents, help someone out. He has done this time and time again. This is how science works at its best. I look forward to continuing to work with Sylvain and wish him all the best in the well-earned success I know is in his future.

This work was supported by many people who were part of "team TCR-CAR" (rebranded "Team ChTCR"). Rachel Prins – not only did you generate so much data, but you made the lab such a fun place. Thank you for your dedication to this project, and for lab potlucks, happy hours and camping trips. Anusha Rajan – thank you for putting up with me and my chaotic 'systems,' and disorganized workspaces. I learned so much from your lab expertise, and so enjoyed getting to know you. I really miss you in the lab! Arul Palani – thank you for all your hard work that really got this project over the finish line. You stepped up as the team got smaller. I appreciate your quiet enthusiasm and dedication. Andrew Stevens – thanks you for helping us get through revisions on this paper, and keeping the lab running smoothly since you have taken over as lab manager, it would be chaos without you

I was had the privileged to work so many others over these last 5 years. Thank you to Carla Jaeger – my fellow 'signaler' in the lab. Thank you also for the enthusiasm and fun you brought to the lab, that is best encapsulated by a brights smile and wave has you skate past on the bike path! Tamer Shabaneh – I learned so much from working with you thank you for your thoughtful support and advice about the industry job search. Thank you also for

hiking/x-country skiing tips and podcast recommendations. Thank you to my fellow Riddell lab grad students. Alec Wilkens – thank you for showing me the ropes on how to be a grad student in Stan's lab, and for your company in the lab, keeping grad student hours is better when you are not alone. Mitch Kluesner and Kirsten Thompson – I wasn't sure if I would get fellow grad-students in the lab these last years and am so happy I did. I have enjoyed spending time with you both, especially pizza night and paddle boarding in the San Juans!

Thank you to my thesis committee, Jarrod Dudakov, Evan Newell, Dan Campbell and David Rawlings. Your guidance and feedback have been so helpful shaping my project. I really appreciate you giving time energy to support my graduate student education.

Thank you to David Han, Yan Li and Larry Samelson who welcomed me into their labs as an undergraduate/post-bac, your mentorship was essential to my grad school career. Thank you to Ana Dios Esponera and Lakshmi Balagopalan whose mentorship in the Samelson lab taught me skills used throughout this thesis and who were excellent scientific role models.

Thank you to my friends Darren, Will, Mark, Miya, Richard and Pam. The best part of graduate school has been meeting you all. You helped me so much over these last years, and so grateful for the lifelong friendships I have gained. An thank you to Helena, whose arrival in Seattle this summer got me over the finish line

Thank you to my family. Mom, Dad, Molly and Annie who have been my greatest support system. My PhD has taken me to the opposite corner of the country, but your constant encouragement and support has kept me going.

Finally, thank you to Will. You have been my rock through it all, supported me through the most stressful of times, boosted my ego and kept me going. Thank you for giving me the time to get all this work done, while I spent weekends and late nights in the lab, and for planning our adventures together that have kept me sane. I couldn't have done it without you.

I would like to dedicate this thesis to two family members who passed away just under a year ago. For my Uncle Chris, who's memory I carry with me on the ski slopes, on hikes in PNW, and listening to live music. Uncle Chris loved and supported his family in so many ways, and he is so deeply missed. He passed away from kidney cancer last winter, and because him, and Granny, and too many loved ones affected by cancer, I am motivated to continue to work on cancer research. For Grandad, who believed in me so much. Thank you for the science kits, museum visits, the graduations attended and all the many ways you supported my education and encouraged and nurtured my scientific interest. Grandad's confidence in me and encouragement is the reason I could make the step from knowing cancer research is important, to knowing I could be one of the scientists leading it.

Chapter 1: Introduction – T cell Signaling and the Development of Chimeric Antigen Receptors

1.1 T cells are critical immune mediators

T-lymphocytes (T cells) are produced in the thymus where they are educated to avoid output of cells with autoreactive T cell receptors. Mature T cells comprise a principal component of the adaptive immune response, orchestrating immune responses against pathogens and abnormal cells. Each T cell expresses a distinct antigen receptor, the receptor on $\alpha\beta$ T cells is comprised of variable alpha and beta chains thereby generating a population of cells with a highly diverse repertoire capable of distinguishing between healthy tissues and those affected by pathogens or mutations that occur in cancer. After encountering an antigen, T cells initiate a targeted response – directly killing affected cells, recruiting additional immune cells, and generating memory cells that protect from future encounters with the same threat [1] .

Understanding the biology of T cells, how they are activated and directed to their effector function, is of critical importance to understanding the human body's native immune defenses. The high specificity and sensitivity of a T cell, and the dynamic effector functions of T cells – cytotoxic activity, cytokine production and activation of other immune cells, and the ability to retain 'memory' – makes them an ideal tool in combating malignancies. Manipulating this natural response, by engineering new specificities into T cells can create powerful therapies to eliminate cancer. This thesis explores how insights into T cell activation can inform the design of novel T cell-based therapies, providing an innovative approach to adoptive T cell therapies for cancer.

1.2 T cell activation

1.2.1 TCR Structure

T cells are activated by engagement of the T cell receptor (TCR) with a peptide bound major histocompatibility complex (p/MHC) molecule on the surface of target cells. Binding of the TCR to p/MHC results in activation of various signal transduction pathways, leading to the activation and proliferation of T cells, and initiation of effector functions. The unique structure of the TCR allows for antigen recognition with incredibly high specificity, and engagement of as little as 10 p/MHC complexes can result in efficient activation of multiple signaling pathways.

The TCR complex is a multimeric receptor created by the assembly of 8 subunits, containing antigen recognition and signaling domains. Antigen recognition and specificity is encoded into two TCR chains, the majority of mature T cells express the TCRα/β subunits, while a small proportion express TCRγ/δ chains [2]. Extracellular regions of the TCR contains two domains, the variable immunoglobulin-like region (V) and the constant immunoglobulin-like region (C) (**Figure 1.1)**. During T cell maturation expression of the RAG1 and RAG2 recombinases results in the rearrangement of gene segments to create vast genetic diversity in the region of the V domain responsible for p/MHC recognition [3]. The C domain allows for interaction with CD3 subunits.

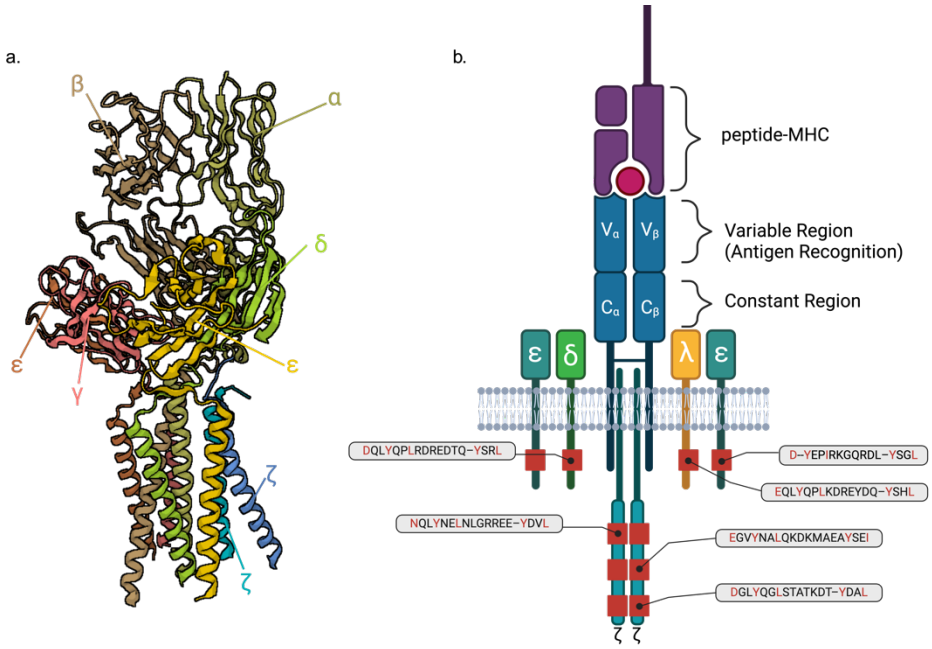

Figure 1.1 T cell Receptor Structure a.) Side view of cryo-EM map of the TCR-CD3 complex, with subunits indicated (PDB:6JXR) b.) Cartoon schematic of TCR-CD3 complex assembly bond to peptide-MHC, ITAM locations indicated in red with sequence notations, red residues indicate conserved sequence motifs

The CD3 subunits contain the signaling motifs that result in signal transduction and T cell activation. TCR chains assemble with three dimers of CD3 proteins, CD3γε, CD3 δε, and CD3ζζ (**Figure 1.1**). Complete assembly of the TCR with all CD3 subunits is required for surface expression of the receptor at the T cell surface [4]. The CD3 subunits contain domains that are critical for signaling after TCR engagement with peptide MHC. These conserved sequences, termed Immune-receptor-Tyrosine-based-Activation-Motifs (ITAMs), consist of YxxL/I motifs separated by an interval (**Figure 1.1b**). ITAMs share consensus sequences, but there is diversity among the ITAM sequences on each CD3 subunit. Variations in the sequences promotes the preferential recruitment of signaling molecules to individual CD3 subunits. This sequence diversity is important to optimal TCR signal transduction [5, 6]

1.2.2 TCR Activation

The ligand of the TCR is peptide-bound MHC molecules, which are categorized into two classes, MHC-I and MHC-II. MHC-I consists of human leukocyte antigens (HLA-A, HLA-B or HLA-C) associated with β2 microglobulin while MHC-II molecules (HLA-DP, HLA-DR, HLA-DQ) are heterodimers of an alpha and beta chain [2]. Peptides that bind to MHC molecules can be generated from the processing of self or mutated proteins, native to MHC-expressing cell, or derived from bacterial or viral proteins, or proteins released from dying cells that are taken up by cells and processed intracellularly into peptides. TCR variable regions are specific for certain p/MHC complexes, recognizing both the MHC molecule and the peptide that is bound. The mechanism that translates ligand binding to receptor activation and signaling is not yet definitively understood. The TCR p/MHC interaction has unique characteristics which distinguishes it from other protein-ligand interactions that

must be considered by mechanisms describing receptor triggering. The TCR binds p/MHC interaction with very low affinity, with K_D in the μM range, resulting from slow association rates and fast off rates. This low affinity interaction is still highly sensitive, capable of triggering T cell activation from interactions with less than ten p/MHC interactions yet retaining the ability to discriminate between highly abundant self p/MHC and less abundant foreign agonist p/MHC [7, 8]

Several models have been proposed that explain how a TCR is able to discriminate between p/MHC molecules with minimal sequence differences, and initiate signaling via phosphorylation of ITAMS by the SRC-family kinase LCK. Hypotheses for TCR triggering can be broadly categorized into three models; aggregation – increased proximity between TCR complexes results in the phosphorylation of adjacent receptors by LCK bound to another receptor; conformational changes – mechanical force of ligand binding results in a conformational change in TCR and/or CD3 subunits that make ITAMs more accessible for phosphorylation; and segregation or redistribution – binding of TCR to p/MHC forces out phosphatases with a large extracellular domain, including CD45, from the region of TCR binding. This exclusion of phosphatases leads to stable phosphorylation of CD3 ITAMs by LCK because of reduced de-phosphorylation events [8-10]. Each of these hypothetical mechanisms are not mutually exclusive, and the mechanism of activation likely involves

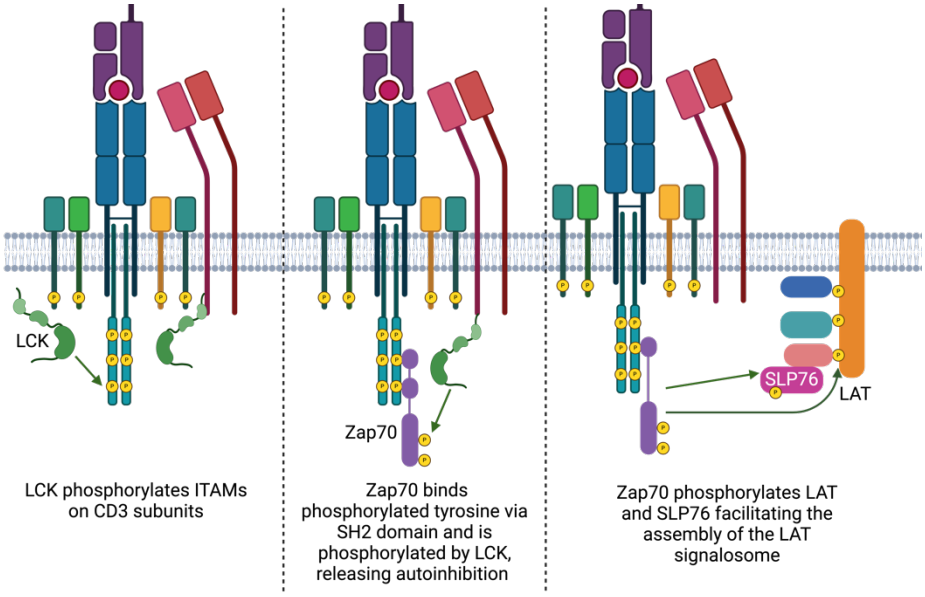

Figure 1.2 Early Events in TCR Signal Transduction TCR signaling is initiated by p/MHC binding, which triggers the phosphorylation of CD3 ITAMs by the kinase LCK. The kinase Zap70 is then recruited to phosphorylated tyrosine on CD3 domains, where it is also phosphorylated by LCK, activating Zap70 kinase activity. Zap70 is then able to phosphorylate molecules including SLP76 and LAT, triggering the assembly and activation of the signalosome that activate T cell function.

elements of each. Regardless of the exact mechanism, binding of p/MHC results in the phosphorylation of if CD3 ITAMs.

Early TCR signaling events are mediated by phospho-tyrosine kinases (PTKs). CD3 ITAMs are phosphorylated by the kinase LCK, and to a lesser extent the kinase FYN (**Figure 1.2)**.

LCK can either be bound to co-receptors CD8 or CD4, to class I and class II p/MHC molecules respectively, and co-localize with p/MHC-bound TCR, or 'free' in the cytosol of the T cell. It is this free form that is most active, and initiates phosphorylation of ITAMs. Additional LCK is brought in by co-receptors, with LCK stabilizing the co-receptor-TCR-p/MHC interaction. LCK has also been shown to be associated with the CD3 epsilon chain after ligand binding, providing an additional mechanism of LCK recruitment to the TCR [11-13]. The PTK Zap70 is recruited to CD3 chains through binding of its tandem SH2 domain to the phosphorylated ITAM tyrosine. The binding of Zap70 SH2 domain to CD3 partially releases Zap70 from an auto-inhibitory state, and the localization of Zap70 to the TCR promotes its phosphorylation by LCK at tyrosine Y319, further releasing its autoinhibition [14-16] (**Figure 1.2**).

1.2.3 TCR signal amplification and diversification via LAT

After activation and TCR localization, Zap70 kinase phosphorylates additional signaling molecules that assembles a larger TCR signalosome comprised of multiple proteins that direct and regulate downstream signaling. Zap70 is the primary mediator of the phosphorylation of LAT (Linker for Activation of T cells). LAT is a membrane associated protein that has a short, four amino acid, extracellular region, a single pass transmembrane region, and long cytoplasmic region that has no identified enzymatic activity. Phosphorylated tyrosines of LAT are binding cites for proteins with SH2-domains. The phosphate-SH2 interaction recruits many proteins to LAT, their recruitment to the plasma membrane brings together kinases and their substrates, along with additional signaling molecules that are critical to the activation of a T cell [17]. Studies of LAT deficient Jurkat T cell lines demonstrates that LAT is required for many TCR-mediated signaling events, including Ca^2 influx, Ras activation, CD69 expression and ERK phosphorylation. Furthermore, LAT deficient mice have no mature $\alpha\beta$ T cells, due to a requirement for LAT in thymocyte development. The diverse signaling pathways mediated by LAT are initiated by the recruitment of different proteins recruited to the LAT signalosome [17].

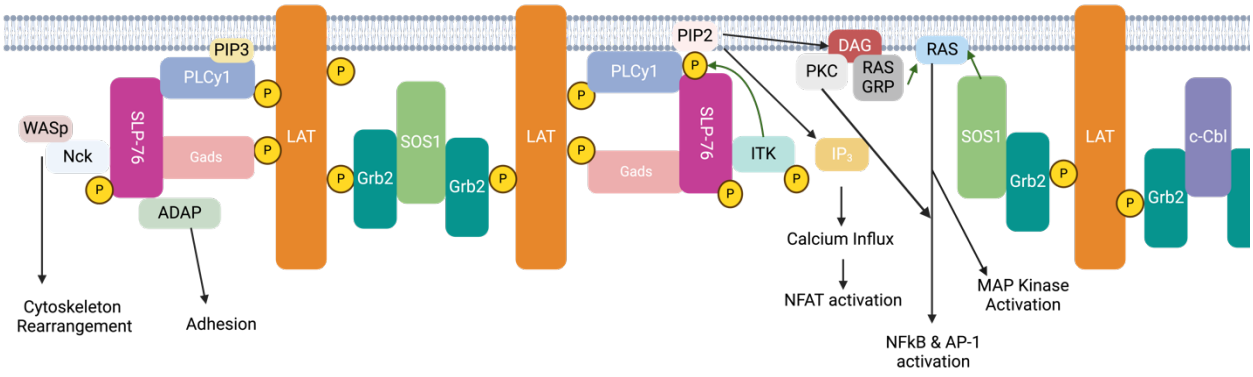

Figure 1.3 Assembly of the LAT signalosome The phosphorylation of LAT by Zap70 allows for the recruitment of many additional proteins to the membrane via SH2-phosphate interaction. Additional proteins are recruited to LAT binding proteins, creating a large signaling complex, that brings together kinases and the ligands, and can oligomerize with other

LAT-nucleated complexes. This large signaling complex form signaling 'microclusters' that can be visualized by microscopy. These complexes initiate multiple signaling pathways with diverse functions including transcription factor activation, cytoskeletal rearrangement, MAP kinase activation and adhesion.

The amino-terminal SH2 domain of phospholipase PLC-γ1 binds phosphorylated LAT tyrosine Y132. While PLC-γ1directly associates with LAT, this interaction is stabilized by the recruitment of the adaptor protein Gads to tyrosine Y171 and Y191, through binding of Gads SH2 domains. An additional adaptor proteins SLP-76 is a ligand for the SH3 domain of Gads. SLP76 binds PLC-γ1 creating a PLC-γ1-LAT-Gads-SLP76 complex that is stabilizes through these multiple interactions (**Figure 1.3**). The association of SLP76 with PLC-γ1 is essential for its function. The kinase Itk binds a phosphorylated tyrosine on SLP-76, leading to activation of Itk, which in turn phosphorylates and activates PLC-γ1. Activated PLC-γ1 hydrolyzes phosphatidylinositol 4,5-bisphosphate (PIP_2) to produce inositol 1,4,5-trisphosphate (IP3) and diacylglycerol (DAG). IP3 is a ligand for IP3 receptor, which release calcium for the endoplasmic reticulum (ER) after binding free IP3. Depletion of calcium in the ER leads in influx of extracellular calcium, which is a critical step towards NFAT activation (**Figure 1.3)** [17-19].

In addition to PLC-γ1activation, the recruitment of SLP-76 to the membrane, by association with LAT-bound Gads, is important for activation of multiple signaling pathways. PI3K, Vav, Itk, and Nck bind the phosphorylated tyrosines of SLP-76. PI3K catalyzes the phosphorylation of PIP2 to generate PIP3, PIP3 accumulation facilitates the recruitment of proteins with PH domains to the membrane. Vav is a guanine nucleotide exchange factor that activates Rho family G-proteins. Furthermore, association between Vav and adaptor Nck and WASp (Wiskott-Aldrich syndrome protein) is important for the initiation of actin polymerization and cytoskeletal re-arrangement (**Figure 1.3**). Additionally, phosphorylated ADAP binds the SH2 domain of SLP-76, the binding of these proteins is critical for adhesion and integrin function in T cells (**Figure 1.3**) [17].

The adaptor protein Grb2 can bind the distal phosphotyrosines Y171, Y191 and Y226 of LAT. Grb2 associates constitutively with Sos1 (Son of Sevenless homology 1), a GEF that actives small G protein Ras, which activates the MAP kinase ERK. Localization of Grb2 and Sos1 to the membrane by binding to LAT facilitates the interaction between Sos1 and membrane-bound Ras. In addition to MAP kinase activation, the association of Grb2 and Sos1 with LAT facilitates the oligomerization of the LAT signalosome. LAT is capable of binding multiple Grb2 proteins, and Sos1 can bind two Grb2 proteins, this creates a 2:1 Grb1:Sos1 complex that brings together multiple LAT molecules (**Figure 1.3**). The additional Grb2 SH3 ligand c-Cbl can also form a 2:1 complex with Grb2 to facilitate LAT oligomerization. LAT oligomerization forms signaling 'microclusters' that can be visualized by TIRF and confocal microscopy. While the functional effects of microcluster formation is not completely understood, decreased T cell signaling, including reduced calcium influx has been observed when microcluster formation is inhibited by mutation to the proline-rich, SH3 binding domain, of Sos1. This effect is most significant with low-antigen stimulation, suggesting LAT complex oligomerization is a critical component for TCR sensitivity [20].

Lastly several molecules that negatively regulate TCR signaling are recruited to the LAT signaling complex. TCR regulation will be covered in more detail in a later section, but briefly, recruitment of the MAP4 kinase HK1 down-regulates ERK-2 and AP-1 and the recruitment of the lipid phosphatase SHIP-1 negatively regulates Zap70 activity. The adaptor protein Gab2 can bring in the phosphatase SHP2 and displace SLP76 from Gads[17]. Together the recruitment of multiple signaling proteins, the oligomerization of signaling complex and the recruitment of regulatory molecules make LAT a critical hub in the activation and function of T cells.

1.2.4 Co-stimulation

Signaling through the T cell receptor alone is not sufficient to activate a naïve T cell [1]. An additional signal, known as 'signal 2', delivered by co-stimulatory molecules is required for the proper activation of naïve T cells in response to antigen, as process known as 'priming'. The canonical, and best described, 'signal 2' for naïve T cell priming is CD28. The co-stimulatory receptor CD28 is constitutively expressed on the surface of naïve T cells, it is activated by its ligands B7.1 (CD80) and B7.2 (CD86) which are expressed primarily on the surface of 'professional' antigen presenting cells including dendritic cells. In conjunction with a TCR signal, CD28 engagement promotes T cell proliferation, cytokine production and cell survival. Upon ligand binding CD28 is phosphorylated by LCK. Phosphorylated CD28 activates PI3K, generating PIP_3, which recruits ITK to the membrane where it can phosphorylate PLC-γ1, synergizing with TCR signaling for maximal activation of PLC-γ1. Maximal activation of PLC-γ1 produces IP_3 and DAG, which ultimately lead to the activation of transcription factor NFAT, NFκB and AP-1, all three act together to stimulate expression of the cytokine IL-2. PIP_3 generation also recruits and phosphorylates AKT, which promotes cell survival [1, 21]. In addition to CD28, naïve T cells constitutively express other co-stimulatory receptors that provide important signals during naïve T cell priming including CD27, which binds to CD70, and CD2, which binds to CD58 [22, 23].

A vast repertoire of co-receptors exists beyond CD28 and have many functions beyond naïve T cell priming. For example, Inducible T cell Co-Stimulator (ICOS), like CD28, is a member of the Immunoglobulin superfamily of receptors. ICOS expression is induced after T cell activation. ICOS also activates PI3K and AKT, however instead of promoting IL-2 production ICOS activation generally supports the expression of cytokines including IL-4, IL-10, IL-21 and IFN-γ. Another class of costimulatory receptors is the tumor necrosis factor receptor (TNF-R) superfamily, which includes the co-stimulatory molecule 4-1BB (CD137). Like ICOS, 4-1BB expression is induced after T cell activation and binds to its ligand 4-1BBL, which is expressed on the surface of B cells, dendritic cells and macrophages. 4-1BB signaling depends on the recruitment of TNF-R associated factors (TRAFs) to initiate signal transduction, which leads to sustained NF-κB activation and the activation of MAPKs. 4-1BB signaling promotes the expression of IL-2, IL-4, IL-5, and IFN-γ that support cell survival and mediate effects on neighboring cells [24].

In general, which co-stimulatory receptors are expressed by the T cell, is determined by the activation state of the T cells, and binding of costimulatory receptors to ligand influences

the function of the T cell. In this way, co-stimulation allows T cells to receive information about their environment, which dictates T cell activation, differentiation, and effector function.

1.2.5 Regulation of TCR signaling

The are multiple mechanisms for TCR signal regulation that act at different stages of signal propagation. The careful control of T cell signaling is important for the generation of an appropriate T cell response. Regulation of TCR signaling is critically for antigen discrimination; loss or mutation of regulatory molecules can result in autoimmunity [25]. Additionally, prolonged high-intensity TCR signaling is associated with effector T cell differentiation and impaired memory formation[26]. It is important that T cells are activated only after receptor engagement. Molecules, including phosphatases, function to prevent or reverse phosphorylation and activation of signaling molecules, countering the positive signaling cascade that is primarily mediated by kinases. The phosphorylation and dephosphorylation of kinases 'tunes' TCR signaling, shifting the balance between phosphatase and kinase activity determines how TCR signaling progresses.

Changing a kinase's phosphorylation state can alter its ability to propagate downstream signaling. This can be seen in the regulation of LCK, which initiates TCR mediated signaling. LCK is phosphorylated at two tyrosines, Y505 and Y394. Auto-phosphorylation of Y394 stabilizes LCK in an active conformation, while phosphorylation of Y505 stabilizes LCK in an inactive conformation. The kinase CSK phosphorylates LCK at Y505, making CSK an inhibitory kinase, while the phosphatase CD45 can dephosphorylate LCK at either site, giving it both positive and negative control over LCK. Several phosphatases including SHP1 have specificity for Y394 providing negative regulation of LCK activity [27]. The activity and availability of CSK, CD45 and other phosphatases targeting LCK tyrosine sites determines whether LCK is active or inactive. For example, TCR clustering and synapse formation separates LCK from CD45 after stable interaction of a T cell and its target, this allows for early interaction of CD45 and LCK to dephosphorylate Y505, followed by the exclusion of CD45, due to its bulky size, from the TCR signaling complex, preventing dephosphorylation of Y394 [28]. Recruitment of phosphatases such as SHP1 to the membrane by LAT-associated molecules, brings LCK and phosphatases in proximity, allowing for dephosphorylation of Y394 and inactivation of LCK [17].Like LCK, the phosphorylation of the kinase Zap70 transitions the molecule from an inactive to active state. Zap70 activity can be stopped by the dephosphorylation of tyrosines Y319 and Y315 by phosphatases included PTPN22 [27].

Phosphatases can be recruited to the immune synapse through association with a number of co-inhibitory molecules that also interact with ligands present on antigen presenting cells to regulate T cell activities. The expression of co-inhibitory receptors is induced after a T cell is activated; in this way T cell activation initiates a circuit that provides for controlled suppression of T cell signaling, stopping sustained T cell activation if antigen is not cleared. T cells can still be activated when co-inhibitory molecules are present but the abundance of phosphatases and other molecules that negatively regulate T cell signaling shift the balance of positive and negative signals, creating a higher threshold for T cell activation

and altering effector functions. Additionally, co-inhibitory receptors can share ligands with co-stimulatory receptors, creating competition for binding, further reducing positive T cell signals. The co-inhibitory receptor CTLA4 competes with CD28 for binding with B7 ligands, and the co-inhibitory receptors TIGIT compete for binding with costimulatory molecule CD226 for the ligands CD155 and CD112 [27]. This direct competition between positive and negative signaling molecules is a direct way T cell signaling is regulated after T cell activation.

Persistent antigen stimulation of T cells, such as in chronic viral infections and cancer can result in a T cell state known as 'exhaustion.' T cell exhaustion is a state in which negative or regulatory signaling in a T cell dominates over productive positive signaling. Characteristics of T cell exhaustion include loss of effector function, sustained upregulation of inhibitory receptors, altered transcription factor expression, a distinct metabolic state, and a failure to transition to quiescence and acquire a memory T cell response[29]. T cell exhaustion can be considered a regulatory state, that is beneficial in cases such as chronic viral infection. It prevents immunopathology and tissue damage that could result from a sustained anti-viral T cell response [29]. However, in the case of cancer, persistent antigen exposure and the expression of inhibitory ligands on tumor cells drives T cell exhaustion, resulting in the disfunction of tumor reactive T cells, and an impaired anti-tumor response [30]

1.2.6 The immune synapse

Many elements of T cell activation and signal regulation are controlled by the organization of the various signaling molecules within the interface between a T cell and its target cell. The organization of this region, known as the T cell or immune synapse, is critical for the initiation and amplification of TCR signaling, the integration of co-stimulatory signaling and the regulation of negative TCR signaling. The T cell synapse is made up of three general regions, organized in a bull's eye pattern. The most central region is the central supramolecular activation cluster (cSMAC) containing TCR-p/MHC interactions, the next ring out is the peripheral SMAC (pSMAC) containing LFA1-ICAM adhesion molecule interaction, and the most distal ring (dSMAC) includes the tyrosine phosphatase CD45 (**Figure 1.4**). One factor that contributes to the formation of this pattern of molecules is the extracellular size of the proteins in the synapse and their ligand on an APC or target cell. The TCR-p/MHC interaction is of low affinity (K_d value in the μM range), and the contact between the T cell and the p/MHC expressing target cell requires spacing of about 13-14 nm between the two cells. Because of the low affinity interaction of the TCR, adhesion molecules present in the pSMAC are required to stabilize the cell-cell interaction. These adhesion molecules bind ligands over a greater space than the 13-14nm of the TCR-p/MHC interaction. Additionally, the phosphatase CD45 has a large extracellular domain of >16nm excluding it to the dSMAC and spatially separating it from the site of signal initiation. These different molecules create compartments with differing synaptic distance requirements, which spatially separates the molecules within the synapse, with shorter interaction accumulating in the center and large molecules remaining in the distal regions (**Figure 1.4b**) [28, 31].

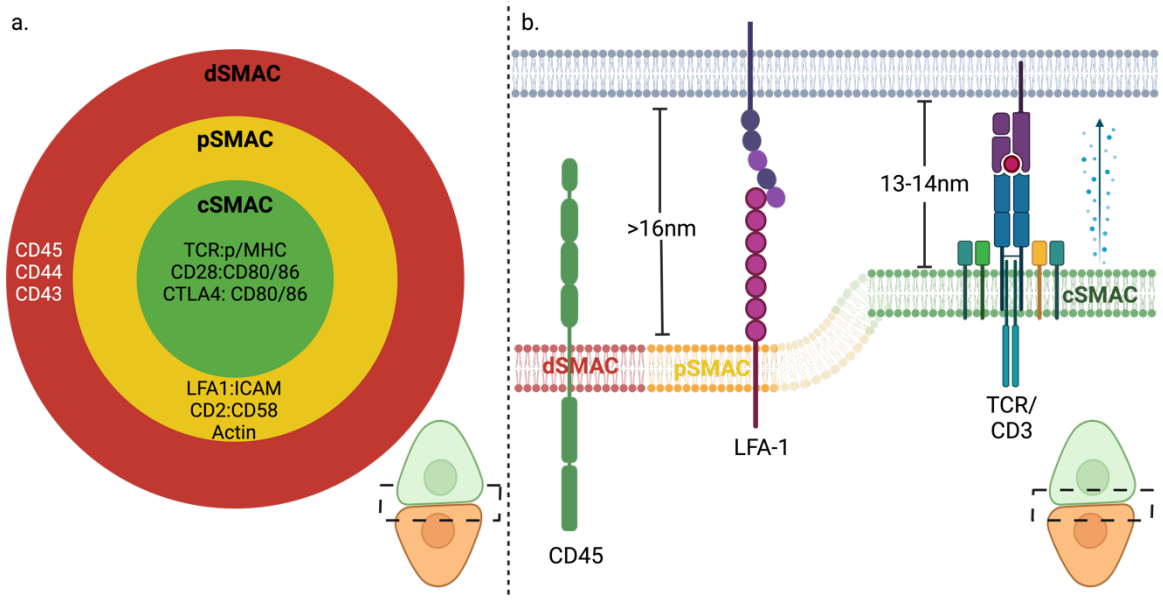

Figure 1.4 Organization of the Immune Synapse a. 'Top view' of distribution of receptors in the immune synapse fall into three main regions, the cSMAC, pSMAC and dSMAC b.) 'Side view', synaptic distance influences distribution of molecules in the synapse, with close-contact interaction of TCR:p/MHC in the cSMAC, and molecules with large extracellular domains, including CD45, in outer regions

The spatial arrangement of the synapse is important for proper TCR signaling and activation upon binding to p/MHC on an antigen presenting cell. The kinetic segregation model is a prominent model of TCR triggering, it hypothesizes that within seconds of TCR p/MHC engagement the close contact forces phosphatase CD45 away from the kinase LCK and CD3 subunits, favoring kinase activity in these regions without the countering of phosphatases [8, 32]. The distinct spatial compartments of the synapse play different roles in T cell activation and function. Despite stable synapse formation ultimately resulting in TCR accumulation in the cSMAC, it has been observed that TCRs form microclusters with signaling molecules in the pSMAC. Phosphotyrosine antibody staining demonstrates that phosphorylation is greater in the pSMAC and is reduced as TCR microclusters move into the cSMAC [33]. This pattern is also affected by antigen stimulation strength, with stronger peptide stimulations resulting in phosphotyrosine accumulation in the pSMAC, and weaker stimulations showing more phosphotyrosine signaling in the cSMAC [34]. Ultimately, TCRs are ubiquitinated and degraded in the cSMAC, making the cSMAC a site of negative regulation after initiation of TCR signaling [35]. Additionally, in cytotoxic lymphocytes (CTLs) the cSMAC is the location for the release of cytolytic granules. It is hypothesized that the synapse structure, including the ring of adhesion molecules surrounding the cSMAC helps to release cytotoxic granules directionally, targeting the bound cells while sparing other nearby cells from the cytotoxic effect [34].

Synapse organization also provides for the integration of co-stimulatory signaling. After binding of the co-stimulatory molecule CD2 to its ligand CD58, CD2 is localized to a region in the synapse on the outside of the ICAM ring of the pSMAC, termed the 'corolla'.

Engagement of CD2 alters the localization of other co-stimulatory and co-inhibitory ligands to this corolla region, where there is an accumulation of phosphorylated signaling proteins including LAT and PLC-γ1, which amplifies TCR mediated signaling. While TCR and CD2 initially co-localize, they segregate as the synapse matures, signaling is likely sustained by the localization of LAT and PLC-γ1 in the corolla [36]. Engagement of CD2, and localization of CD28 in the corolla has also been shown to increase IL-2 production demonstrating an amplification of CD28 signaling with corolla localization [36, 37].

1.3 The impact of TCR signaling on T cell differentiation

Characteristics of the initial TCR signaling cascade influence T cell function, including development, activation, proliferation and survival. Sensing and responding to activating signals of different strength is essential to the development of a diverse T cell repertoire without autoimmunity. As T cells develop in the thymus, they undergo two selection processes, dictated by the strength of signal initiated by the TCR. First positive selection leads to the survival and maturation of only T cells that receive enough signal from self-p/MHC complexes. Next, T cells that have high-affinity interaction of p/MHC undergo apoptosis as a result of strong signaling, eliminating highly reactive TCRs target self-antigen [38]. T cells continue to sense antigen strength after T cells mature and leave the thymus. The strength of the TCR-pMHC interaction can dictate the fate of the T cell which may include no response, T cell activation, activation-induced cell death (AICD), or non-response to future antigen encounter [39].

The 'strength' of a TCR-p/MHC interaction is dictated by a variety of factors, including antigen abundance, the affinity of the receptor-ligand interaction and the duration of the interaction. How the T cell senses a 'strong' signal is still an active field of investigation. Some studies have focused on CD3 ITAM multiplicity, demonstrating mono-phosphorylation of ITAMs, resulting from weak receptor agonism, is associated with inhibitory ITAM function, recruiting phosphatases to ITAMs to suppresses signal amplification [40]. Downstream of ITAM phosphorylation, the phosphorylation of Zap70 has been identified as a key determinant of the threshold of T cell activation, sufficient Zap70 phosphorylation is required for signal transduction, inefficient Zap70 phosphorylation due to low antigen affinity or quantity prevents further signal transduction [41, 42]. Similarly, slow phosphorylation of LAT by Zap70, particularly at the PLC-γ1 binding tyrosine residue Y132, has been implicated in TCR ligand discrimination. This slow phosphorylation step is incomplete from short, weak interactions but occurs during prolonged strong receptor interaction [43].

Once a mature T cell responds to antigen, it can differentiate into many different cell states that contribute to an effective adaptive immune response. Effector function is partly determined by TCR signal calibration, which is influenced by receptor levels, antigen density, and inflammatory cues. As previously described, distinct signaling check points are present to discriminate weak antigens and provide a threshold for activation. Less is known about how distinct signaling qualities influence T cell differentiation. It has been hypothesized that distinct signalosomes form in response to weak or strong ligands, but an

exact mechanism has not been revealed [44]. However, associations between signal strength and differentiation have been identified. For naïve CD4 T cells, strong TCR signal leads to differentiation to Th1, interferon producing cells, while weaker signaling leads towards a Th2, IL-4/IL-5 producing lineage. T_{FH} differentiation is also favored by a strong TCR signal, but the link between TCR signal strength and differentiation of less clear for other CD4 T cell subsets. A general trend that has been observed is that weaker signaling favors memory formation and stronger signaling favors cytotoxic function. Weaker potency TCRs induce memory-associated transcription factors like EOMES and Tcf-1, while stronger TCRs limit their expression.[44].

Signaling strength has been shown to alter CD8 effector T cell function and fate. High and low affinity interaction can produce T cell activation and effector cell differentiation. While most effector T cell cells will be short-lived, some have potential to become 'effector' (T_{EM}) or 'central' T_{CM} memory T cells. Signal strength can impact which memory populations are produced. One study demonstrated that high level of TCR signaling, as indicated by high Nur77 reported expression preferentially differentiated to $T_{CM,}$ showing that TCR signaling strength can impact T_{EM} vs. T_{CM} fate decision[45] Additionally, effector functions can be influenced by signaling strength particularly due to TCR affinity. CTLs stimulated with high-affinity ligands show increased expression of inhibitory receptors such as CD39 and transcription factors like TOX, which are associated with T cell dysfunction and exhaustion. This dysfunctional state can result in loss of the ability to respond to antigen. Although low-affinity ligand stimulation may still induce inhibitory receptor expression, such cells are more likely to retain effector function. Very low TCR signaling can result in insufficient activation and functional inertness[26].

1.4 The T cell response to cancer

The theory of immune surveillance, which was introduced in the early 1900s, proposes that a critical function of the immune system is to detect and eliminate tumors. Evidence for this hypothesis includes observations in both mice and humans that gene knock-outs or mutations that result in immune deficiencies, can lead to increased cancer occurrences. Failure of this surveillance and control is described with a complementary theory of cancer immunoediting, the process by which tumors must evolve under immune pressure to escape immune recognition. The potential for the immune system to recognize and eliminate tumors has become the basis for the development of novel cancer therapeutics. In less than two decades, immune-based cancer therapies have revolutionized the way cancers are treated, and it remains an active and growing field of research [1, 46, 47].

1.4.1 The native T cell response to cancer

Some of the earliest evidence that T cells could control tumor growth came from studies of RAG-$2^{-/-}$ mice. RAG-$2^{-/-}$ mice cannot undergo rearrangement of the TCR genes, and therefore do not produce mature, peripheral α/β T cells, B cells, NKT cells or γ/δ T cells. In multiple studies, RAG-$2^{-/-}$ mice developed tumors, either chemically induced or spontaneously, at a greater rate that wild-type mice, demonstrating a role of lymphocytes

in protecting from tumor formation [47]. Since these early experiments much more has been learned about how T cells recognize and respond to tumor cells.

The process of initiating an anti-cancer immune response has been summarized into a framework known as the Cancer-Immunity Cycle. The cycle comprises of several key steps. First, antigens derived from mutated proteins (neoantigens) or from overexpressed or aberrantly expressed self-proteins in tumors are taken up and processed by dendritic cells (DCs), typically in draining lymph nodes (Step 1). Next, DCs present cancer-specific antigens on MHCI and MHCII molecules for recognition by T cells (Step 2). T cells that recognize MHC-presented peptides are 'primed' resulting in the activation of an effector response against the tumor (Step 3). After activation, tumor-specific T cells then traffic to the tumor site (step 4), infiltrate the tumor (step 5), recognize and kill tumor cells presenting antigen on MHCI (steps 6 and 7) As tumor cells are killed, additional tumor-associated antigens are released, perpetuating this cycle. [48].

Over time, this framework has been expanded to account for the involvement of innate immune cells within the tumor microenvironment. These cells shape the T cell response through both immune stimulating or immune suppressing signals [49]. However, failure at any point in the Cancer-Immunity Cycle can result in tumor progression and metastasis. For example, DCs may fail to process and present tumor antigens, cutting off the cycle before T cell recognition (Step 2). Alternatively, the DC-T cell interaction may induce a regulatory response, in which the tumor-associated antigen is treated as 'self' rather than foreign. Failure can also occur after T cell priming. T cells may also fail to traffic to and infiltrate into the tumor. T cells may have their effector function suppressed by the tumor microenvironment or acquire a dysfunctional state known as T cell exhaustion. Finally, tumor cells may lose expression of MHC molecules or downregulate antigen processing machinery, rendering them insensitive to T cell attack. Cancer immunotherapies attempt to rescue the Cancer-Immunity Cycle by providing a support to or circumventing one or more steps in the cycle.

1.4.2 Approaches to augment the T cell response to cancer

Checkpoint Blockade

T cells received inhibitory signals at many steps in the priming, activation and effector response stages that dampen their activity. These signals serve an important role in regulating the T cell response to ensure antigen is cleared but prevent uncontrolled T cell expansion and activation that can result in toxicities. However, particularly in the setting of cancer, these controls or 'checkpoints' can prevent the desired immune response. Inhibitors of these regulatory molecules are now currently being used as cancer therapeutics, collectively known as immune checkpoint therapy, to improve the native T cell response to cancer.

Cytotoxic T lymphocyte-associated protein-4 (CTLA-4) is expressed by activated T cells and is a homolog for the co-stimulatory receptor CD28. CTLA-4 has a higher affinity and avidity

for B7 ligands, allowing it to outcompete CD28 for ligand binding, thereby inhibiting CD28-supported T cell proliferation and IL-2 production [50]. In addition to disrupting CD28 binding, phosphorylation of CTLA-4 recruits the phosphatase SHIP-2, which dephosphorylates CD3 subunits and LAT, providing a mechanism for inhibition of both CD28 and CD3/TCR signaling [51]. CTLA-4 interferes with the priming of T cells by blocking the co-stimulatory 'signal 2' and inhibits priming and effector activation of T cells by cancer antigen-presenting DCs (step 3 of the Cancer-Immunity Cycle). Treatment with anti-CTLA-4 antibody blocks the interaction of CTLA-4 with B7, allowing for CD28 to bind, and provide signals for T cell priming (**Figure 1.5**). Anti-CTLA-4 treatment has been shown to cause increased expansion of effector CD4 and CD8 T cells and when used alone in clinical trials provides durable responses in approximately 25% patients with metastatic melanoma. Anti-CTLA-4 (Ipilimumab) is now FDA approved for the treatment of unresectable or metastatic melanoma.

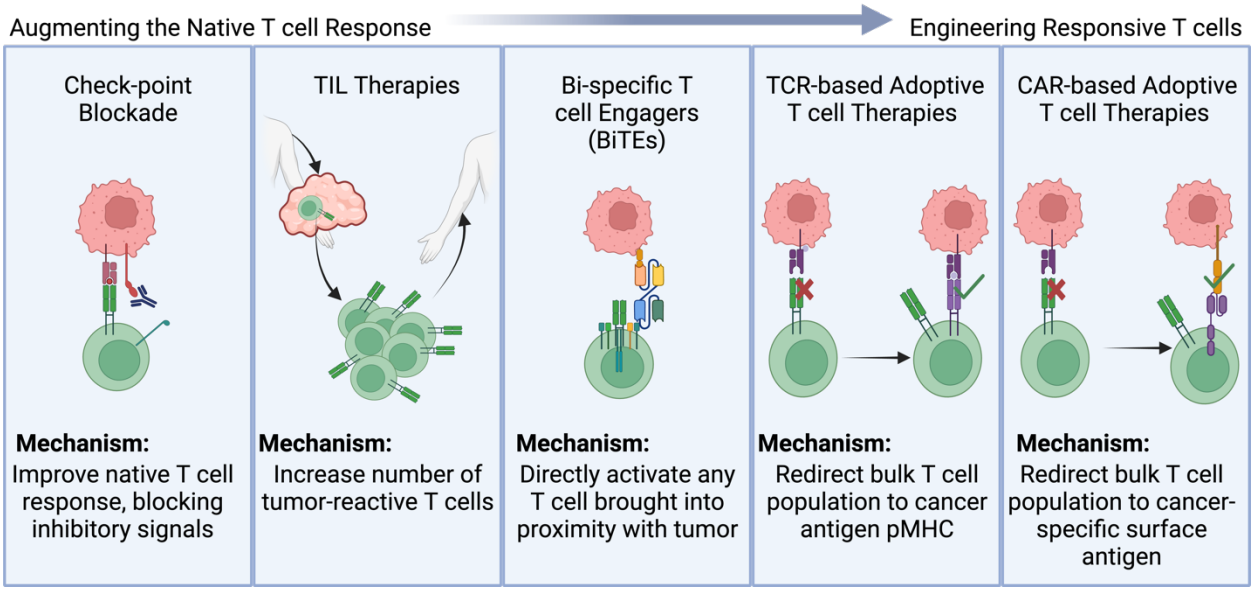

Figure 1.5 T cell-based cancer immunotherapies Immune-based therapies for caner function by acting on T cells in a variety of ways. Some approaches aim to improve the native T cell response to a tumor, while others engineer tumor specificity into the T cells through engaging TCR common chains with tumor antigen or expressing new receptors with tumor specificity in patient T cells.

Programed death 1 (PD-1) is an additional T cell checkpoint receptor, which is expressed by activated T cells. PD1 engagement with its ligand PD-L1 or PD-L2 results in recruitment of phosphatases SHP-1 and SHP-2, which dephosphorylate TCR signaling molecules including CD3ε, Zap70, and CD28 to interfere with TCR signaling. PD-1 functions to prevent excessive T cell activation, and autoimmunity. High expression of PD-L1on tumor cells dampens the T cell anti-tumor response, preventing the elimination of tumor cells by cytotoxic T cells – step 7 of the Cancer-Immunity Cycle [50, 52]. Treatment with either anti-

PD-1 or anti-PD-L1 antibodies, blocks receptor-ligand interactions and the activation of PD-1 inhibitory signaling, improving the T cell mediated anti-tumor response (**Figure 1.5**). After initial FDA approval of anti-PD1 (Nivolumab or Pembrolizumab) for treatment of metastatic melanoma, anti-PD1 and anti-PDL1 antibodies have been approved for the treatment of many additional cancer types.

Anti-CTLA4 and anti-PD-1/anti-PD-L1 therapies function at different stages of T cell activation and the Cancer-Immunity Cycle and the combination therapy of both antibodies can increase anti-tumor efficacy. The combination of anti-CTLA4 and anti PD-1 is approved for use in multiple settings including the treatment of metastatic melanoma, previously treated colorectal cancer, unresectable hepatocellular carcinoma and non-small cell lung cancer (NSCLC). Additional 'checkpoint' targeted antibody therapies are also being tested in clinical trials, including those targeting LAG-3, TIM-3 and TIGIT [50].

While checkpoint blockade therapies have been successful in many settings, there are limitations to their use. Checkpoint blockade functions to 'boost' or un-inhibit an endogenous T cell response and is dependent on existing tumor-specific T cells to act on. Cancers with high mutational burdens, such as melanoma, are best at generating tumor-specific T cell responses, and it is these tumor types that checkpoint blockade therapies are most beneficial. Resistance to checkpoint inhibitors can develop through multiple mechanisms. Tumors may gain genetic or epigenetic alteration that prevent antigen presentation on MHC-I, preventing recognition by a CD8 T cell [50, 53]. In addition to escaping recognition, genetic alteration in tumor may aid in tumor escape of the T cell response. Mutations to interferon-receptor-associated kinases Janus Kinase 1 (JAK1) and Janus Kinase 2 (JAK2) have been observed in tumors from patients with acquired resistance to PD-1 blockade, allowing tumors to become insensitive to INF-γ produced by T cells[54]. Furthermore, stromal and immune cells in the tumor microenvironment may act to prevent T cell infiltration into the tumor blocking T cell-tumor cell interactions [49].

Tumor-Infiltrating-Lymphocyte (TIL) Adoptive Cell Therapy (ACT)

Adoptive cell therapies (ACT) are cell-based therapies that use either patient or donor derived cells to improve a patient's immune response. Adoptive transfer of tumor infiltrating lymphocytes (TIL) is one approach to improve the T cell response to cancer. The concept is that by expanding TIL outside of the body and reinfusing large numbers the number of a tumor-reactive T cells in the patient can be dramatically increased. Briefly, tumors are extracted surgically from a patient, processed and cultured ex-vivo in cytokines to promote T cell growth, then further expanded by a rapid expansion protocol (REP), where T cells are co-cultured with feeder cells and low-doses of anti-CD3 antibody and IL-2. This process can generate many millions of T cells from only a few thousand starting inputs. The

expanded TILs are then re-infused to the patient (adoptive transfer), typically after a patient received lymphodepletion therapies (**Figure 1.5**). Preclinical development of TIL therapy began in the 1980's. The adoptive transfer of tumor reactive to T cells in mice showed clearance of liver and lung metastasis in mice with colon adenocarcinomas [55]. The successful translation of TIL treatment to patients required the addition of lymphodepleting chemotherapy prior to T cell transfer. Patients are also treated with high-dose IL-2 after TIL infusion to promote the survival and proliferation of the transferred TILS in vivo. Patients with metastatic melanoma treated with TILs have experienced complete and durable remission, with objective response rates ranging from 30-40% [56, 57].

TIL ACT aims to overcome the suppressive tumor microenvironment that can limit the local expansion of tumor reactive T cells. With this approach, a heterogenous population of T cells, enriched for tumor reactivity due to their localization to the tumor, are expanded ex-vivo, in the absence of suppressive factors of the tumor microenvironment. Like check-point blockade, this approach 'boosts' an endogenous T cell response by giving T cell the opportunity to overcome suppressive signals. This strategy relies on the presence of cancer antigen-specific T cells that can enter the tumor microenvironment. TIL therapies are therefore most suitable for tumors with high mutational burdens that will elicit a cancer-specific T cell response, and that have resectable tumors with T cell infiltration [58]. TIL therapies have been used in clinical trials for metastatic melanoma, cervical cancer and NSCLC. In 2024 the FDA approved a TIL product (lifileucel) for treatment of refractory metastatic melanoma [56].

Bispecific T Cell Engager (BiTE)

Checkpoint blockade and TIL ACT depend on the generation of tumor-reactive T cells through the cancer-immunity cycle. Bispecific T Cell Engagers (BiTEs) bypass the need to produce and then modify this specific population, and instead engages T cells within tumors, regardless of their natural antigen specificity. BiTEs consist of two antibody domains connected by a small linker peptide (**Figure 1.5)**. The antibody domains are typically single-chain variable fragments (scFV), which are derived from the variable light and heavy chains of an antibody. One scFV of a BiTE binds to the CD3ε chain, while the other scFV is specific for an antigen expressed on the surface of the targeted tumor. Simultaneous engagement of CD3ε and a tumor antigen with a BiTE results in the establishment of a immunological synapse between the T cell and tumor cell, activation of the T cells that then secrete perforin and other cytolytic cytokines, killing the tumor cell [59, 60]. The BiTE architecture is adaptable to targeting of multiple different tumor antigens, by altering the specificity of the scFV. BiTEs have gained FDA approval for the treatment of

multiple hematological malignancies, and efforts continue to expand their use to solid tumors [61, 62].

While BiTEs have shown successes in the treatment of hematological malignancies they have some limitations. Unlike checkpoint blockade and TIL ACT, BiTEs improve the T cell response to one specified antigen. This required the identification of a surface-expressed tumor-specific antigen, that is either not expressed on healthy tissue or that has an expression pattern such that on-target off-tumor targeting can be tolerated. Additionally, successful clearing of tumor requires homogenous expression of the target antigen, tumor clones that lack target expression cannot be directly targeted by BiTEs. In addition to these mechanistic limitations, BiTEs have some challenges for practical application. Many BiTEs have a very short half-life that requires long-term continuous IV administration, although efforts to generate half-life extended (HLE) BiTEs are resolving this limitation. Finally, BiTEs need to localize to the tumor site this may be more difficult to achieve in solid tumors that are less accessible than hematological malignancies. Furthermore, the use of BiTE therapies for solid tumors is limited by the availability of tumor-specific surface antigens that would allow for the targeting of tumors which sparing normal healthy tissue [59].

Genetically Engineered T cells for Adoptive Cell Therapies (ACT)

While BiTEs redirect T cell specificity through engagement with an extracellular molecule on the tumor, another approach to engineering tumor-specificity into bulk T cell populations is to introduce a new receptor into the T cell itself, either by removing T cells from the patient and transducing them ex vivo or as recently demonstrated by performing the gene transfer in vivo [63]. Ex vivo genetically engineered T cell therapies generally use a lentivirus to deliver DNA encoding the new receptor into T cells isolated from patients. These engineered T cells are expanded ex-vivo, then infused into a patient where they have the capability to target the intended tumor antigen, proliferate and provide a durable memory T cell response. Genetically engineered ACT includes both the introduction into a T cell of a transgenic TCR or a CAR directed at a p/MHC or cell surface antigen, respectively.

TCR T cell therapies utilize TCR sequences that have been identified as specific to tumor antigen, presented as a peptide on MHC-I molecules. TCR sequences used for TCR ACT target tumor-specific peptides, typically those arising from neoantigens, self antigens derived from the re-expression in tumors of proteins expressed during embryonic development or in the testes, or virally derived peptides - in the case of tumors that have viral origins. (**Figure 1.5**). However, identifying tumor-specific TCR sequences continues to be a challenge. Traditionally TCR identification involves expansion of individual TCR clones after co-culture with tumor cells or candidate tumor antigens and sequencing. Identification of antigen-reactive T cell markers has been aided in the identification of

phenotypic markers of potential tumor-reactive T cells [64], and computational predative approaches may eventually help with the design of reactive TCRs given a tumor-specific target [65, 66]. An additional challenge to TCR identification is the genetic restriction of TCR recognition. The HLA genes that encode MHC are polymorphic in the population. TCR recognition is highly specific for a single p/MHC, therefore ACT with a TCR is restricted to patients with a particular HLA-type [53]. Despite these challenges in development, TCR therapies are actively being testing in clinical trials, and have produced responses in melanoma and sarcomas. Recently a MAGE A4 specific TCR gained FDA approval for the treatment of soft tissue sarcomas in 2024 [67].

An alternative approach to genetically engineering tumor specificity into patient T cells is use of Chimeric Antigen Receptors (CARs), discussed in more detail in Chapter 2. CARs are synthetic receptors that are a hybrid of multiple T cell signaling domains, fused with an antibody-based recognition domain, typically an scFV (**Figure 1.5, Figure 2.1**). CARs are capable of recognizing surface proteins on a tumor cell by binding of the scFV domain, which activates intracellular signaling domains of the CAR, initiating signaling and a cytotoxic response by the T cell. Intracellular cellular domains vary among CAR designs, however currently FDA-approved products share a similar architecture, fusing a membrane proximal co-stimulatory domain with a distal CD3ζ domain. In this way, the CAR provides both the conical 'signal 1,' CD3ζ ITAMs, and 'signal 2' co-stimulation within one molecule [53]. Initial CAR designs used CD28 as their costimulatory domain, however designs that used signaling domains of the costimulatory domain 4-1BB showed less tonic signaling, that is signaling without receptor binding to antigen, and less T cell exhaustion than CARs using the CD28 domain[68]. Comparisons between CARs with CD28 and 4-1BB costimulatory domains have also demonstrated that 4-1BB CARs have improved in-vitro persistence, with increased central memory differentiation, and mitochondrial programing that supports long term persistence including mitochondrial biogenesis [69]. CAR T cells have been FDA approved for targeting CD19 and BCMA expressed on B cell malignancies and multiple myeloma, respectively [70]. A major limitation in the use of CARs is the identification of tumor-specific surface antigens that can be targeted by CARs while sparing healthy tissues. Furthermore, while CARs have been successful in the context of targeting B cell malignancies, their expanded use in targeting other cell types, including solid tumors derived from epithelial tissues, have had much more limited successes. Target selection for solid tumors, together with immunosuppressive tumor microenvironment remain major hurdles for expanding CAR T cell therapy to solid tumor, however this remains an active field of study [71].

Chapter 2: Chimeric Antigen Receptor T cell Therapies

2.1.1 The development of chimeric antigen receptors

Early attempts to generate T cell receptors that bypass MHC recognition was described in the 1980s by groups in Japan and Isreal. The first approach, produced in the lab of Dr. Yoshikazu Kurosawa, replaced TCR variable chain regions with antibody heavy and light chains (**Figure 2.1**). The group expressed these chimeric molecules in a mouse T cell line and showed calcium influx after antigen engagement [72]. This was the first example of an antibody-TCR chimeric receptor activating T cells. Shortly after this publication, Dr. Zelig Eshhar's group also expressed chimeric antibody-TCR receptors in mouse T cells, showing receptor mediated IL-2 production and target cell killing [73]. A major difficulty in expressing these chimeric receptors was that they required infecting T cells with two different retroviral vectors, each encoding a single chain of the antibody-TCR hybrid receptor, which was very inefficient. To bypass this need, Dr Eshhar's group designed single-chain receptors, fusing a single chain antibody fragment (scFV) with a lymphocyte intracellular signaling domains, either T cell CD3ζ or B cell FcεRIγ creating a 'scFvR', which became known as a first-generation CAR (**Figure 2.1)** [74].

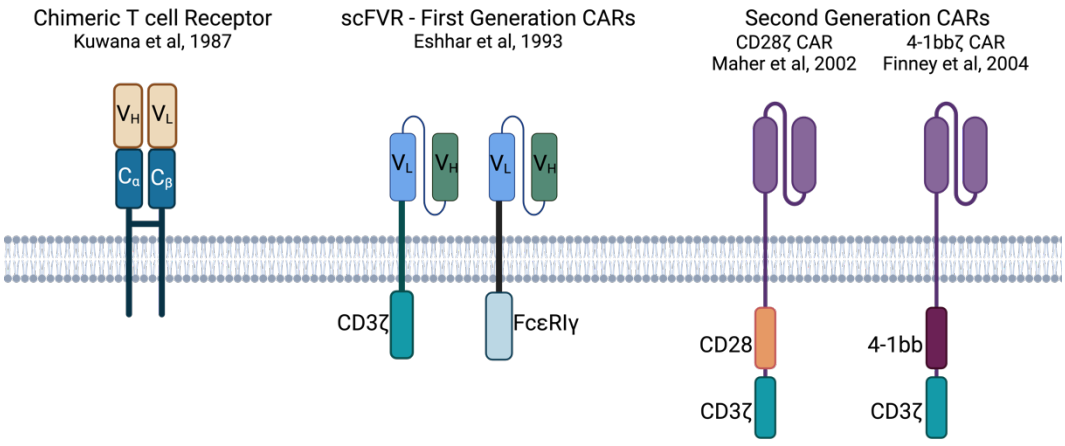

Figure 2.1 Evolution of MHC-independent receptor design Chimeric TCRs were first proposed in the 1980s, however introduction of two proteins from independent viral vectors was limiting. Single-chain receptors were proposed, linking antigen recognition with ITAM domains of TCR or BCR receptors, these receptors were further developed to include TCR 'signal 1' CD3ζ and 'signal 2' co-stimulatory domains

First generation CARs showed antitumor activity in murine tumor models and were advanced to clinical trials in ovarian cancer and metastatic renal cell carcinoma with autologous T cells designed with scFVs against the alpha folate receptor (ovarian cancer)[75] or Carbonic Anhydrase IX (renal cell carcinoma)[76]. However, these trials did not show tumor regression and there was no evidence of engineered T cells in the blood

obtained from treated patients 1-2 months after infusion. Some first-generation CARs showed limited efficacy and persistence in patients with lymphoma treated with an anti-CD20 CAR or neuroblastoma treated with anti-GD2 first-generation CAR. However, the limited efficacy of first-generation CARs over all demonstrated a need to improve the receptor design [70].

It was hypothesized that T cells expressing first generation CARs, which delivered only 'signal 1' through activation be the chimeric receptor, failed to persist due to lack of co-stimulation. To enhance CAR T cell persistence, second-generation CARs were developed to provide co-stimulation signaling upon antigen recognition. Initially this was achieved by fusing an scFV with a CD28 domain alone [77]. Later designs incorporated both a CD28 costimulatory domain and a CD3ζ domain fused to an scFV. These 'second generation CARs, which delivered both 'signal 1' and 'signal 2' after recognition of a single antigen (**Figure 2.1**), showed improved proliferation, cytokine production and antigen-directed killing in-vitro compared to receptors without the costimulatory domain[78]. In a clinical trial, a small number of patients with lymphoma received a co-infusion of T cells expressing a first-generation CAR and T cells expressing a second-generation CAR with CD28 co-stimulation (28ζ CAR). T cells expressing the 28ζ CAR showed improved expansion and persistence compared with T cells expressing the first-generation CAR [79]. This demonstrated the utility of incorporating co-stimulation domain directly into the CAR architecture to improve CAR T cell expansion and persistence.

In addition to CD28, the co-stimulatory molecule 4-1BB has been incorporated to the CAR structure to make a different 'second generation' CARs (**Figure 2.1**). The use of a 4-1BB co-stimulatory in place of the CD28 co-stimulatory domain has several advantages. Like 28ζ CARs, T cells expressing 4-1BBζ CARs have improved cytokine production and proliferation compared to first-generation CARs [80]. Functional differences between CARs with CD28 and 4-1BB co-stimulatory domains have been described. 4-1BBζ CARs generally show lower levels of tonic signaling, signaling without antigen binding, and 4-1BBζ CAR expressing T cells have improved persistence in patients compared to 28ζ CARs [68, 70]. 4-1BB co-stimulation in CARs also impacts the differentiation of T cells expressing these CARs. Expression of 4-1BBζ CARs promoted the expansion of central memory T cells, which higher respiratory compacity and mitochondrial biogenesis, these conditions promote the long-term survival and function of T cells expressing the 4-1BBζ CAR. 28ζ CARs, in contrast, expanded to produce more effector memory cells that with high glycolytic activity, resulting is poorer persistence compared to 4-1BBζ CAR T cells[69].

2.1.2 Clinical Translation of CAR T Cells

Between 2017 and 2023, 7 CAR T cell products have been FDA approved, and thousands of patients have received these therapies. CARs expressing anti-CD19 scFVs were developed to target malignant B-cells, and show remarkable success in treating relapse or refractory (R/R) B cell lymphomas, which had previously very poor outcomes after salvage chemotherapy [81-83]. Multicenter trial of CD19 CAR T cell therapies show complete response rates (CR) of 40-50% for patients with diffuse large B cell lymphoma and mantle cell lymphoma[84], 67% -74% for patients with indolent B cell lymphomas[85, 86] These trials lead to the FDA approval of CD19-directed CARs for these indication. Additionally, a multi-center CD19-CAR trial for treatment of R/R B cell acute lymphoblastic leukemia (B-ALL), show CR rates ranging from 71-81% [87, 88]. CD19 CARs are now FDA approved for treatment of ALL, providing a new therapy for patients with limited options. CAR T cells targeted B cell maturation antigen (BCMA) have also shown success in treating R/R multiple myeloma. Clinical trials of BCMA-directed CARs had an overall response rate (ORR) of 73-98% [89-91]. BCMA-directed CARs are now FDA approved for treatment of R/R multiple myeloma.

All FDA approved CAR T cell products are generated by lentiviral transduction to introduce the CAR transgene, and the receptors are second-generation CARs containing either CD28 or 4-1BB co-stimulatory domains. Treatment with CAR T cells is proceeded by administration of lymphodepleting chemotherapy to improve CAR T cell engraftment. CAR T cells have shown impressive initial successes treating a cohort of patients with limited alternative treatment options[81]. Since the first patients treated with CARs were treated just over a decade ago, long term follow-up of patients receiving CAR T cell therapies is limited to this timeframe. However, studies of these patient cohorts have revealed both the long-term success for a subset of patients and also the limitations in achieving sustained remission in a majority of patients.

The CD19-directed 28ζ Axicabtagene Ciloleucel or ‘axi-cel’ was approved for treatment of R/R Large B Cell lymphoma. Patients treated with axi-cel have been followed for 5 years, demonstrating the long-term efficacy of this therapy. The five-year progression-free survival rate was 29%, and the overall survival rate at 5 years was 40%, with the lymphoma-specific survival rate of 53%. In general relapses beyond one year were rare, while non-lymphoma specific deaths occurred due to infections or additional cancer occurrences[92]. These data indicate some patients (29%) maintained sustained, durable responses at the 5-year time point, showing the impressive function of CAR T cell therapies, and their potential for achieving long-term remission in patients with limited treatment options. However, improvements to CAR T cell therapies are necessary to improve the proportion of patients that experience this long-term success, and this is best accomplished by addressing the mechanisms by which tumor escape CAR T cell recognition.

2.2 Mechanisms of Tumor Recurrence after CAR T cell therapies

2.2.1 Clinical Observations: Antigen Loss and Downmodulation

Mechanisms that account for loss of CAR T cell efficacy include poor CAR T cell product quality, an immunosuppressive tumor microenvironment (TME) and antigen escape. The most common mechanism for tumor escape of CAR T cell recognition is antigen escape. Loss of target antigen expression, or mutation to the target antigen results in the inability of the CAR to recognize antigen and activate the CAR-expressing T cell . There are multiple mechanisms that have been identified explaining alterations of antigen expression in tumors. These have been studied in the context of CD19 expression in B cell malignancies and BCMA expression in multiple myeloma. Complete CD19 antigen loss is observed in some cases. One mechanism for this loss of expression is disrupted trafficking of CD19 to the cell surface [93]. Cases of complete CD19 loss demonstrate that CD19 is not essential for tumor survival, even though it is a co-stimulatory molecule for B cell receptor signaling, making CD19-targeted CAR therapies vulnerable to loss of efficacy due to target expression loss. In addition to complete loss of CD19 expression, alternative splicing events have been identified, which maintain some intracellular signaling functions of CD19, while eliminating the epitope that is recognized by the CD19 CAR scFV [94, 95]. While these mutations are identified post-treatment, studies have also demonstrated that these CD19 isoforms exist prior to CD19-targeted treatment, identifying a cell population that never had the ability to be directly targeted by CD19 CAR. Similarly, acquired BCMA loss or expansion of pre-existing BCMA negative clone during BCMA-targeted therapies have been observed [96, 97]. These findings demonstrate that antigen loss is a major mechanism of CAR resistance, that can either be acquired or pre-exist in the tumor population. CARs and other therapies that target one antigen are vulnerable to loss of efficacy with antigen loss. Therapies that target multiple antigens may improve efficacy by limiting this mechanism of escape.

Patients can relapse with target antigen positive tumors, even with continued presence of CAR T cells in circulation. This demonstrates that CAR T cells have lost the ability to respond to antigen positive tumor. While mutations to the targeting epitope may explain some cases of escape from CAR recognition, decreased antigen expression has been widely observed and provides another explanation for the inability of CAR T cells to respond to antigen positive tumor. Lower antigen levels on tumor cells present at the time of relapse compared to pre-treatment levels have been observed in multiple settings including after CD19, CD22 and BCMA- targeted CAR T cell therapies [98-100]. This observation shows that CAR T cells provide a selective pressure on these tumors, selectively responding to and eliminating high-antigen tumor cells, while being ineffective

against low-antigen tumor. This suggests that CAR T cells have a minimum threshold of antigen expression on the tumor that is for recognition and tumor elimination. The threshold of antigen expression for CAR activation has been directly studied in vitro and the data supports the clinical observations. In general, CAR T cell activity increases with increased antigen density on target cells, with typical second-generation CAR T cells requiring antigen levels in the range of 1000s of molecules on each target cell to induce cytokine production and proliferation[101, 102]. In some cases, this threshold for activation can be used to advantage. When a particular antigen is overexpressed compared to healthy tissue, targeting this antigen with a CAR that has low sensitivity for antigen allows for the selective targeting of antigen-high tumor cells [103, 104]. However, for tumors with low target antigen expression, or 'safe' antigens where off-tumor on-target cytotoxicity is tolerable, improving CAR sensitivity will be critical to improve the efficacy of these therapies against tumors with heterogenous antigen expression levels.

2.2.2 CAR vs. TCR Signaling and Sensitivity

Clinical and experimental evidence suggests that CAR T cells require 1000s of antigens present on the target cell surface to activate a CAR expressing T cell, while TCR expressing T cells can be activated with as little as 10s of p/MHC molecules [42, 105]. While CAR designs aim to recapitulate TCR activation signals by incorporating TCR signaling motifs, CARs do not incorporate all signaling motifs of the native TCR (**Figure 2.2**). These differences result in different signaling events down-stream of receptor activation, and a requirement for higher antigen levels on target cells. Traditional 'second generation' CARs incorporate the CD3ζ signaling domain to provide 'signal 1' for T cell activation. While the three ITAMS of CD3ζ provide sufficient signal to activate the T cell, in both the context of CARs and TCRs [74, 106], the native TCR associates with dimers of three additional CD3 subunits and a second CD3ζ, providing for a total of 10 ITAMs compared to the three in a CAR (**Figure 2.2**). Many groups have demonstrated the importance of both the number and diversity of ITAMs for TCR function. Individual ITAMS, CD3ζ and CD3ε, can initiate a TCR activation signal similar to a complete TCR complex, suggesting ITAMs may be functionally redundant, but additive [106-109]. However, individual ITAMs may have diverging roles in TCR activation. Sequence diversity in the ITAMs motifs (**Figure 1.1**) results in preferential recruitment of individual signaling molecules, including both kinases such as Zap70 and regulatory molecules including p85 and SHP1 [5, 40]. In addition to ITAM motifs, CD3 subunits contain other sequence motifs, include proline-rich sequences (PRS) and basic residue sequences (BRS) that also mediate protein-protein interactions, contributing to the recruitment of proteins to the TCR complex [110]. Together, these data suggest that the lower ITAM multiplicity and diversity in CARs would result in differences in signaling that contribute to reduced antigen sensitivity compared to the TCR.

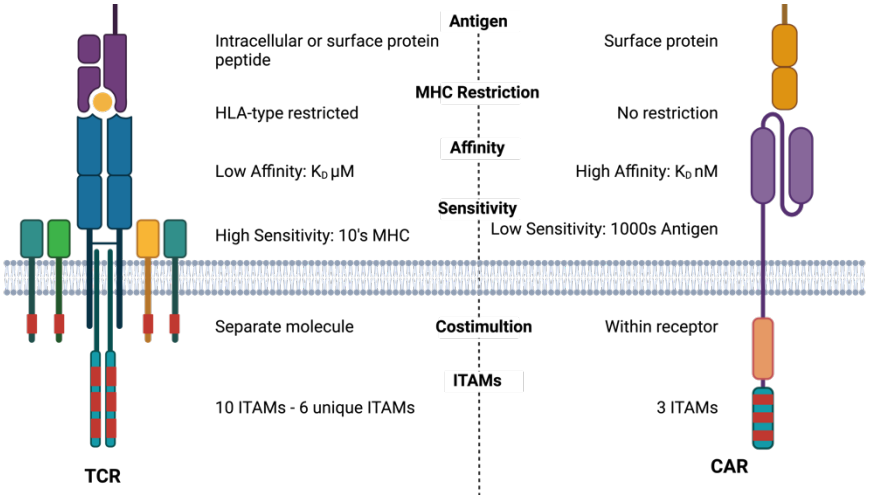

Figure 2.2 Comparison of TCR and CAR Structure Differences between TCR and CAR architecture lead to differences in receptor function

Additional differences between CAR and TCR signaling have been observed downstream of ITAM signaling. Phosphoproteomic analysis has demonstrated that the adaptor proteins LAT is less intensely phosphorylation downstream of 4-1BBζ CAR activation compared to TCR activation [111]. Additionally, microscopy studies demonstrated that CARs have a similar deficiency in Zap70 phosphorylation, showing 100-fold increase in the amount of antigen necessary to recruit Zap70 to the immune synapse compared to TCR [42]. In addition to reduced phosphorylation of specific signaling molecules, the topology of immune synapses formed by CAR T cells may contribute to altered receptor-mediated signaling. Instead of the well-organized bull's eye synapse typical of T cells, CAR T cells tend to form primitive and disorganized immune synapses [112]. Since conical synapse formations aid in signaling amplification, propagation and regulation, these benefits may not be provided to CAR T cells.

In addition to diminished antigen-induced signaling, CAR T cells demonstrate evidence of signaling in the absence of antigen binding. This 'tonic signaling' results in baseline production of cytokines and if prolonged or intense, results in the induction of activation marker expression indicative of an 'exhausted' T cell phenotype. Excessive tonic signaling can render CAR T cells less effective in-vivo and may contribute to toxicities in patients treated with CAR T cells Multiple factors related to the structure and design of CARS have been suggested to cause of tonic signaling. Oligomerization of CAR receptors through interaction of the scFV may induce signaling without antigen binding. Individual scFVs, such as the anti-GD2 scFV (14g2a), have increased tonic signaling over CARs with different scFVs but the same intracellular domains [113]. Transmembrane domains may also contribute to basal CAR oligomerization and signaling. CARs can use a variety of

transmembrane domains, from other surface receptors including CD8 and CD28, the CD28 transmembrane domain has been shown to promote receptor oligomerization [114]. The use of the CD28 costimulatory domain within the CAR architecture also increases tonic signaling over the use of 4-1BB [68]. Receptor density also contributes to tonic signaling, lowering the expression of the CAR can reduce tonic signaling, but this approach may also reduce receptor sensitivity [115].

2.3 Approaches to overcome antigen escape from CAR T cell Therapies

The loss of CAR activity due loss or low levels of antigen expression remains a key challenge to the success of CAR T cell therapies. The poor sensitivity of CARs for antigen compared to TCRs and the observation that monospecific T cell therapies are vulnerable to single antigen loss needs to be addressed in new receptor designs to make CAR therapies effective long-term treatments.

2.3.1 Improving CAR signaling and sensitivity

Additional costimulatory domains

One approach to improving CAR T cell signaling has been the inclusion of additional co-stimulatory domains into the CAR architecture. These 'third generation CARs' incorporate multiple co-stimulatory domains, most frequently both CD28 and 4-1BB, with the aim of achieving an additive effect from each domain (**Figure 2.3**). Preclinical models showed success in this approach, with improved proliferation, persistence and anti-cancer activity to T cells that expressed CARs incorporating two costimulatory domains compared to T cells that expressed CARs including only one. However, clinical trials of these CAR T cells showed increased occurrence of severe side effects and accelerated T cell exhaustion associated with the use of multiple costimulatory domain [116]. Furthermore, while the 'third generation' approach showed increased potency in pre-clinical models, this method of CAR design did not address issues of sensitivity or provide recognition of more than one antigen, leaving these CARs vulnerable to the same limitations of 'second generation' CARs.

In additions to adding costimulatory domains, another approach has been to incorporate alternative costimulatory domains, replacing CD28 and 4-1BB. One alternative co-stimulatory domain that has been proposed is CD28-family co-stimulatory molecule ICOS. ICOS-CARs were proposed to improve CAR T cell persistence by promoting Th17 differentiation and T cell persistence. In mouse models ICOS CARs did show increased Th17 differentiation and improve T cell persistence when compared to CARs with CD28 or 4-1BB domain[117]. Pooled screens comparing many co-stimulatory domains have become useful tool and have identified domains from co-stimulatory molecules including

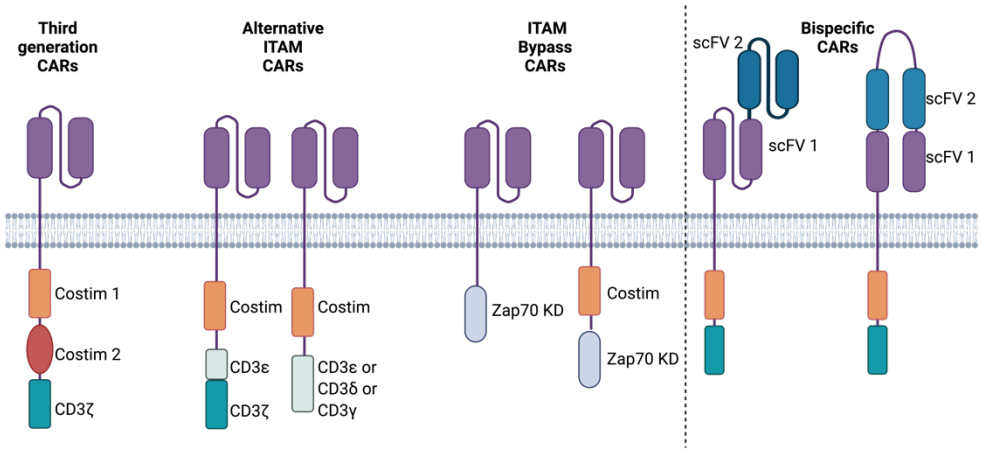

Figure 2.3 CAR architecture to improve sensitivity and specificity CARs designed to improve function over second-generation CARs include the inclusion of multiple costimulatory domain (Third Generation CAR), adding or replacing CD3 subunit domains (Alternative ITAM CARs), and replacing CD3 subunits with down-stream signaling molecules (Bypass CARs). Bispecific CARs have been generated to target multiple tumor antigen in the same receptor.

as CD40 and BAFF-R, as improving CAR T cell function[118]. However, these screens typically use T cell functions, including cytokine production and proliferations, to select domains and have not evaluated antigen sensitivity. While evidence from these studies suggests that some alternative signaling domains may provide additional or distinct functionalities by engaging different signaling networks, these also do not address antigen sensitivity. In summary, inclusion of costimulatory domains has been shown to add functionality to CARs, as seen in the improved functionality from 'first-generation' to 'second-generation' receptors However, altering TCR 'signal two' alone will not fully address the need for improved antigen sensitivity or provide additional antigen recognition. A better first step to improve CARs may be to improve 'signal one' to increase antigen sensitivity and then approach the problem of how to tackle complete antigen loss.

Incorporation of additional or alternative ITAMs

As previously discussed, the typical CAR design utilizes only the CD3ζ ITAMs for signal 1, which may limit the sensitivity and diversity of signaling initiated by the CAR. It has been shown that high ITAM multiplicity reduces the number of receptors required to trigger a TCR T cell response, and that decreasing the ITAMS available to a CAR further reduced CAR T cell response to low antigen-density targets [119]. To increase both ITAM multiplicity and ITAM diversity, a novel CD19 CAR was designed [110], that incorporates a CD3ε motif in addition to the conventional CD3ζ, providing a total of 4 ITAMs (**Figure 2.3**). This receptor showed improved antitumor function in mouse models compared to 28ζ and 4-1BBζ CARs, however receptor sensitivity for antigen recognition was not studied [110]. In another study, individual CD3 ζ,ε,δ or γ domains were paired with a 4-1BB costimulatory domain in a CD19 CAR and screened for both in-vitro function and efficacy in a mouse model. All CD3

subunits were sufficient for activation of downstream signaling after receptor ligation and CD3ε,δ and γ CARs outperformed CD3ζ in-vivo in a Nalm-6 tumor model. CD3δ containing CARs also demonstrated a more 'stem-like' phenotype after multiple antigen stimulations, compared to other CD3 subunit usage. This was attributed to the association of the phosphatase SHP-1 with CD3δ, demonstrating a potential benefit of ITAM diversity beyond signal 'strength' [120]. This study demonstrated the differential efficacy between CD3 domains incorporated into a CAR, but did not directly address sensitivity. Together these CAR designs demonstrate the advantage of diverse CD3 chain usage. However, it is likely that CAR architecture, or the expression of a single molecule, will limit the total number of ITAMS or CD3 domains that can be incorporated into one receptor. Instead, engaging native CD3 subunits will likely be the best way to recapitulate TCR signaling through CD3 subunits.

Bypassing CD3 signaling

An alternative approach to improving CAR proximal signaling is to 'bypass' CD3-mediated signaling by directly engaging downstream signaling molecules (**Figure 2.3**). This type of receptor was first described in 1998 and termed 'scFV-PTK'[121]. These scFV-PTK receptors fused a scFV antigen recognition domain with an intracellular protein kinase domain. A scFV-Syk receptor could produce IL-2 and lyse target cells in co-culture, demonstrating the efficacy of these receptors for signaling T cell effector functions [121, 122]. Years later, similar receptors were designed, including chimeric receptors containing LCK, Fyn, the Zap70 Kinase Domain (Zap70KD), LAT, SLP76, and PLCγ1. Zap70KD and PLCγ1 CARs were capable of activating T cells, and an anti-GD2 Zap70KD receptor outperformed 4-1BBζ CARs in mouse models [123]. Additional 'bypass' receptors have incorporated multiple signaling molecules, fusing multiple steps in the TCR signaling cascade, including a CD19-targeting LAT-Zap70 fusion molecule. However, this receptor showed high levels of tonic signaling. An alternative design fused a downstream signaling molecule with costimulatory domain, providing similar architecture to a second-generation CAR, creating a CD19-directed CAR with a CD28-Zap70KD fusion molecule. This receptor showed improvement in mouse models over 28ζ CARs, and similar effectiveness to 4-1BBζ CARs [124]. While these studies did not directly address antigen sensitivity, bypass receptors demonstrate the further engagement of downstream signaling molecules can improve CAR function.

2.3.2 TCR-based Chimeric Receptors

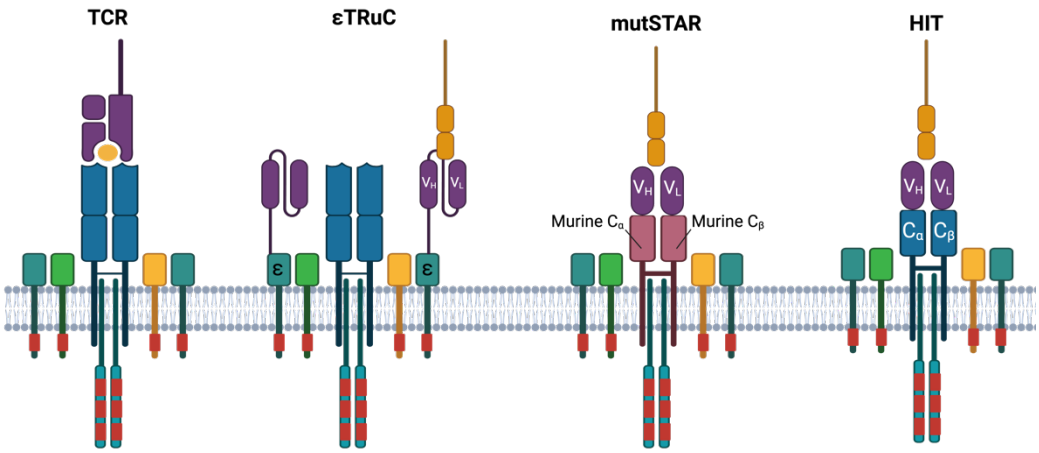

Figure 2.4 Engaging native TCR subunits Multiple receptors designs have been proposed that fuse an antibody recognition domain directly to TCR subunits. This approach permits the assembly a receptor complex containing all CD3 subunits, with the aim to better recapitulate TCR signaling and sensitivity.

The earliest chimeric receptor designs proposed direct engagement of TCR subunits (**Figure 2.1**), however these receptors were not further developed due to difficulties expressing multi-subunit receptors [72, 73]. However, the direct engagement of the native TCR complex has been re-visited, and made more feasible due to use of improved lentivirus vectors that can encode multiple proteins from one vector. These approaches offer the ability to engage all CD3 subunits, and better engage proximal signaling molecules without the needing to directly engineer these proteins into the receptor. Initial studies of these receptors show promise in overcoming CAR signaling deficiencies and improving receptor sensitivity.

Direct fusion of antibody with TCR subunits

The first description of a TCR-scFV fusion molecule was in the context of identifying which TCR subunits are necessary for trigger TCR activation [125]. This receptor design was refined for tumor antigen targeting with the development of T cell Receptor fusion Construct 'TRuC' receptors. Receptors were generated by fusing an scFV-linker with full TCRα chain, TCRβ chain, or each of the CD3 δ,ε, γ subunits. The TCR-chain fusion molecules showed poor expression, however the ε-TRuC expressed well in T cells. Co-immunoprecipitation demonstrated that ε-TRuC associated with all TCR subunits. ε-TRuC outperformed 28ζ and 4-1BBζ CARs in mouse models and had improved in-vitro antigen sensitivity over 28ζ CAR, as measured by cytokine production against low antigen [126, 127]. A phase 1/2 clinical trial of an anti-mesothelin ε-TRuC targeting mesothelin-expressing solid tumors, showed radiological tumor regression in 93% of patients treated with an overall disease control rate of 77%. These finding demonstrate the safety and feasibility of this approach, and a phase 2 trail is ongoing [128].

STAR and HIT receptors

Advances in gene delivery have made chimeric receptors that directly fuse antibody chains to TCR constant chains feasible. These chimeric receptors have been reported by multiple groups and have showed improved sensitivity over standards second-generation CARs. While gene delivery was a major hurdle to prevent their implementation, another difficulty for these receptors is the potential for mispairing between the introduced synthetic receptor and the native TCR. Two groups have proposed methods to minimize this mispairing allowing for intact synthetic receptor expression. A Synthetic TCR Antigen Receptor "STAR" was designed, replicating the design from Dr. Kurosawa's group in the 1980's, fusing antibody variable heavy and light chains directly to the constant regions of the α/β TCR. To prevent mispairing with endogenous TCR chains, a "mutSTAR" was introduced, that utilized mouse TCR chains, which would preferentially pair with each other rather than the endogenous TCR chains (**Figure 2.4**) [129]. An alternative approach to prevent mispairing was proposed with the HLA-independent T cell Receptor "HIT." This receptor used the same general format as the STAR, directly fusing antibody variable chains to the TCR α and β chains. The HIT receptor used human chains, and attempted to prevent mispairing by knocking-in the receptor chains to the TCR α chain (TRAC) locus using CRISPR-Cas9 gene editing [130]. HIT expressing T cells showed improved sensitivity over second-generation CAR T cells for targeting CD19, CD70 and BCMA and mutSTAR expressing T cells showed improved sensitivity in targeting EGFR, EGFRvIII, GPC3 and CD19 [131]. HIT and mutSTAR receptors showed similar antitumor efficacy in-vivo, with improvement over second-generation CARs in some models, and similar function to CARs in others. HIT receptors showed improved efficacy over 28ζ CAR in antigen-low tumor mouse model. For both the HIT and the mutSTAR, engineering co-stimulation into the receptor was required for the most optimal function and largest improvement over second-generation CARs [129, 130]. This demonstrates one potential limitation of this receptor class. These receptors may provide better engagement of the TCR signaling apparatus for signal 1 but face the same challenges of 'first-generation' CARs where co-stimulation is necessary for optimal function. A second limitation is that the mutSTAR and HIT receptors are monospecific and could not target tumors that have lost expression of the antigen. However, these receptors do demonstrate that direct engagement of the TCR complex is a feasible approach to improving engineered T cell sensitivity, addressing one of the major limitations of CAR T cell therapies.

2.3.3 Overcoming antigen loss: Bi-specific CARs

CARs that target multiple tumor antigens have been designed to reduce the ability of the tumor to escape by losing expression of a single antigen. These receptors are engineered to

respond to two targets independently, creating a receptor that can respond when either antigen is present. This would allow for continued efficacy of the receptor if the expression of one antigen is lost. Bispecific CARs have been designed and brought to clinical trials for multiple antigen pairs including CD19/CD22 for leukemia and lymphoma [132-134], CD19/CD20 for lymphoma [135, 136], and BCMA/CD38 or BCMA/CD19 for multiple myeloma [137, 138]. Though this is a promising approach, effective use of bispecific receptors has faced many hurdles, including the same barrier to efficacy that monospecific CARs have, poor antigen sensitivity. Bispecific CAR T cells are constructed by including two scFVs into the CAR molecule or by expressing two scFvs in the same T cell. scFVs can be added in tandem, sequentially linking two scFVS, or can be generated using a 'loop' architecture, generating a single chain 'loops' back on itself to match scFV pairs (**Figure 2.3**). These designs allow for the delivery of a single molecule capable or targeting two antigens. However, there is evidence that the fusion of two scFVs may limit the function of the receptor compared to monospecific receptors for either antigen. Studies have found compromise receptor expression, antigen binding and down-stream signaling in the bispecific receptors compared to monospecific CARs [139]. Further evidence of loss of function against individual antigen targeting can been seen in clinical trials of some bi-specific CARs. Patients treated with a bispecific CD19/CD22 'Loop CAR', had tumors that were still CD22 positive at relapse, with similar expression levels seen prior to treatment [132]. This contrasts with clinical data from monospecific CD22 CARs, where patients that relapsed with CD22 positive tumors had lower CD22 expression, suggesting some selective pressure from the effective targeting of the CAR to CD22 tumor [99]. Head-to-head comparison of the bispecific CAR and the CD22 monospecific CAR in-vitro showed less cytokine production in bispecific CAR T cells compared to cells expressing the monospecific receptor, confirming the bispecific was not effectively targeting CD22 [132].

The reduced efficacy of the bispecific CAR compared to the monospecific receptor may be due to the fusion of to scFVs. Other approaches to dual-targeting therapies is the expression of two CARs in the same cells, 'bicistronic' CARs, or treatment with two separate CAR products. Bicistronic CARs also show limited efficacy compared to monospecific CARs, likely due to lower receptor expressions levels because of the large viral construct required to deliver both CARs into the T cells, and due to competition between the two receptors for downstream signaling molecules such as LCK and Zap70 [139]. Co-infusion or sequential infusion of two different CAR T cell products is an alternative approach to two-antigen targeting. While trials have indicated early success with this approach [140], the production two CAR T cell products adds complexity and expense. Additionally, preferential expansion of one product over the other may led to the dominance of one cell product, preventing lasting bispecific targeting. Ultimately each of

the proposed CAR-based methods of dual-antigen targeting are vulnerable to low antigen escapes, as seen in monospecific CARs. There is a need for a receptor that is capable of bispecific targeting with high antigen sensitivity.

Chapter 3: Sensitive bispecific chimeric T cell receptors for cancer therapy

Contents of this chapter have been submitted and accepted for publication

Sylvain Simon[†], Grace Bugos[†,] Rachel Prins, Anusha Rajan, Arulmozhi Palani, Kersten Heyer, Andrew Stevens, Longhui Zeng, Kirsten Thompson, Pinar A. Atilla, Jason P. Price, Mitchell G. Kluesner, Carla Jaeger-Ruckstuhl, Tamer B. Shabaneh, James M. Olson, Xiaolei Su, Stanley R. Riddell[*], Sensitive bispecific chimeric T cell receptors for cancer therapy, *Nature Cancer, In Press*

Abstract

The adoptive transfer of T cells expressing synthetic chimeric antigen receptors (CARs) is effective in many patients with B cell malignancies. However, the persistence of cancer cells that evade detection due to low levels or complete absence of the target antigen frequently leads to tumor recurrence, highlighting the need for immune receptors with enhanced sensitivity and multispecificity. We introduce a novel synthetic chimeric T cell receptor (ChTCR) that is highly expressed in primary T cells, confers superior antigen sensitivity compared to previous hybrid TCR designs, and is readily adapted for sensitive bispecific targeting. ChTCRs replicate the structure of natural TCRs, form classical immune synapses and demonstrate potent TCR-like signaling. T cells expressing bispecific-ChTCR (Bi-ChTCRs) are more effective than bispecific CAR T cells in eradicating tumors with heterogeneous antigen expression in vivo. The Bi-ChTCR architecture is resilient and can be designed to target different B cell and multiple myeloma antigens. These findings provide a widely applicable strategy to combat tumor heterogeneity and prevent relapse seen with current CAR therapies

Introduction

Adoptive immunotherapy with T cells expressing a chimeric antigen receptor (CAR T) specific for B-cell lineage antigens induces rapid regression of relapsed or refractory lymphoma, acute leukemia and multiple myeloma [83, 89, 91, 141-143]. Despite high response rates, many patients relapse after CAR T treatment due to outgrowth of tumor cells that have low levels or complete loss of the target antigen [83, 89, 91, 97, 98, 132, 142, 143]. Genomic analysis of tumors identified preexisting or emergent clones that evade CAR T cells because of bi-allelic loss of the gene encoding the target antigen, point mutations in the epitope, or downregulation of antigen expression due to epigenetic silencing [96, 144]. These findings illustrate the need for T cell therapies that provide highly sensitive and multispecific antigen recognition.

CAR design was inspired by the understanding that two signals mediated by the T cell receptor (TCR) and a costimulatory molecule were required for full T cell activation[21]. Each TCR assembles with CD3d, CD3e, CD3g, and CD3z homo- or heterodimers providing 10 immune-receptor-tyrosine-based-activation-motifs (ITAMs) for modification [110, 145]. The first CAR design fused a single chain variable fragment (scFv) of a monoclonal antibody to the CD3z subunit, which has only three ITAMs [74]. Costimulation was added by incorporating one or more costimulatory domains into the receptor architecture[78, 80, 114, 146]. Differences between CARs and TCRs are evident by comparison of signaling after engaging antigen. CAR T cells exhibit reduced phosphorylation of ZAP-70 and LAT compared to a TCR [42, 111, 147], which may contribute to their reduced antigen sensitivity

[42, 148-150]. To improve sensitivity, receptors that better engage the TCR apparatus have been designed [126, 129, 130, 151]. The HLA independent T cell receptor (HIT) and the synthetic T cell and antigen receptor (STAR) fuse the VH and VL chains of an antibody to TCR constant alpha (TRAC) and beta (TRBC) chains respectively[129, 130]. To reduce mispairing with endogenous TCR chains, the HIT receptor transgene was inserted into the TRAC locus, and the STAR receptor fused VH and VL chains with murine TCR constant chains that contained an interchain disulfide bond to promote pairing (mutSTAR)[129, 130]. T cells expressing HIT and mutSTAR receptors were more sensitive for a single antigen than conventional CARs but these approaches do not eliminate mispairing and competition for assembly with CD3 chains, and would not prevent outgrowth of antigen negative tumors.

We sought to develop a chimeric T cell receptor (ChTCR) that could target two antigens with high sensitivity. We first constructed a monospecific receptor termed the "full ChTCR" where the scFv, rather than a VH or VL fragment, is fused to the TRAC chain while the TRBC chain is left void of an antigen binding domain. Base editing was used concurrent with ChTCR gene transfer to eliminate expression of endogenous TRAC and TRBC, preventing mispairing with the ChTCR. T cells expressing the full ChTCR recognized lower levels of antigen than T cells expressing CD28/z or 4-1BB/z CARs and were also superior to mutSTAR and HIT receptors. The full ChTCR format enabled bispecific antigen targeting by linking a second scFv specific for a different tumor antigen to the TRBC chain. Bispecific ChTCRs (Bi-ChTCRs) were more effective in eliminating heterogeneous and antigen low leukemia and multiple myeloma cells in vitro and in vivo, compared to monospecific ChTCRs and bispecific CARs. This new Bi-ChTCR design can be broadly applied for sensitive targeting of multiple pairs of antigens on B cell malignancies and multiple myeloma and holds promise for clinical translation.

Results

Chimeric TCRs recapitulate TCR structure, synapse formation and signaling

We designed two variations of CD19-specific ChTCRs, a "split" format in which VH and VL fragments of the CD19-specific antibody (FMC63) were fused to TRAC and TRBC chains of the TCR respectively[130], and a "full" ChTCR format where the scFv (V_L-linker-V_H) was fused to TRAC while TRBC was co-expressed but left void of a ligand binding domain (**Fig. 3.1a and Extended Data Fig 3.1a**). For comparison, we utilized clinically approved CD19-specific CD28/CD3z[143] and 4-1BB/CD3z CARs [142] (**Fig. 3.1a and Extended Data Fig 3.1a**).

Split and full CD19 specific ChTCRs and CARs were expressed in $CD8^+$ T cells by lentiviral delivery. We used cytosine base editors (CBE) to knockout endogenous TCRab expression

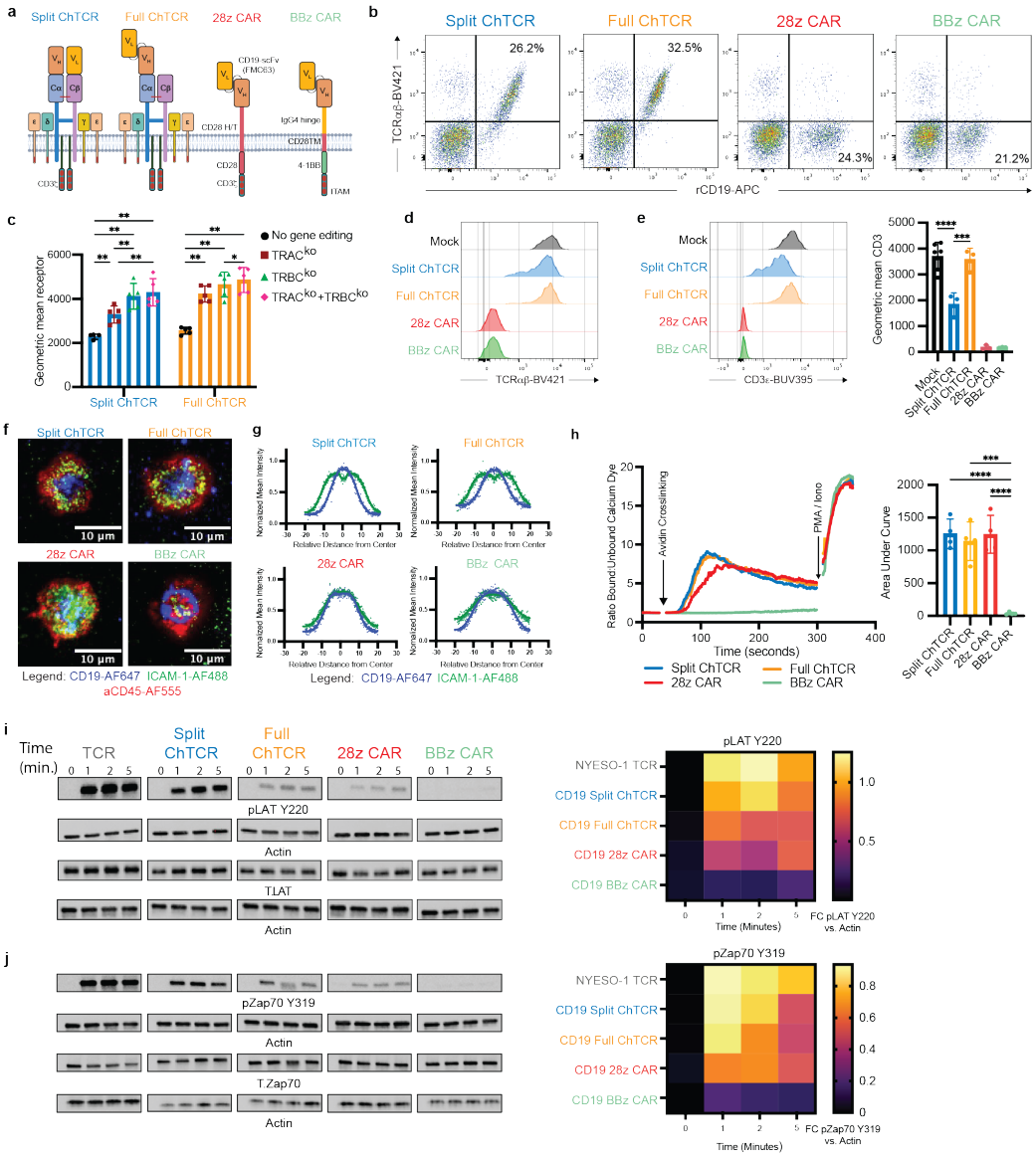

Figure 2.1 Chimeric TCRs expressed in T cells reproduce canonical TCR structure, synapse formation and proximal signaling a. Schematic of CD19-specific ChTCRs and CARs: Left to right - Split ChTCR V_HC_α: FMC63 variable heavy chain-TCR alpha constant chain, V_LC_β: FMC63 variable light chain-TCR beta constant chain; Full ChTCR: FMC63V_LV_H-C_α:C_β TCR. Both ChTCRs are shown in association with endogenous CD3εδ, CD3ζζ and CD3γε subunits. CD28z CAR with FMC63 V_LV_H scFv linked to CD28 hinge/transmembrane and co-stimulatory domain, and CD3ζ; BBz CAR with FMC63 V_LV_H scFv linked to IgG4 hinge, CD28 transmembrane domain, 4-1BB co-stimulatory domain and CD3ζ. **b.** Representative flow plots of primary CD8 T cells stained with anti-TCRab antibody and recombinant CD19 protein after lentiviral transduction and base editing to knock-out endogenous TCRab expression. **c.** Geometric mean of rCD19-APC binding to primary T cells transduced with Split or Full ChTCRs with and without base editing of TCRa, TCRb or both TCRab chains (n=5 biological independent samples). *P<0.05, **P< 0.01 using two-way ANOVA. **d.** Representative TCRab expression by mock unedited and TCRab gene edited ChTCR$^+$ and CAR$^+$ T cells. **e.** Left: Representative CD3e expression by mock unedited and TCRab gene edited ChTCR$^+$ and CAR$^+$ T cells. Right: geometric mean ± SD of CD3e-BUV395 fluorescence (n=4 independent donors). *** P< 0.001, **** P< 0.0001 by two-way ANOVA. **f.** Left: Representative TIRF microscopy images of ChTCR$^+$ and CAR$^+$ T cells interacting with a soluble lipid bilayer functionalized with ICAM-1 extracellular domain (green), CD19 extracellular domain (blue) and stained with an anti-CD45-AF555 antibody. Scale bars = 10μm. **g.** Normalized mean intensity of ICAM-1-AF488 (green) and CD19-AF647 (blue) staining across cell radiuses in synapses; dots represent mean at each position with solid trend line, n=100 cells. **h.** Left: Representative calcium flux measured

after antigen crosslinking of T cells expressing each of the specified receptors. The y-axis shows the ratio of calcium bound to unbound Indo-1 dye over time on the x-axis. Arrows indicate crosslinking of receptors and addition of PMA/ionomycin**.** Right: Area under the curve of calcium flux measurements over 300 seconds after antigen cross-linking, (n=4 independent experiments). *** P< 0.001, **** P< 0.0001 by two-way ANOVA. **i.** Left: Representative western blot of LAT $pTyr^{220}$, Actin and LAT after antigen activation of T cells expressing each of the indicated receptors. Right: heat map of mean band intensity of LAT $pTyr^{220}$ normalized to actin loading control (n=3 independent experiments). **j.** Left Representative Western Blot analysis of Zap70 $pTyr^{319}$, Actin and Zap70 after antigen activation of T cells expressing each of the indicated receptors. Right: Heat map of mean band intensity of Zap70 $pTyr^{319}$ normalized to actin loading control (n=3 independent experiments).

to prevent mispairing of the ChTCR with endogenous TCR chains and competition for CD3 subunits (**Extended Data Fig. 3.1b**). TCR^{ko} efficiency was greater than 90% and improved the expression level and frequency of split and full $ChTCR^{+}$ T cells compared to no knockout and single $TRAC^{ko}$ or $TRBC^{ko}$ T cells **(Fig. 3.1b-c and Extended Data Fig. 3.1c-d)**. ChTCRab chains and CD3e subunits were expressed at the cell surface demonstrating association of ChTCRs with endogenous CD3e **(Fig. 3.1d-e)**. CD3e expression was significantly higher on full $ChTCR^{+}$ T cells than on split $ChTCR^{+}$ T cells and was comparable to unedited T cells, suggesting the full format more efficiently assembled with CD3 chains and trafficked to the cell surface **(Fig. 3.1e)**. Confirmation that ChTCRs associated with all CD3 subunits was shown by tagging receptors with HA, immunoprecipitation with anti-HA, and immunoblotting for individual CD3 subunits **(Extended Data Fig. 3.2)**.

T cells form a well-organized synapse with cognate peptide/MHC (p/MHC) that amplifies and regulates signaling[34, 152]. TCRs are concentrated in a central supramolecular complex (cSMAC) with adhesion molecules such as LFA-1, a ligand for ICAM-1, at the periphery of the synapse (pSMAC), and the CD45 phosphatase excluded to the distal SMAC. We examined immune synapses formed between ChTCR or CAR expressing T cells and soluble lipid bilayers containing fluorescently labeled CD19 and ICAM-1 using TIRF microscopy. The synapses of CD28/z and 4-1BB/z CD19 CAR T cells were disorganized with CD19 and ICAM-1 intertwined across the synapse, as previously described[112]**.** In contrast ChTCR T cells formed an organized cSMAC containing CD19 surrounded by a peripheral ring of ICAM-1, similar to that described for a TCR **(Fig. 3.1f and 3.1g)**.

Many CARs tonically signal without binding antigen, which can drive T cell exhaustion, limit persistence *in vivo,* and increase toxicities[68, 153]. To evaluate tonic signaling, we transduced Jurkat reporter cells with split and full CD19 ChTCRs, 28/z and 4-1BB/z CARs, and an NY-ESO-1-specific TCR. A low frequency of cells expressing the TCR, 4-1BBz CAR or either of the ChTCRs showed NFAT and NFkB activation, whereas a high frequency of cells expressing the 28z CAR activated NFAT and NFkB in the absence of antigen **(Extended Data Fig. 3.3a-c)**. After binding antigen, intracellular signaling by CARs is distinct from that mediated by TCR recognition of p/MHC[42, 111]. We evaluated intracellular signaling in primary T cells expressing CD19-specific ChTCRs and CARs, first by measuring calcium influx after crosslinking receptors with CD19 antigen. Split and full ChTCRs and the 28z CAR fluxed calcium with similar magnitudes, whereas calcium influx was barely detectable

in T cells expressing the 4-1BBz CAR **(Fig 3.1h)**. We then compared phosphorylation of LAT and Zap70 after antigen activation of CAR, ChTCR, or TCR expressing T cells. T cells expressing the split and full ChTCRs exhibited rapid phosphorylation of LAT Y220 and Y171 and Zap70 Y319 at one-minute, matching the kinetics of the NY-ESO-1 TCR **(Fig 3.1i, j and Extended Data Fig. 3.3d)**. In contrast, T cells expressing CARs showed less intense and a later peak in LAT and Zap70 phosphorylation. Thus, both ChTCR formats assemble with all CD3 chains, form TCR-like synapses, lack tonic signaling, and induce rapid antigen-specific signaling.

The CD19 full ChTCR has superior antigen sensitivity and anti-tumor efficacy

To determine antigen sensitivity, we flow-sorted $CD8^+$ T cells for split and full ChTCR, CD28z CAR, and 4-1BBz CAR expression and tested recognition of Nalm-6 cells expressing high, medium, and low levels of CD19 (23999, 2619 and 230 molecules respectively) **(Fig 3.2a)**. When co-cultured with $CD19^{High}$ tumor, CD28z CAR T cells produced more IL-2 and IFNg compared to 4-1BBz CAR and ChTCR T cells **(Fig 3.2b and 3.2c)**. However, when co-cultured with tumor cells expressing medium or low levels of CD19 antigen, T cells expressing split and full ChTCRs produced markedly higher levels of IL-2 and IFN-g than 4-1BBz and CD28z CAR T cells. Strikingly, T cells expressing the full ChTCR produced higher levels of IL-2 and INF-g than T cells expressing the split ChTCR **(Fig 3.2b and 3.2c)**. Consistent with the cytokine data ChTCR T cells proliferated more than CAR T cells when co-cultured with $CD19^{Mid}$ and $CD19^{Low}$ Nalm-6 cells, and full ChTCR T cells proliferated more than split ChTCR T cells in response to $CD19^{Low}$ tumor **(Fig 3.2d)**. The expression and function of each of the CD19-specific ChTCRs and CARs was also studied in CD4+ T cells. $CD4^+$ T cells transduced with the full ChTCR expressed higher levels of the chTCR and CD3e compared to those expressing the split ChTCR (**Extended Data Figure 3.4a-c**), and produced more IL-2 and IFN-g in response to $CD19^{Low}$ tumor cells compared to split ChTCR T cells and 28z and 4-1BBz CAR T cells (**Extended Data Figure 3.4e-f)**. Consistent with superior recognition of $CD19^{Low}$ tumor cells, T cells expressing the full ChTCR exhibited more robust LAT phosphorylation compared to CAR+ and split ChTCR+ T cells following co-culture with Nalm-6 $CD19^{Low}$ cells (**Fig 3.2e**). Thus, ChTCRs conferred improved recognition of $CD19^{Low}$ tumor cells by CD8+ and CD4+ T cells compared to CARs, and the full ChTCR was superior to the split ChTCR.

To compare the in vivo antitumor activity of T cells expressing ChTCRs and CARs, cohorts of NSG mice were engrafted with Raji lymphoma and treated with each of the transduced T cells **(Fig 3.2f)**. T cells expressing the full ChTCR quickly eradicated tumor cells in all treated mice and improved survival compared to mice treated with split ChTCR, CD28z or 4-1BBz CAR T cells **(Fig 3.2g-i).** We then tested $ChTCR^+$ T cells for antigen sensitivity *in vivo* by treating NSG mice engrafted with Nalm-6^{Low} cells that lack expression of CD80 and

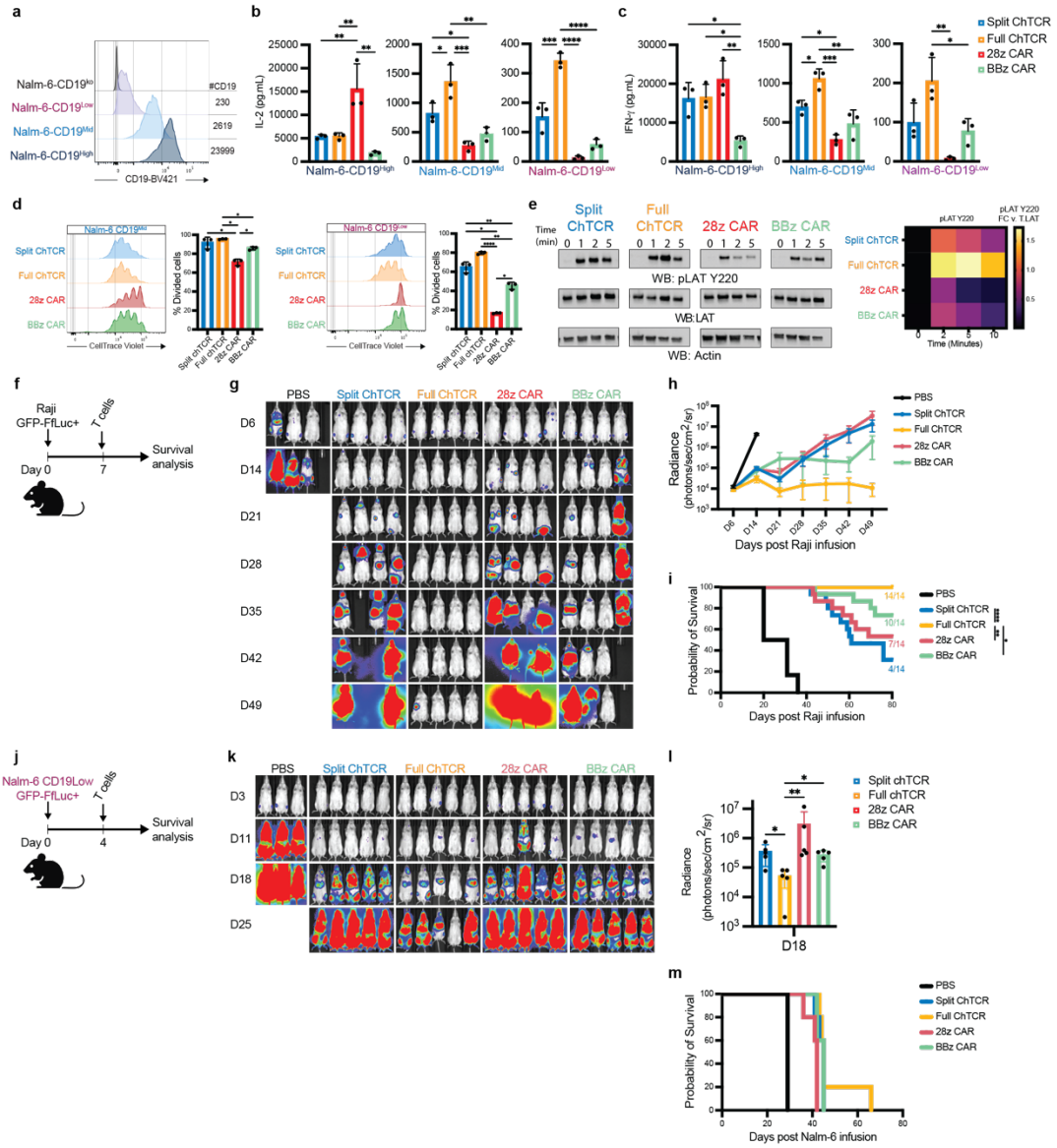

Figure 3.2 T cells expressing the CD19-specific Full ChTCR recognize CD19 low tumor cells and have superior anti-tumor effect in vivo a. Flow histograms of CD19 expression in Nalm-6 cells with varying levels of CD19. **b.** Concentration of IL-2 in culture supernatant after overnight co-culture of T cells expressing each of the indicated receptors with Nalm-6 CD19^{High}, CD19^{Mid}, and CD19^{Low} cells at an effector to target ratio (E:T) of 1:1. Data is shown as the mean ± SD for 3 independent experiments. *P<0.05, **P<0.01, ***P<0.001, ****P<0.0001 by two-way ANOVA **c.** Concentration of IFN-γ in culture supernatant for each experimental group described in **1b**. Data is shown as the mean +/SD for 3 independent experiments. *P<0.05, **P<0.01, ***P<0.001 by two-way ANOVA. **d.** Left: Representative histograms of CellTrace Violet (CTV) dye dilution in T cells expressing the indicated receptors measured after 3 days of co-culture with Nalm-6 CD19^{Mid} and Nalm-6 CD19^{Low} tumor cells. Right: Percent of divided cells (mean ± SD) for 3 independent experiments, *P<0.05, **P<0.01, ****P<0.0001 by two-way ANOVA. **e.** Left: Representative western blot of LAT pTyr^{220}, Actin and LAT after co-culture of CD8 T cells expressing each of the indicated receptors with Nalm-6 CD19^{Low} tumor cells. Right: heat map of mean band intensity of LAT pTyr^{220} normalized to total LAT control (n=3 independent experiments). **f.** Schematic of the Raji GFP-ffluc^{+} NSG mouse model. **g.** Representative bioluminescence images of Raji-ffluc tumor burden in NSG mice treated with 2x10^{6} T cells expressing each of the indicated receptors. **h.** Tumor burden (mean ± SD radiance (photons/sec/cm^{2}/steradian) of Raji GFP-ffluc^{+} bearing NSG mice treated as described in **f**. (n=4 or 5 mice per group; 3 independent experiments). **i.** Kaplan-Meier survival of Raji GFP-ffluc^{+}-bearing NSG mice treated as described in **f** (n=14 mice per treatment group). *P <0.05, **P<0.01, ***P<0.001. **j.** Schematic of the Nalm-6 CD19^{Low} GFP-ffluc^{+} NSG mouse model. **k.** Representative bioluminescence images of NSG mice inoculated with Nalm-6 CD19^{Low} GFP-ffluc^{+} tumor cells

and treated with $2x10^6$ T cells expressing the indicated receptors (n=5 mice per group). **l.** Tumor burden (mean ± SD radiance (photons/sec/cm^2/steradian)) of Nalm-6 $CD19^{Low}$ GFP-ffluc$^+$-bearing NSG mice 18 days after treatment with T cells expressing the indicated receptors (n=5 mice per group). *P <0.05, **P<0.01 by non-parametric Kruskal Wallis test. **m**. Kaplan-Meier survival of Nalm-6 $CD19^{Low}$ GFP-ffluc$^+$-bearing NSG mice treated as described in **j** (n=5 mice per treatment group).

CD86 co-stimulatory ligands expressed by Raji cells. Even with a low dose of T cells and the absence of any $CD19^{High}$ tumor cells to drive T cell proliferation in vivo, T cells expressing the full ChTCR exhibited superior antitumor activity early after infusion compared to T cells expressing the split ChTCR, or CD28z or 4-1BBz CARs, although the anti-tumor activity was transient and did not translate into improved survival over other treatment groups **(Fig 3.2j-m)**. These data show that CD19 ChTCRs were more sensitive for recognizing antigen low tumor cells compared to conventional CARs and that the full ChTCR is the most effective receptor *in vitro* and *in vivo*.

Endogenous TCR^{ko} maximizes expression and function of HLA-independent chimeric TCRs

We evaluated how expression and function of the full and split ChTCRs compared to previously described mutSTAR and HIT receptors, which share a similar architecture to the split ChTCR. Unlike our approach, the strategies for expressing the HIT and mutSTAR in T cells did not eliminate expression of both endogenous TCR chains. The mutSTAR used murine TRAC and TRBC chains to facilitate preferential pairing of the transgenic TCR and the HIT receptor was introduced by targeted knock-in to the TRAC locus, thereby eliminating one of the two endogenous TCR chains. We constructed a CD19-specific mutSTAR composed of murine TCR chains fused to the VL and VH domains of FMC63[129, 131] (**Extended Data Fig. 3.5a-b**) and expressed the mutSTAR, split and full ChTCRs using lentiviral delivery in primary T cells, either without TCR^{ko} as originally described[129, 131], with $TRAC^{ko}$ or $TRBC^{ko}$ only, or with KO of both TCR chains. As observed previously, expression of full and split ChTCRs was higher in T cells with KO of both TCR chains (**Extended Data Fig. 3.5c-e**). The mutSTAR was expressed at the cell surface in T cells without TCR^{ko} consistent with prior data[129, 131] (**Extended Data Fig. 3.5c-d).** However, the level of mutSTAR expression determined by staining of the murine TRBC chain and binding to recombinant CD19 protein was significantly higher with KO of both endogenous TCR chains to eliminate competition for assembly with CD3 subunits (**Extended Data Fig. 3.5e-g**). MutSTAR TCR^{ko} T cells expressed similar levels of CD3e at their surface as split ChTCR T cells but both were expressed at lower levels than the full ChTCR (**Extended Data Fig. 3.5h**). Higher expression of mutSTAR achieved with $TCRab^{ko}$ resulted in superior antigen sensitivity in response to $CD19^{Low}$ tumor cells compared to the non-TCR^{ko} T cells, although sensitivity was still inferior to $TCRab^{ko}$ cells expressing the full ChTCR (**Extended Data Fig. 3.5i-j).** We then expressed the HIT receptor using a CRISPR-Cas9-mediated

targeted insertion within the TRAC locus, with or without concomitant TRBC^{ko} (**Extended Data Fig. 3.6a-b**). The frequency of HIT+ T cells and the expression level of the HIT receptor were increased when targeted integration was combined with TRBC^{ko} (**Extended Data Fig. 3.6b-d**). HIT TCR^{ko} T cells showed lower TCRab and CD3e levels than both split and full ChTCR T cells (**Extended Data Fig. 3.6e-g**), suggesting that receptor expression with targeted knock-in to the TCRa locus is inferior to that achieved by lentiviral delivery, although we cannot exclude potential effects of a different scFv. Higher expression of HIT receptors achieved with TCRab^{ko} resulted in superior antigen sensitivity in response to CD19^{Low} tumor cells compared to the non-TCR^{ko} T cells (**Extended Data Fig. 3.6h-j)**, although sensitivity was still inferior to TCRab^{ko} cells expressing the full ChTCR constructed with FMC63 (**Extended Data Fig. 3.6k,l).** These data demonstrate the importance of editing both endogenous TCR chains to avoid competition for CD3 subunits and TCR chain mispairing and achieve high level expression of HLA independent chimeric T cell receptors.

Design of a sensitive CD22 monospecific ChTCR

The unoccupied TRBC chain in the CD19 specific full ChTCR could allow targeting of a second antigen by fusing a scFv of different specificity to TRBC. Bispecific targeting of CD19 and CD22 is of clinical interest because CD19 and CD22 negative or low relapses occur after monospecific therapies targeting these antigens[99, 132]. Unfortunately, a CD19/CD22 bispecific CAR, termed the “Loop” CAR, demonstrated compromised sensitivity to each antigen compared to the respective monospecific CARs, and patients treated with the Loop CAR relapsed with CD19$^{Low/Neg}$ CD22^{+} tumor[132]. We sought to determine if the ChTCR platform could provide a more effective bispecific CD19/CD22 receptor.

We first evaluated monospecific ChTCRs by fusing the m971scFv, which is used in the Loop CAR and targets a membrane proximal epitope, or the 9A8 scFv, which targets a more membrane distal epitope, to TRBC **(Fig 3.3a)**[154]. ChTCRs were constructed in both V_HV_L and V_LV_H orientations, expressed in TRBC and TRAC edited T cells, and compared to conventional 4-1BBz CARs constructed with the same scFvs **(Fig 3.3a)**. T cells expressing all constructs bound soluble recombinant CD22, with the m971 CAR and ChTCR showing a higher MFI of CD22 binding than observed with 9A8 **(Fig 3.3b, c)**. However, when T cells were co-cultured with WT Nalm-6 cells, m971 ChTCR^{+} T cells produced less IL-2 and INF-□ and proliferated poorly compared to T cells expressing the 9A8 ChTCR **(Fig 3.3d-f; Extended Data Fig. 3.7a)**. CAR T cells constructed with each scFv were functional in these assays, with m971 CAR T cells producing higher cytokine levels and proliferating better

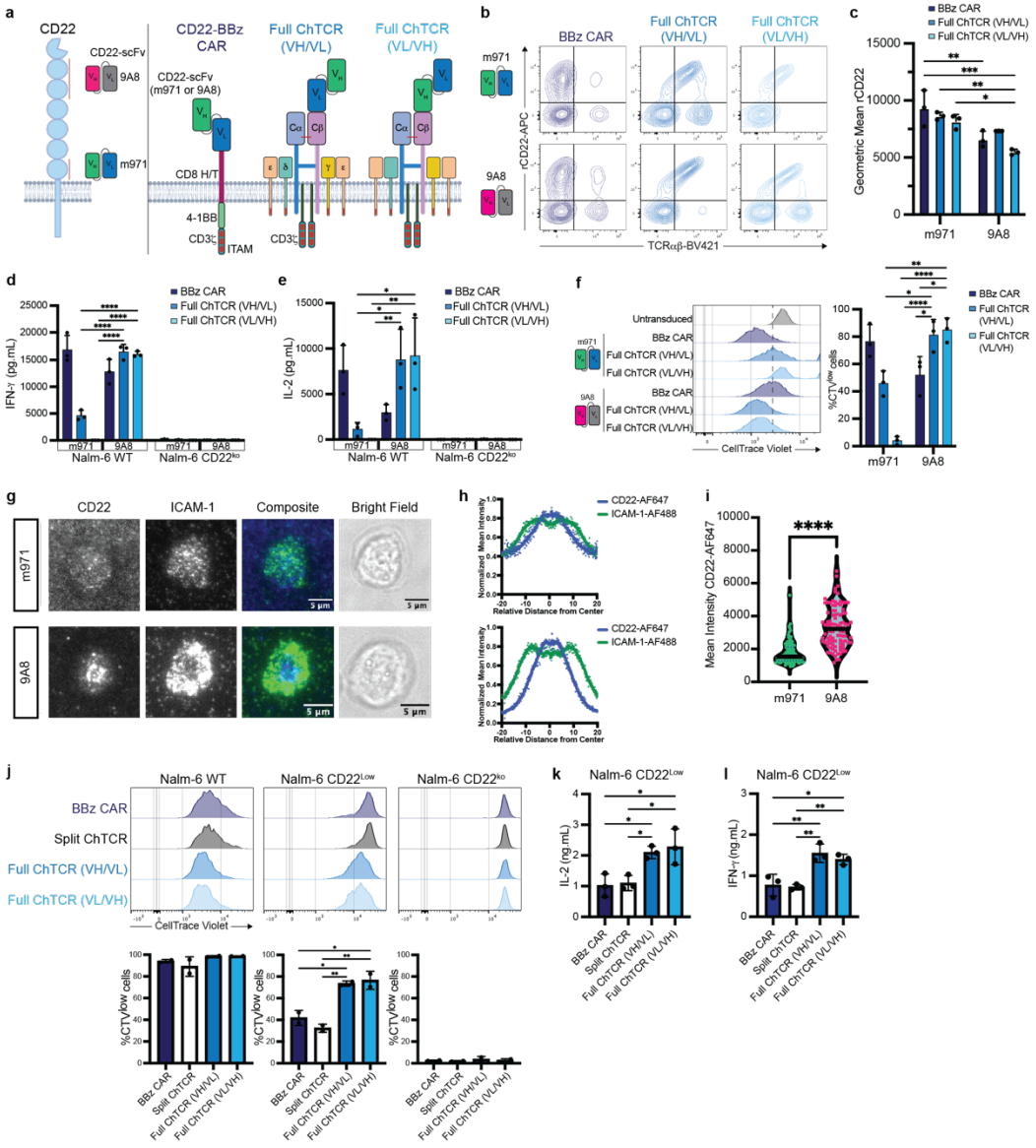

Figure 3.3 Design of a sensitive CD22-specific Full ChTCR a. Left: Schematic of the CD22 molecule with locations of epitopes recognized by m971 and 9A8 scFvs. Right: Structure of CD22-specific receptors: CD22-BBz CAR: anti-CD22 scFV V_H-V_L (m971 or 9A8), CD8 hinge and transmembrane domain, 4-1BB co-stimulatory domain, and CD3ζ domain; CD22 Full ChTCRs: m971 or 9A8 in VH/VL or VL/VH orientations linked to TRBC and shown associated with endogenous CD3 subunits. **b.** Representative flow plots of primary CD8 T cells stained with anti-TCRab and recombinant CD22 protein after lentiviral transduction and base editing to knock-out TCRab. Top row: T cells expressing CAR and ChTCRs constructed with the m971 scFV; Bottom row: T cells expressing CAR and ChTCRs constructed with the 9A8 scFv. **c.** Geometric mean ±SD of recombinant CD22-APC binding to CAR and ChTCR T cells constructed with either m971 or 9A8 scFv. Data is shown for T cells from 3 independent donors. *P< 0.05, **P< 0.01, ***P< 0.001 by two-way ANOVA. **d and e:** Concentration of IFN-γ (d) and IL-2 (e) in culture supernatant after overnight co-culture of T cells expressing each of the indicated receptors with Nalm-6^{WT} or CD22^{ko} cells. Data is shown as the mean ±SD for T cells from 3 independent healthy donors. *P< 0.05, **P< 0.01, ****P< 0.0001 by two-way ANOVA. **f.** Left: Representative histograms of CellTrace Violet (CTV) dilution measured after 72h co-cultures of T cells expressing each of the indicated receptors with Nalm-6 cells. Right: Frequency of divided cells. Data is shown as the mean ± SD for 3 independent healthy donors. *P< 0.05, **P< 0.01, ****P< 0.0001 by two-way ANOVA. **g.** Representative TIRF microscopy images of CD22 ChTCR T cells constructed with the m971 scFv (top) or 9A8 scFv (bottom) interacting with a soluble lipid bilayer functionalized with ICAM-1 extracellular domain (green) and CD22 extracellular domain (blue), or brightfield. Scale bars = 5µm. **h.** Normalized mean intensity of

ICAM-1-AF488 and CD22-AF647 staining across cell radiuses in synapses; dots represent mean at each position, with trend line (n=100 cells). **i.** Mean intensity of CD22-AF647 within the synapse of 100 T cells expressing ChTCRs constructed with the m971 scFv or 9A8 scFv. **** P<0.0001 by two-tailed t-test. **j.** Top: Representative flow histograms of CellTrace Violet (CTV) dilution measured after 72h co-culture of T cells expressing the indicated receptors with Nalm-6 cells expressing different levels of CD22 or CD22 knockout. Bottom: Frequency of divided cells in each group. Data is shown as the mean ± SD for 3 independent healthy donors. *P< 0.05, **P< 0.01, ****P< 0.0001 by two-way ANOVA. **k and l.** Concentration of IL-2 (k) and IFN-γ (l) in culture supernatant after overnight co-culture with Nalm-6 $CD22^{Low}$ cells. Data is shown as the mean ± SD for 3 independent experiments. *P<0.05 and **P< 0.01 by 2-way ANOVA test.

than 9A8 CAR T cells **(Fig 3.3d-f)**. A ChTCR in which the m971 scFv was fused in VL/VH or VH/VL orientations to the TRAC chain also bound soluble CD22 but did not function against $CD22^{+}$ tumor cells (**Extended Data Fig. 3.7b-f**). The discrepancy between binding of soluble CD22 by m971 and 9A8 ChTCRs and function in response to tumor suggested that the m971 epitope on membrane bound CD22 is less accessible to a ChTCR. This was supported by analysis of synapses formed by CD22-specific ChTCR T cells. T cells expressing the 9A8 ChTCR formed a synapse with CD22 localizing to the center surrounded by ICAM-1 whereas T cells expressing the m971 ChTCR showed minimal CD22 accumulation in the synapse (**Fig 3.3g-i)**.

We next compared antigen binding and sensitivity of T cells expressing the 9A8 ChTCRs to a 9A8 4-1BBz CAR (**Extended Data Fig. 3.8a).** CD22 binding to T cells expressing the full ChTCR (V_HV_L and V_LV_H) and 4-1BBz CARs was similar and higher than T cells expressing the split ChTCR (**Extended Data Fig. 3.8b, c).** T cells expressing the full ChTCR also showed higher TCRab expression than T cells expressing the split ChTCR (**Extended Data Fig. 3.8d**). To evaluate antigen sensitivity, we used Nalm-6 $CD22^{WT}$ (11912 molecules/cell) and $CD22^{Low}$ cell lines (959 molecules/cell) as target cells (**Extended Data Fig. 3.8e**). T cells expressing the full and split ChTCRs and the 4-1BBz CAR proliferated similarly after co-culture with Nalm-6^{WT} cells (**Fig 3.3j)**, however T cells expressing full ChTCRs demonstrated greater proliferation compared to split ChTCR and CAR T cells after co-culture with Nalm-6 $CD22^{Low}$ cells. Full ChTCR T cells also produced more IL-2 and IFN-g in response to Nalm-6 $CD22^{Low}$ cells compared to split ChTCR and 4-1BBz CAR T cells (**Fig 3.3k, l)**. Because CD28z CAR T cells have higher antigen sensitivity than 4-1BBz CAR T cells in some contexts[155, 156], we also evaluated T cells transduced with a CD28z CAR designed with the 9A8 scFv. The CD28z CAR T cells produced lower levels of cytokines after co-culture with Nalm-6 $CD22^{Low}$ cells than 4-1BBz CAR T and ChTCR+ T cells (**Extended Data Fig. 3.8f-g)**. These findings demonstrate that the CD22 full ChTCR provided better recognition of $CD22^{Low}$ tumor than the CD22 split ChTCR, CD28z, and 4-1BBz CARs, and provided the rationale to evaluate a bispecific ChTCR comprised of CD19 and CD22 scFvs fused to each individual TCR chain.

Design of a bispecific CD19/CD22 ChTCR

We fused the CD19-specific FMC63 scFv to TRAC in a V_HV_L orientatio and the CD22 specific 9A8 scFv to TRBC in a V_LV_H orientation and transduced TCR^{ko} CD8+ T cells **(Fig 3.4a; Extended Data Fig. 3.9a)**. For comparison, T cells were transduced with CD19 monospecific 4-1BBz CAR, CD22 monospecific 4-1BBz CAR using the m971 scFv, and the Loop CAR [99, 154] **(Fig 3.4a-b)**. The MFI of rCD19 and rCD22 binding was superior for T cells expressing the Bi-ChTCR compared to the Loop CAR **(Fig 3.4b-d)**. Expressing two scFvs on the same ChTCR could result in tonic signaling or affect synapse formation. When expressed in Jurkat TPR cells, Bi-ChTCR exhibited minimal antigen-independent activation of NFAT, NF-kB and AP-1 similar to the monospecific CD19 and CD22 4-1BBz CARs while the Loop CAR exhibited high antigen-independent activation **(Extended Data Fig. 3.9b-d)**. The Bi-ChTCR formed an organized synapse with a soluble bilayer functionalized with CD19 and CD22 proteins with CD22 taking a more central position than CD19 in the cSMAC **(Fig 3.4e)**, perhaps due to the more distal location of the 9A8 epitope.

We tested T cell recognition of WT Nalm-6 cells and gene edited Nalm-6 cells that expressed only CD19 (Nalm-6 $CD22^{ko}$), only CD22 (Nalm-6 $CD19^{ko}$), or neither CD19 nor CD22 (Nalm-6^{dko}) (**Extended Data Fig. 3.9e**). Bi-ChTCR T cells demonstrated robust proliferation and cytokine production in response to Nalm-6^{WT} and Nalm-6 cells expressing only CD19 or CD22 (**Fig. 3.4f-h and Extended Data Fig. 3.9f**). In contrast, Loop CAR T cells showed reduced functions when co-cultured with $CD19^{ko}$ cells compared to Nalm6 WT or $CD22^{ko}$, and CD19 and CD22 mono-specific CAR T cells only responded to tumor cells expressing their cognate antigen **(Fig. 3.4f-h and Extended Data Fig. 3.9f)**. T cells expressing the Bi-ChTCR lysed Nalm-6 WT, Nalm-6 $CD22^{ko}$, and Nalm-6 $CD19^{ko}$ cells, while T cells expressing the Loop CAR lysed Nalm-6 $CD22^{ko}$ cells but lysed Nalm-6 $CD19^{ko}$ target cells poorly (**Extended Data Fig. 3.9g)**. Monospecific CAR T cells failed to recognize Nalm-6 cells lacking cognate antigen (**Extended Data Fig. 3.9g**).

We next evaluated in vivo therapy of a tumor inoculum with heterogeneous antigen expression. NSG mice were engrafted with an equal mixture of Nalm-6^{WT} ($CD19^+/CD22^+$), Nalm-6 $CD19^{ko}/CD22^+$, and Nalm-6 $CD19^+/CD22^{ko}$ tumor cells (**Fig. 3.4i**). Mice treated with Bi-ChTCR T cells showed improved tumor clearance and survival compared to monospecific or bispecific CAR T cells (**Fig. 3.4j-l**). In control untreated mice, tumor cells harvested at euthanasia were predominantly $CD19^+CD22^+$ with a smaller frequency of $CD19^+$ $CD22^-$ and $CD19^-$ $CD22^+$ cells than in the initial tumor inoculum, illustrating a proliferative advantage for Nalm-6^{WT} tumor in vivo. Mice that received CD19 CAR or Loop CAR T cells relapsed with predominantly $CD19^-CD22^+$ tumor cells and minor populations of $CD19^{Low}CD22^+$ and $CD19^-CD22^-$ tumor cells. In CD22 CAR T treated mice, the persisting tumor was predominantly $CD19^+CD22^-$ with a small frequency of $CD19^+$ $CD22^{+/Low}$ and $CD19^-$ $CD22^-$ cells **(Fig. 3.4m-n).** Analysis of one mouse with progressive tumor in the Bi-

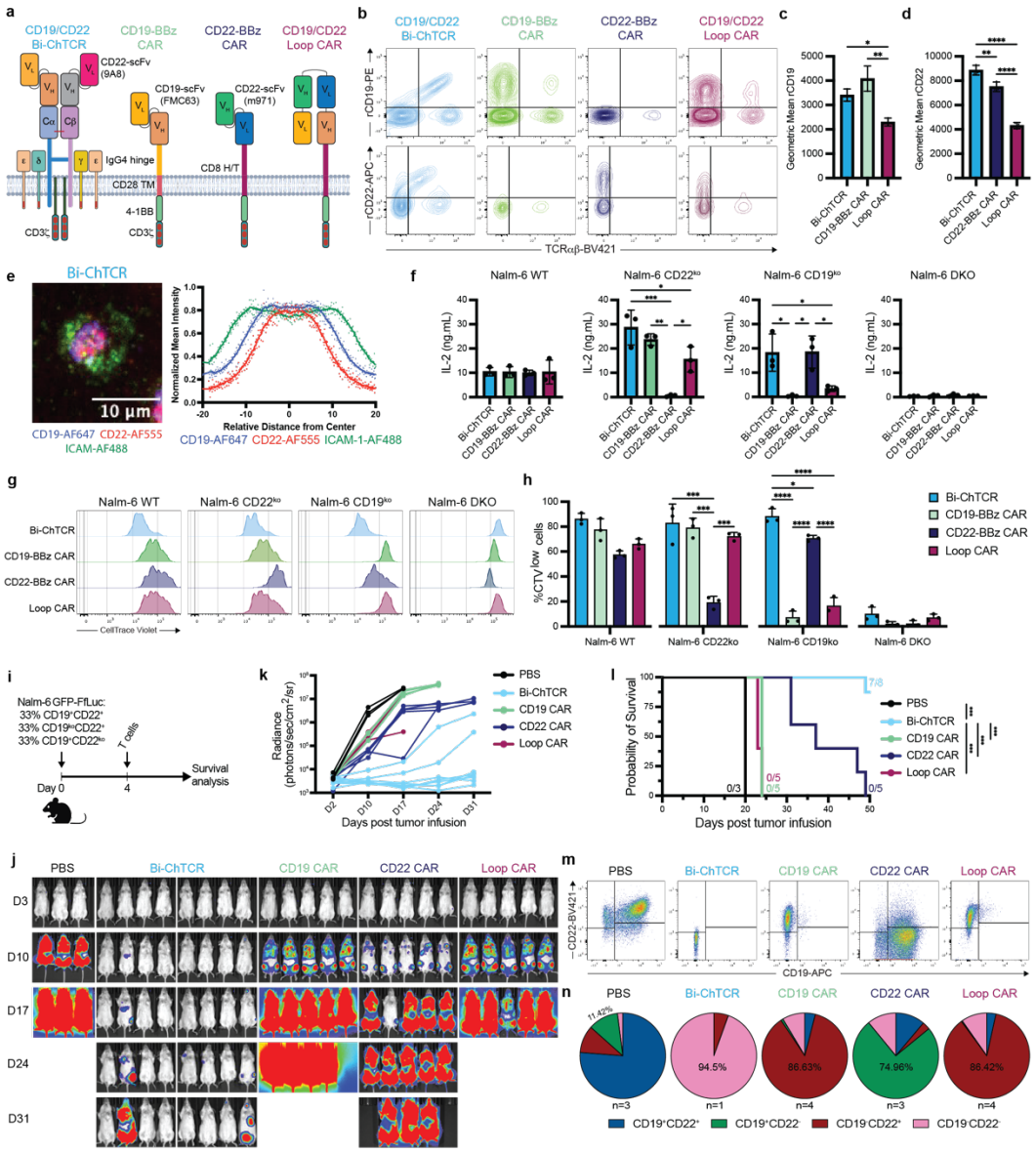

Figure 3.4 A CD19/CD22 Bi-ChTCR confers T cell recognition of both CD19 and CD22 a. Schematic of bispecific CD19/CD22 ChTCR, monospecific CD19 and CD22 4-1BB/CD3z CARs, and bispecific CD19/CD22 CAR [7]. The CD19-specific FMC63 scFv and the CD22-specific 9A8 scFv were used in the Bi-ChTCR construct; FMC63 and m971 scFvs were used in all CAR constructs. **b.** Representative flow plots of transduced and TCRab base edited primary CD8 T cells stained with anti-TCRab and recombinant CD19 (top) or CD22 proteins (bottom). **c. and d.** Geometric mean ± SD of CD19-PE (c) or CD22-APC (d) binding to T cells expressing the indicated receptors (n=3 independent experiments). *P< 0.05, **P< 0.01, ****P< 0.0001 by two-way ANOVA. **e.** Left: Representative TIRF microscopy image of CD19/CD22 Bi-ChTCR T cells interacting with a soluble lipid bilayer functionalized with ICAM-1 extracellular domain (green), CD19 and CD22 extracellular domains (blue and red respectively). Scale bars = 10μm. Right: Normalized mean intensity of ICAM-1-AF488, CD19-AF647 and CD22-AF555 staining across the cell radiuses in synapses. Dots represent mean at each position, with trend line (n=100 cells). **f.** Concentration of IL-2 in culture supernatants after overnight co-culture of T cells expressing the indicated receptors with Nalm-6^{WT}, Nalm-6^{CD22ko}, Nalm-6^{CD19ko} and Nalm-6^{DKO} cells. Data is shown as the mean ± SD for T cells from 3 independent healthy donors. *P< 0.05, **P< 0.01, ***P< 0.001 by two-way ANOVA. **g.** Representative flow histograms of CellTrace Violet (CTV) dilution measured after 72h co-culture of T cells expressing the indicated receptors with Nalm-6 cells expressing CD19 and CD22 or knocked out for one or both targets. **h.** Frequency of divided cells (CTV^{low} cells) measured after 72h co-culture of T cells expressing the indicated receptors with Nalm-6 cells. Data is shown as the mean ± SD from 3 independent healthy donors. *P< 0.05, ***P< 0.001, ****P< 0.0001 by two-way ANOVA. **i.** Schematic of NSG mice engrafted with Nalm-6 GFP-ffluc^{+} cells that are heterogeneous for CD19 and CD22

expression. **j.** Representative bioluminescence images of Nalm-6 GFP-ffluc$^+$ tumor burden in mice treated with 2x10^6 T cells expressing the indicated CARs or the Bi-ChTCR. **k.** Tumor burden (mean ± SD radiance (photons/sec/cm^2/steradian)) of tumor-bearing NSG mice treated with T cells expressing the indicated CARs or the Bi-ChTCR (n=5 to 8 mice per group). **l.** Kaplan-Meier survival of Nalm-6 GFP-ffluc$^+$-bearing NSG mice treated with CARs or Bi-ChTCRs (n=5-8). *P <0.05, **P<0.01, ***P<0.001. **m. and n.** Representative flow plots (n) and pie graphs (o) of CD19 and CD22 expression on Nalm-6 GFP-ffluc+ tumor cells harvested from the bone marrow at the time of euthanasia for each of the treatment groups (n=1-4 mice per group).

ChTCR T cell treated group showed that tumor cells were predominantly CD19$^-$CD22$^-$ with a small fraction of CD19$^-$ CD22^{Low} cells. These data show that heterogeneity in antigen expression limits the antitumor activity of mono- and bispecific CAR T cells, and this barrier is overcome by Bi-ChTCR T cells.

Bi-ChTCR T cells maintain sensitivity to each antigen in vitro and in vivo

Signaling or sensitivity of the Bi-ChTCR for each single antigen could be compromised by having two scFvs in proximity. LAT phosphorylation was comparable in intensity and kinetics between the Bi-ChTCR and the monospecific CD19 or CD22 full ChTCRs, and greater than the Loop CAR **(Fig. 3.5a-b)**. To evaluate antigen sensitivity, we compared T cell recognition of Nalm-6 CD22^{ko} cells expressing low levels of CD19, and of Nalm-6 CD19^{ko} cells low levels of CD22 **(Fig 3.5c)**. T cells expressing the CD19/CD22 Bi-ChTCR exhibited strong proliferation **(Fig 3.5d and g)** and cytokine production against both CD22^{ko}CD19^{Low} and CD22^{Low}CD19^{ko} tumor cells **(Fig 3.5e, f, h and i)** that was equivalent to mono-specific CD19 and CD22 full ChTCRs and superior to the Loop CAR.

We then evaluated the in vivo efficacy of Bi-ChTCR T cells for eliminating a tumor inoculum comprised of Nalm-6 cells expressing high and low levels of CD19 and CD22 **(Fig 3.5j)**. Having demonstrated previously that monospecific and bispecific CAR T cells failed to control heterogeneous tumors with high antigen levels **(Fig 3.4i-n)**, we compared Bi-ChTCRs T cells to CD19 and CD22 4-1BBz CAR T cells co-infused at 1:1 ratio, a therapeutic strategy being employed clinically to address tumor heterogeneity[154, 157]. Bi-ChTCR T cells showed superior anti-tumor efficacy and improved survival compared to mice treated with the mixed CD19 and CD22 BBz CAR T cell product **(Fig 3.5k-m)**, and superior efficacy correlated with greater expansion of CD4+ and CD8+ ChTCR+ T cells in the blood **(Fig 3.5n-o)**. It is notable that the Bi-ChTCR T cells were more effective against a tumor inoculum containing CD19^{low}CD22^{low} Nalm-6 and Nalm-6^{WT}, than the monospecific CD19 full ChTCR was for CD19^{low} Nalm-6. It is possible that Nalm-6^{WT} drove greater proliferation of the Bi-ChTCR T cells or that the higher density of CD22 on CD22^{low} Nalm-6 contributed to better efficacy. These nuances notwithstanding, the data shows that Bi-ChTCR T cells maintain superior antigen sensitivity against each target antigen in vitro and are more effective than two CAR T cell products for eliminating tumors with heterogeneous and low antigen levels.

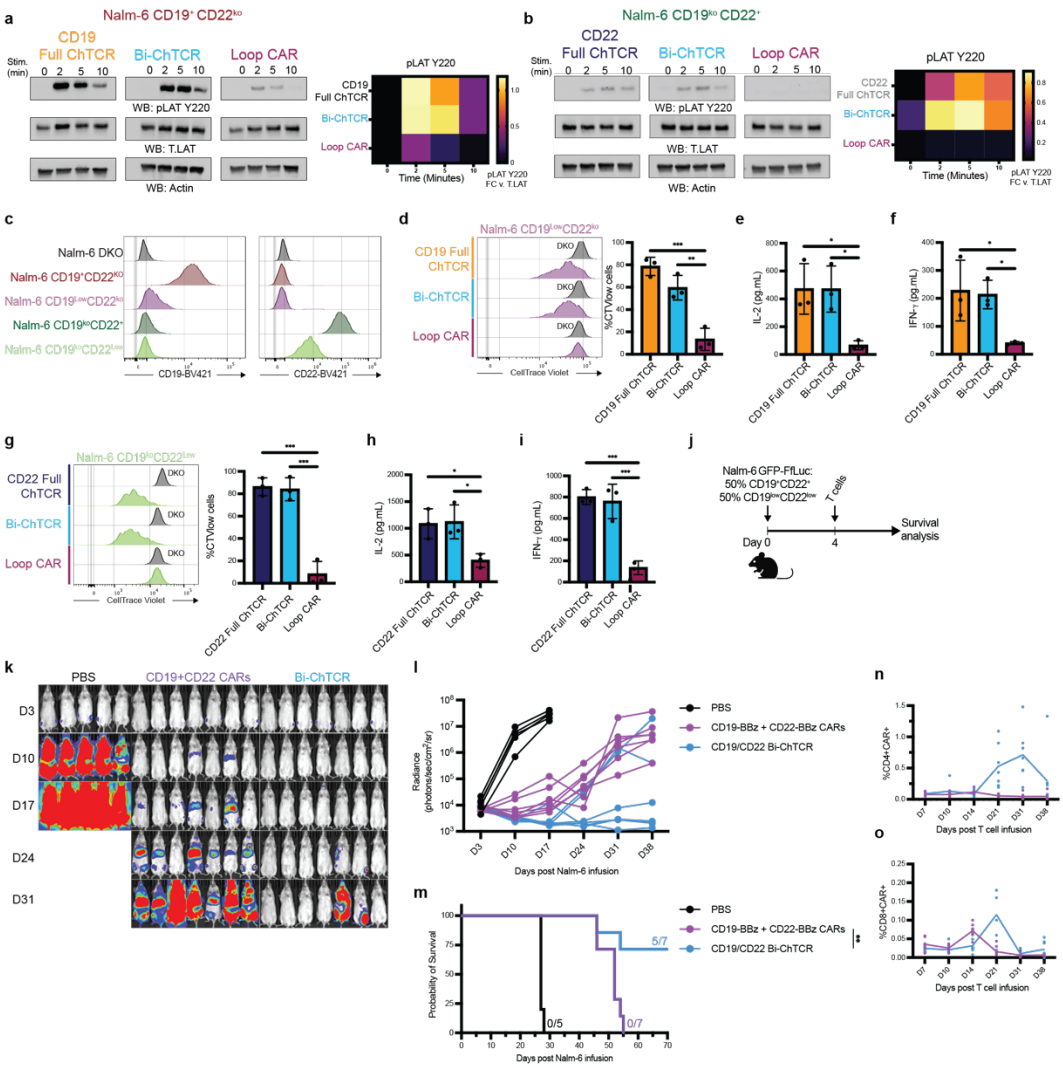

Figure 3.5 T cells expressing the CD19/CD22 Bi-ChTCR have exquisite sensitivity for both antigens and potent anti-tumor activity a. and b. Representative western blot for LAT pTyr^{220}, Actin and LAT in lysates from T cells expressing the indicated receptors after stimulation with Nalm-6 CD19^{+}CD22^{ko} cells (a) or Nalm-6 CD19^{ko}CD22^{+} cells (b) for the indicated times. Right: Heat map of mean band intensity of LAT pTyr^{220} normalized to LAT (n=3 independent experiments). **c.** Flow plots depicting CD19 and CD22 expression levels on Nalm-6 cells after gene knockout. **d.** Left: Representative flow histograms of CellTrace Violet (CTV) dilution measured after 72h co-culture with Nalm-6 cell CD19^{ko}CD22^{ko} (DKO, control) or Nalm-6 CD19^{Low}CD22^{ko} cells. Right: Frequency of divided cells (CTV^{low} cells) measured after 72h co-culture with Nalm-6 CD19^{Low}CD22^{ko} cells (mean ± SD) (n=3 independent healthy donors). P values from two-way ANOVA test, **P< 0.01, ***P< 0.001. **e-f.** Concentration of IL-2 (e.) and IFN-g (f.) in culture supernatant after overnight co-culture with Nalm-6 CD19^{Low}CD22^{ko} cells (mean ± SD) (n=3 independent healthy donors). P values from two-way ANOVA statistical test, *P< 0.05. **g.** Left: Representative flow histograms of CellTrace Violet (CTV) dilution measured after 72h co-culture with Nalm-6 DKO cells or Nalm-6 CD19^{ko}CD22^{Low} cells. Right: Frequency of divided cells (CTV^{low} cells) measured after 72h co-culture with Nalm-6 CD19^{ko}CD22^{Low} cells (mean ± SD) (n=3 independent healthy donors). P values from two-way ANOVA statistical test, **P< 0.01, ***P< 0.001. **h-i.** Concentration of IL-2 (h) and IFN-g (i) in culture supernatant after overnight co-culture with Nalm-6 CD19^{ko}CD22^{Low} cells (mean ± SD) (n=3 independent healthy donors). P values from two-way ANOVA test, *P< 0.05. **j.** Schematic of NSG mice engrafted with a mixture of Nalm-6 GFP-ffluc^{+} cells CD19^{+}CD22^{+} and CD19^{Low}CD22^{Low} treated with 2x10^{6} T cells expressing CD19- and CD22-BBz CARs (1:1 ratio) or the CD19/CD22 Bi-ChTCR. **k.** Representative bioluminescence images of Nalm-6 GFP-ffluc^{+} tumor burden in mice treated with 2x10^{6} T cells. **l.** Tumor burden (mean ± SD radiance (photons/sec/cm^{2}/steradian)) of tumor-bearing NSG mice treated with T cells expressing CD19+CD22-BBz CARs or CD19/CD22 Bi-ChTCR (n=5 to 7 mice per group). **m.** Kaplan-Meier survival of Nalm-6 GFP-ffluc^{+}-bearing NSG mice treated with CD19+CD22-BBz CARs or CD19/CD22 Bi-ChTCR (n=5-7). **P<0.01. **n. and o.**

Frequency of CD4+ (**n.**) and CD8+ (**0.)** T cells expressing the CARs or Bi-ChTCR in the blood at indicated timepoints (% of Live+Lymphocyte+).

Bi-ChTCR specific for multiple myeloma antigens

To determine whether the Bi-ChTCR architecture could be used to target two multiple myeloma antigens, we designed BCMA/SLAMF7 Bi-ChTCRs. We tested different guide RNAs to delete expression of SLAMF7 and avoid the potential for fratricide since SLAMF7 is expressed on some T cells [158] (**Extended Data Fig 3.10a)**. Simultaneous editing of SLAMF7 with sgRNA1 and TCRab was highly efficient in primary T cells (**Extended Data Fig 3.10b-c)**. We then transduced T cells with monospecific split and full ChTCRs using the HuLuc63 (anti-SLAMF7) scFv and compared antigen sensitivity of flow-sorted ChTCR+ T cells using titrations of plate-bound antigen. Similar to CD19 and CD22, the surface expression of the SLAMF7 full ChTCR was higher on T cells than the split ChTCR and this translated into higher antigen sensitivity (**Extended Data Fig 3.10e-h)**. Split and full monospecific BCMA ChTCRs were also constructed with the C11D5.3 scFv. In this case, the split ChTCR showed higher expression and improved sensitivity over the full ChTCR illustrating the need to compare split and full formats for individual scFvs (**Extended Data Fig 3.10i-m)**. Nonetheless, the BCMA full ChTCR showed robust reactivity and was used in the design of BCMA/SLAMF7 Bi-ChTCRs.

We designed 4 formats of BCMA/SLAMF7 Bi-ChTCRs and expressed them in TCR^{ko} Jurkat cells (**Extended Data Fig. 11a**). All 4 Bi-ChTCRs were expressed at similar levels at the cell surface as measured by binding to rBCMA and rSLAMF7 and restored cell surface expression of CD3e (**Extended Data Fig. 3.11b-e)**. We proceeded with analysis of format 1 since the VH/VL orientation provided a direct comparison to previously designed BCMA and SLAMF7 CARs (**Extended Data Fig. 3.12a, Fig. 6a**). The BCMA/SLAMF7 Bi-ChTCR and monospecific BCMA and SLAMF7 CARs were expressed in T cells with simultaneous CBE of endogenous TRAC, TRBC and SLAMF7[158]. Gene edited SLAMF7 and BCMA/SLAMF7 Bi-ChTCR T cells expanded in culture and had the same viability as BCMA CAR T cells (**Extended Data Fig. 3.12b-c**). Binding of soluble BCMA and SLAMF7 was significantly higher for T cells transduced with the monospecific CARs compared to the Bi-ChTCR (**Fig 3.6b-d**). However, Bi-ChTCR T cells exhibited more rapid and intense phosphorylation of Zap70 compared to monospecific BCMA and SLAMF7 CAR T cells (**Fig.3. 6e and f),** and produced higher amounts of IFN-g when cultured with titrated levels of plate-bound antigen (**Extended Data Fig. 3.12d,e)**. BCMA/SLAMF7 Bi-ChTCR T cells recognized the INA-6 MM cells expressing both BCMA and SLAMF7, and INA-6 engineered to express only a single antigen, whereas monospecific CAR T cells only recognized INA-6 cells that expressed their cognate antigen (**Fig. 3.6g-i**).

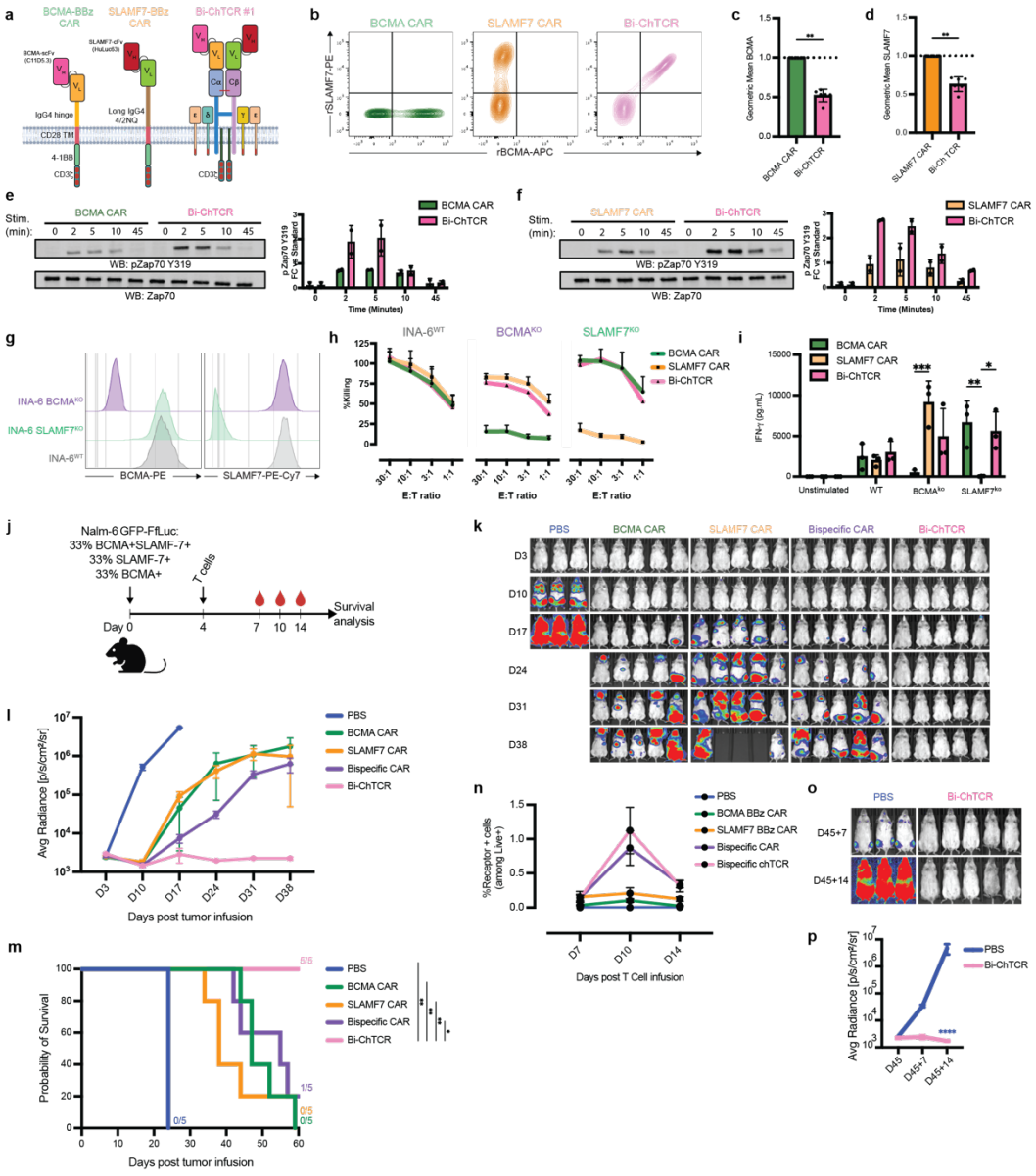

Figure 3.6 BCMA/SLAMF7 Bi-ChTCR for targeting Multiple Myeloma a. Schematic of CARs and a Bi-ChTCR specific for BCMA and SLAMF-7. The BCMA BBz CAR was constructed with the C11D5.3 scFV V_H-V_L linked to an I_gG4 hinge, CD28 transmembrane domain, and 4-1BB and CD3ζ signaling domains. The SLAMF7 BBz CAR was constructed with the HuLuc63 V_H-V_L linked to a long IgG4 4/2NQ hinge, CD28 transmembrane domain, and 4-1BB and CD3ζ signaling domains; The BCMA/SLAMF7 Bi-ChTCR was constructed with the C11D5.3 scFV V_H-V_L fused to TRAC and the HuLuc63 V_H-V_L fused to TRBC. **b.** Representative flow plots of transduced and TCRab and SLAMF7 based edited primary CD8 T cells stained with recombinant SLAMF7-PE and BCMA-APC. **c. and d.** Normalized geometric mean ± SD of binding of BCMA-APC (c.) or SLAMF7-PE (d.) to CD8 T cells expressing each CAR or the Bi-ChTCR. Data is shown for 6 independent experiments. **P< 0.01 by paired t-test. **e and f.** Left: Representative western blot analysis of lysates from BCMA CAR and Bi-ChTCR (h) or SLAMF7 CAR and Bi-ChTCR (i) for pZap70 pTyr^{319} and Zap70 after crosslinking the receptor with antigen-coated beads. Right: Fold-change in mean intensity of pZap70 pTyr^{319} normalized to actin per stimulation timepoints. **g.** Flow histograms of BCMA (left) and SLAMF7 (right) expression in INA-6 WT, INA-6 SLAMF7^{ko} and INA-6 BCMA^{ko} myeloma cells. **h.** Cytotoxic activity of CAR or Bi-ChTCR T cells against the indicated INA-6 cells measured by chromium release assay. Data is shown as the mean ± SD for 3 independent experiments. **i.** Concentration of IFN-γ in culture supernatant after overnight co-culture of T cells expressing the indicated receptors with wild-type and single antigen knock-out INA-6 cells. Data is shown as the mean ± SD for 3 independent experiments. P< 0.05, **P< 0.01, ***P< 0.001 by two-way ANOVA

j. Schematic of NSG mice engrafted with Nalm-6 cells that are heterogeneous for BCMA and SLAMF7 antigen expression and treated with $2x10^6$ CAR or ChTCR T cells. **k.** Bioluminescence imaging of Nalm6-ffluc tumor burden in mice after treatment with T cells expressing monospecific or bispecific CARs or the Bi-ChTCR. **l.** Mean ± SD radiance (photons/sec/cm^2/steradian) of Nalm-6 GFP-ffluc tumor burden for each treatment group (n=3-5 mice per group). **m.** Kaplan-Meier survival of Nalm-6 GFP-ffLuc-bearing mice in each treatment group (n=3-5 mice per group). *P<0.05, ** P <0.01. **n.** Frequency of CAR+ and Bi-ChTCR+ T cells in the blood at indicated timepoints (% of Live+Lymphocyte+). **o.** Bioluminescence images of tumor burden in mice rechallenged with a mixture of BCMA+SLAMF7+, BCMA-SLAMF7+ and BCMA+SLAMF7- Nalm-6 GFP-ffluc cells 45 days after initial tumor infusion. **p.** Mean of Nalm-6 GFP-ffluc tumor burden in new control group or mice previously treated with Bi-ChTCR T cells and rechallenged (mean radiance ± SD) (photons/sec/cm^2/steradian) (n=3-5 mice per group). ****P<0.0001 by two-way ANOVA.

Before analyzing the in vivo function of the BCMA/SLAMF7 Bi-ChTCR, we compared expression and signaling to a previously described BCMA/SLAMF7 bispecific CAR[159]. We observed superior binding of BCMA and SLAMF7 to the Bi-ChTCR compared to the bispecific CAR (**Extended Data Fig. 3.13a-c**), and Bi-ChTCR T cells exhibited more rapid and intense Zap70 phosphorylation after stimulation with bead-coated BCMA and SLAMF7 antigens alone, or together (**Extended Data Fig. 3.13d-e).** We then asked whether BCMA/SLAMF7 Bi-ChTCR$^+$ T cells could eliminate a Nalm-6 tumor inoculum that was heterogeneous for BCMA and SLAMF7 expression (**Fig. 3.6j).** Bi-ChTCR$^+$ T cells rapidly eliminated tumors in all mice, while bispecific CAR$^+$ T cells showed a moderate improvement in tumor control and survival over each monospecific CAR$^+$ T cell product **(Fig. 3.6k-m)**. Bi-ChTCR T cells demonstrated superior expansion in the blood compared to all other treatment groups, despite the absence of a costimulatory domain in the receptor (**Fig. 6n**). We rechallenged mice that were tumor free after the administration of Bi-ChTCR with the same mixture of Nalm-6 cells. Control mice quickly developed tumors, whereas all mice from the Bi-ChTCR treated group were protected from tumor challenge (**Fig. 3.6o-p**). Collectively, the data demonstrates that Bi-ChTCRs can sensitively target pairs of B cell lineage antigens relevant for therapy of leukemia, lymphoma and multiple myeloma.

Discussion

Outgrowth of tumor cells that have downregulated or lost the target antigen is a major mechanism for the failure of CAR T cells [91, 96, 132, 144, 160, 161]. Improving efficacy requires the development of receptors that are both highly sensitive and capable of recognizing multiple tumor antigens. Bispecific CARs often exhibit reduced sensitivity for each individual antigen, enabling escape of low antigen expressing tumor cells [132, 162]. Here, we describe chimeric TCRs that simultaneously target two tumor antigens with high sensitivity.

The concept of linking an antigen binding domain to the TCR to improve sensitivity is not new but as shown here for mutSTAR and HIT receptors, mispairing of chimeric TCR chains with endogenous TCR chains and competition for CD3 molecules compromises cell surface expression and sensitivity [72, 73, 126, 129, 130]. We employed base editing to

efficiently disrupt endogenous TRAC and TRBC expression without inducing double-strand DNA breaks which can lead to chromosome losses, translocations and/or recombinations[163, 164]. Base editing can disrupt expression of multiple genes in T cells with high efficiency and is being used for editing T cells in clinical trials [165]. Our data shows that eliminating endogenous TCR chains was required for optimal expression of split and full ChTCRs, and improved both the surface expression and sensitivity of HLA-independent mutSTAR and HIT receptors.

The monospecific full ChTCR, in which an scFv is linked to a single TCR constant chain, demonstrated superior antigen sensitivity in vitro and antitumor activity in vivo compared to the split ChTCR for three of the four targets we tested. CD19, CD22 and SLAMF7 full ChTCRs had higher receptor expression levels and improved sensitivity compared to the split ChTCRs. When expression of the full ChTCR was lower, as in the BCMA ChTCR, antigen sensitivity was reduced. It is possible that other factors including structural elements of ChTCRs may contribute to improved expression and sensitivity. Modeling of ChTCRs alone and bound to target antigen may help further elucidate why the full ChTCR structure is generally superior to split formats and could facilitate scFv selection for new targets[166].

ChTCRs assemble with all CD3 subunits, which provides diversity in ITAM sequences and may contribute to TCR-like synapse formation[6, 110, 167]. Immune synapses play a pivotal role in regulating T cell activation, from signal initiation, propagation and termination [31]. This regulation is likely to be preserved in ChTCR T cells and may be important in achieving optimal antigen sensitivity. Other studies have incorporated specific signaling portions from CD3e, d or g subunits into CARs to provide additional CD3 motifs and improve CAR T cell function. CD3e CARs in particular exhibited improved T cell persistence and function in vivo. However, the antigen sensitivity, synapse formation and signaling of CD3e modified CARs was not evaluated[13, 110, 120].

It is notable that ChTCR^{+} T cells secrete lower levels of cytokines compared to CD28z CAR T cells in response to high antigen expressing tumor cells, which may relate to the lack of a costimulatory domain in the ChTCR. High cytokine levels correlate with the severity of cytokine release syndrome and neurotoxicities observed with CAR T cell therapy[168], and it is reasonable to expect a better toxicity profile with ChTCRs when the majority of tumor cells express high antigen levels. Despite the absence of receptor intrinsic costimulation, CD19 full ChTCR T cells were more effective in vivo against antigen high tumors than CD28z and 4-1BBz CAR T cells. Costimulation is provided to T cells by a variety of molecules including LFA-1 and CD2 that participate in the synapse [36, 127, 169]. Thus, the necessity for additional costimulation may depend somewhat on the ability to form TCR like synapses, which differs with CARs. When mice were engrafted with a tumor inoculum

comprised only of Nalm-6^{CD19Low} tumor cells, T cells expressing the full ChTCR were only modestly superior to CAR T cells. In this scenario providing additional costimulation to ChTCR T cells might further improve efficacy, as shown for the HIT receptor[170]. Approaches to incorporate costimulation into our ChTCRs without driving excessive cytokine release is the subject of ongoing work.

We leveraged the superior monospecific full ChTCR format to design bispecific ChTCRs that target CD19 and CD22, or BCMA and SLAMF7. Given the absence of rules for designing optimized ChTCRs, we constructed monospecific CD22 ChTCRs with two CD22 scFvs that had similar binding affinities (m971 and 9A8) but were specific for membrane-proximal and membrane-distal epitopes, respectively[154, 171]. Surprisingly, while T cells expressing ChTCRs using each scFv bound soluble CD22 protein, only T cells expressing the 9A8 ChTCR formed an organized immune synapse and recognized CD22 positive tumor cells. In contrast, the m971 scFv specific for a membrane proximal epitope in CD22 was superior to 9A8 in CAR T cells[172]. These findings highlight potential differences between CARs and ChTCRs perhaps related to distinct synaptic distance requirements between the two receptor classes[28, 173]. Unlike CARs, ChCTRs do not possess a hinge domain between the TCR constant chains and the scFv, which could limit the flexibility necessary to engage the membrane-proximal epitope of a bulky protein like CD22. These findings underscore the need for further work to define rules for optimal ChTCR design, informed by functional screening of large numbers of scFvs of known epitope specificity.

T cells expressing Bi-ChTCRs targeting CD19 and CD22 or BCMA and SLAMF7 recognized target cells expressing one or both target proteins and exhibited superior sensitivity for tumor with low antigen levels compared to T cells expressing monospecific and bispecific CARs. In vivo models that mimic therapy of tumors with heterogeneous antigen expression and with low levels of antigen showed improved efficacy of Bi-ChTCR T cells compared to bispecific CAR T cells[99, 159]. Bispecific targeting with CARs can also be achieved by the infusion of two mono-specific CAR products either at the same time or sequentially. This strategy could overcome complete antigen loss, but the poor sensitivity of CAR T cells would allow escape of antigen low tumor cells, as demonstrated in our study. Additionally, the use of two products adds manufacturing complexity and cost[162, 174]. A potential limitation of the ChTCR approach is that the presence of the endogenous TCR may be necessary to improve in-vivo persistence of CAR T cells in immunodeficient mice[175]. Long term persistence of CAR T cells is not essential for clinical efficacy and we observed sufficient persistence of Bi-ChTCR T cells to reject a later tumor re-challenge [176].

Collectively, these data identify a new and adaptable approach for sensitive and potent recognition of two target antigens with a single engineered T cell product that holds

promise for reducing antigen escape and relapse in both B cell malignancies and multiple myeloma.

Methods

Cell Lines

Lenti-X 293T cell line was acquired from Takara Bio USA. Jurkat 76 TPR cells were previously described [177] and a kind gift from Dr. Mirjam Heemskerk (University Medical Center, Utrech). Nalm-6 (CRL-3273), Raji (CCL-86), H929 (CRL-3580), INA-6 and Jurkat E6.1 (TIB-52) were acquired from American Type Culture Collection. MOLP8 cell line was acquired from DSMZ (ACC569). Lenti-X 293T were maintained in complete culture media (DMEM (Gibco, 11965-092), 10% fetal bovine serum (Corning, 35-011-CV), 2mM L-glutamine (Gibco, 25030-081), 1x penicillin/streptomycin (Gibco, 15140-122), 25mM HEPES (Gibco, 15630080)). NALM-6, Raji, INA-6 and Jurkat cell lines were obtained from ATCC and maintained in RPMI 1040 medium (Gibco, 22400-089) supplemented with 10% fetal bovine serum, 2mM L-glutamine, 1x penicillin/streptomycin. MOLP8 and H929 were maintained in RPMI 1040 medium (Gibco, 22400-089) supplemented with 20% fetal bovine serum, 2mM L-glutamine, 1x penicillin/streptomycin. Cells were split every 2-3 days and replated at a density of 0.3-0.6x10^6 cells/mL. Tumor cell lines were authenticated in the Fred Hutchinson Cancer Center Genomics Core and all cell lines were routinely checked to ensure they were negative for mycoplasma contamination.

Generation of Nalm-6 lines

Nalm-6 cell lines expressing various levels of CD19 and CD22 were generated as described previously [155]. Briefly, CD19, CD22, or both were knocked out of Nalm-6 cells using CRISPR Cas9, and negative cells were transduced with a lentiviral vector encoding either a truncated CD19 protein (extracellular and transmembrane domains only, Uniprot P15391). Briefly, 1x10^6 cells were resuspended in SF buffer (Lonza, V4XC-1032) mixed with 20nM of ribonucleoprotein protein complex formed with CRISPR Cas9 enzyme (Horizon Discovery, CAS12207) and sgRNAs of interest (Horizon Discovery). NALM-6 cells negative for the antigen of interest were sorted by flow cytometry, transduced with the lentiviral vector, subjected to single cell flow sorting to obtain cell lines with different levels of CD19 and CD22 expression, and expanded for analysis. Nalm-6 cells expressing BCMA and/or SLAMF7 were generated by transduction with a lentiviral plasmid encoding for the extracellular and transmembrane domains of BCMA (Uniprot: Q02223) or SLAMF7 (Uniprot: Q9NQ25) and sorted by flow cytometry for purity.

Generation of constructs and Lentivirus preparation

Lentivirus vector (HIV7) was used for transduction of T cells. CAR and ChTCR sequences were synthesized after codon optimization and inserted into the HIV7 lentivirus plasmid backbone under the EF1a promoter by Gibson assembly, or in some cases full plasmids were synthesized commercially (Twist Biosciences). Sequences for scFvs were previously described; anti-CD19 FMC63 [178], anti-CD22 m971 [99], anti-CD22 9A8 [154], anti-BCMA C11D5.3 [179], and anti-SLAMF7 HuLuc63 [158]. To generate split ChTCRs, human TCR constant beta chain (UniProt P01850, amino acids 1-176) was inserted immediately after the antibody V_L chain. A furin site, a P2A sequence and a GM-CSF signal peptide were inserted between the TCR chains. The TCR constant alpha chain sequence (UniProt P01848, amino acids 1- 140) was inserted immediately after the antibody V_H sequence from the scFv. Full ChTCR were designed by expressing the TRBC chain, fused to a furin site, a P2A sequence and a GM-CSF signal peptide before the entire scFv sequence (V_L-linker-V_H) and the TRAC chain. For Bispecific ChTCRs, each target-specific scFv was fused to a TCR chain. TRBC S56C and TRAC T47C substitutions were made to improve chain pairing [180]. The mutSTAR receptor was designed using sequences previously described [129, 131] and was comprised of the VL and VH domains from FMC63 fused to murine TRBC1 (UniProtKB-P01852, amino acids 146 to 173) and TRAC (UniProtKB-P01849, amino acids 113 to138) sequences respectively with the following mutations: mTCR-Cα S48C, mTCR-Cβ S57C, and mTCR-Cα transmembrane domain LSVMGLRIL mutated to LLVIVLRIL. The HIT receptor sequence incorporating the CD19-specific scFv SJ25C1 was described in Mansilla-Soto et al [130]. In some experiments, the CAR and ChTCR constructs included an HA tag to facilitate immunoprecipitation. Replication-deficient lentivirus was produced by transient transfection of Lenti-X cells using pPAX2, pVSVG and receptor-encoding lentiviral vector using Xfect polymer transfection reagent (Takara Bio, 631318), according to the manufacture's protocol. Lentiviral supernatant was harvested after 48 hours and filtered using a 0.45-mm PES syringe filter. Virus was further concentrated with Lenti-X Concentrator (Takara Bio, 631232) according to the manufacturer's recommended protocol.

T cell isolation

Peripheral blood was collected from healthy adults enrolled in an IRB approved study at Fred Hutchinson Cancer Center or obtained from Bloodworks Northwest after informed consent. Peripheral blood mononuclear cells (PBMCs) were isolated by density gradient using SepMate-50 (Stem Cell Tech., 85450) and lymphocyte separation media (Corning, 25-072-CV). Bulk CD8+ and CD4+ T cells were isolated using EasySep T cell Isolation kit (Stem Cell Tech, 17953) following manufacturer's instructions. T cells were cryopreserved for later use.

T cell transduction and gene editing

Bulk $CD8^+$ and $CD4^+$ T cells were activated using Dynabeads Human T-Activator CD3/CD28 (Gibco, 11131D) at a 3:1 bead to T cell ratio. T cells were cultured in T cell media (CTL) (RPMI 1040 (Gibco, 22400-089), 10% Human serum (Bloodworks Northwest) 2mM L-glutamine (Gibco, 25030-081), 1x penicillin/streptomycin (Gibco, 15140-122), 0.5mM b-mercaptoethanol) supplemented with IL-2 (50 IU/mL). The next day concentrated lentiviral supernatant was added to activated T cells with LentiBOOST Solution B (100x) (SIRION Biotech SB-P-LV-101-12) and polybrene (Millipore, TR-1003-G) at a final concentration of 4.4mg/mL. T cells were spinoculated at 800g, 32° C for 90 min, after overnight incubation beads removed prior to gene editing. Cytidine base editing was performed to knock-out expression of endogenous TRAC, TRBC or both, and SLAMF7 in some experiments. $1x10^6$ T cells were resuspended in P3 buffer (Lonza, V4XP-3032), mixed with 1mg concentration of RNA guide and 1.5mg of CBE BE4max mRNA (Addgene plasmid 112093) (Aldevron), and electroporated using the Lonza 4D device (Lonza) [181]. Sequences for sgRNAs are described in Table S1. T cells were cultured in CTL supplemented with IL-2 (150IU/mL), IL-7 (5ng/ml), IL-15 (5ng/mL) initially, and then maintained in CTL supplemented with IL-2 (50IU/mL) for one week before being used for assays. CAR+ and ChTCR+ T cells were purified by flow cytometry and cultured for 3 days before functional assays. For assays requiring larger cell numbers (western blot analysis and Calcium flux assays), flow sorted CAR and ChTCR specific T cells were expanded using OKT3 (30ng/mL) or PHA-L (500x) (Thermo Fisher Scientific, 00-4977-93), g-irradiated lymphoblastoid cell line (LCL) (8000 rad), and g-irradiated PBMCs at a LCL to T cell ratio (100:1) and PBMC to T cell ratio (600:1). IL-2 was added 24-hours after co-culture, and OKT3 or PHA-L was washed out on day 4. Cultures were fed with CTL supplemented with IL-2 (50IU/mL) and rested without IL-2 addition before use in assays.

ssDNA production and TRAC-targeted Kin

ssDNA incorporating CTS sequences were produced as in Shy et al[182]. and used as HDRT for targeted Kin experiments. Briefly, a plasmid encoding the HIT receptor with flanking homology arm sequences was ordered from Twist Bioscience and served as a template for generating a PCR amplicon. CTS sequences and a 5' biotin modification were added during the PCR reaction. dsDNA was purified using SPRI beads. ssDNA was then isolated as in Wakimoto et al. and Shy et al [182, 183]. Complimentary oligos to CTS sequences were mixed at 4:1 molar ratio to ssDNA and annealed by heating at 95 °C before cooling gradually. ssDNA templates were then immediately used in electroporation experiments. The sequence of the HDRT encoding the HIT receptor, PCR primers and TRAC or TRBC specific sgRNAs are described in Table S1. Ribonucleocomplexes (RNPs) of Cas9

enzyme (Dharmacon Horizon) and sgRNAs were produced by complexing sgRNAs to Cas9 (molar ratio of sgRNA–Cas9 of 2:1). ssDNAenh electroporation enhancer was added to sgRNA solution before mixing with Cas9 [184]. RNP mixtures were incubated at 37 °C for 15–30 min after mixing. 50 pmol of RNP was used for each electroporation. 2ug of ssDNA encoding the HIT receptor and TRAC-targeting RNPs were mixed and incubated for at least 5 min, then combined with activated T cells resuspended in P3 buffer and electroporated using the Lonza 4D device using program EH-115 (Lonza). When indicated RNPs targeting TRBC were also added.

Flow Cytometry

T cells were stained to detect CAR or ChTCR expression with the appropriate recombinant proteins (Acro bioystems, CD19 (CD9-H82E9), BCMA (BCA-H82E4), CD22 (Siglec-2) (SI2-H82E3) and SLAMF7 (HL7-H82E0)), and with anti-TCRa/b-BV421 1:50 (BD, 744778) and anti-CD3e-BUV395 1:50 (BD, 563546) antibodies. When protein directly conjugated to a fluorescent label was not available, biotinylated recombinant protein was used, followed by incubation with fluorescently labeled streptavidin (BioLegend, APC (405207), PE (405204), BV421 (405226), BD Biosciences BUV395 (564176)). Tumor lines were stained for detection of target proteins with the following BioLegend antibodies (CD19 (302212), CD22 (363512), BCMA (357520), SLAMF7 (331810)) and stained with fluorescently tagged isotype controls when indicated. Antigen density was quantified using Quantibrite beads (BD Biosciences, 240495 or custom made). Data were collected on BD FACSymphony A5 and BD FACSCelesta cytometers. FlowJo version #10.8.2 was used to analyze flow cytometry files.

Generation and fluorescent labeling of extracellular protein domains and density quantification

12X His-tagged CD19 (N138Q) and ICAM-1 extracellular domains were produced using the "Daedalus" mammalian expression system [185]. Briefly, HEK293F cells were transduced with lentivirus expressing CD19(N138Q)-12x His tag or ICAM-1-12x his tag constructs. Proteins were captured from expression culture supernatant by HisTrap FF crude (Cytiva, 11000458) Ni-affinity chromatography and polished by Superdex 200 (Cytiva, 28-9909-44) size exclusion chromatography. Purified proteins were flash frozen in liquid nitrogen in 1X PBS and stored at -80 °C. Extracellular domain of CD22-10x His tag was commercially available (Acrobiosystems, CD2-H52H8). For labeling, 100mg of His-tagged extracellular proteins were concentrated to 1mg/mL using Amicon Ultra Centrifugal Filters (Milipore, UFC500396), and pH adjusted to 8.3 by addition of $NaHCO_3$. Proteins were incubated with Alexa Fluor 488 TFP ester, Alexa Fluor 647 NHS ester or Alexa Fluor 555 NHS ester (ICAM_AF488, CD19_AF647, CD22_AF555, CD22_AF647) at room temperature for 15

minutes. Non-reactive dye was removed by size-exclusion chromatography, followed by repeat buffer exchange with Amicon Ultra Centrifugal Filters. Aliquots of protein were frozen and stored at -80° until use. Molecular density of extracellular domains in the soluble lipid bilayer (SLB) was determined using SLB-coated silica beads as previously described [36]. Briefly, silica microspheres (Bangs Laboratories Inc, SS05003) equaling the surface area of a single 96-well chamber were washed and resuspended in PBS. Beads were incubated with lipids (as described in section "soluble lipid bilayer generation and TIRF imaging") and washed following the same steps as bilayer preparation on 96-well plate. His-tagged proteins were serially diluted and incubated with SLB-coated silica beads for 30 min with gentle shaking. Beads were run on a flow cytometry machine (BD FACSCelesta) along with Quantum Alexa Fluor 488 MESF or Quantum Alexa Fluor 647 MESF (Bangs Laboratories Inc, 647A/488A). Degree of labeling of proteins was determined by 280 and fluorescent absorption, and MESF standards were used to determine the absolute molecular density of proteins on silica beads.

Soluble lipid bilayer generation and TIRF imaging

Soluble lipid bilayers were generated on 96-well chambered coverslips as previously described [186]. Briefly, 96-well plates (Ibidi, 89627) were washed overnight with 5% Hellmanex III (Sigma, Z805939) and rinsed with ultrapure water. Wells were incubated with 20% HCL 3X, for 1 hr on 50° hot plate. Small unilamellar vesicles (SUV) were generated using 97.5% POPC (Avanti, 850457C-200mg), 0.5% PEG-5000-PE (Avanti, 880230), 2% DOGS-NTA (Avanti, 790404). SUVs were generated by repeated (35X) freeze thaw cycles, moving between liquid nitrogen and a 37° water bath, followed by centrifugation at 33,500xg for 45 minutes at 4°C. SLBs were generated by covering wells with SUV, incubating for 1 hr at 37°, then washed 3X with PBS. SLBs were incubated with his-tagged proteins at determined concentrations (ICAM 200 molecules per mm^2, CD19 and CD22 50 molecules per mm^2) for 2 hours, then washed 3X with PBS. T cells were washed and resuspended in cell imaging buffer (RPMI w/o phenol red (Gibco, 11835-03H), 1%FBS, 25mM HEPES), and incubated on bilayer for 40 minutes, followed by fixation with 4% PFA. Bilayers were washed 3X with PBS prior to imaging. Imaging was performed using a Nikon Eclipse Ti2 stand equipped with iLas2 module (Gataca Systems) using the Apo TIRF 100x/1.49 objective and 488nm (515/30), 561nm (595/31) 640nm (860/42) laser lines. Images were acquired with an Andor iXon-L-897 EMCCD camera. The microscope was controlled using Nikon NIS Elements software (version 5.41.01). Distribution of protein within synapse was quantified based on a previously described method [187]. Briefly, radial averages were generated by rotating cell images to all angles 1-359°, all rotated images were compressed to a single stack and z-project of mean intensity was taken.

Radial averages combined from all cells measured and intensity values were normalized to max intensity. Analysis was performed in Fiji (ImageJ2, version 2.9.0/1.53t).

Multiplexed calcium flux measurement by flow cytometry

CAR T cells and ChTCR T cells were harvested and washed once with phosphate buffer saline (PBS). Cells were stained with anti-human CD45 antibody (clone HI30), so that each receptor was stained with a unique CD45 fluorescent barcode (single or double stain with APC-CD45 (Biolegend, 304012), PE-CD45 (BD, 555483), PerCp-Cy-5.5-CD45 (BD, 564105), FITC-CD45 (Biolegend, 304006), BUV805-CD45 (BD, 612891)). Cells were washed three times, pooled 10^7 cells total. Cells were stained with 5μM indo-1AM dye (Invitrogen, I1223) in calcium stain buffer (phenol-free RPMI, 1%FBS, 0.5 mM probenecid (Sigma, P8761-100G), 10 mM HEPES) at 37° for 45 minutes. Cells were then washed twice with calcium stain buffer, resuspended in 4 mL calcium stain buffer, and split into 4 tubes. Prior to calcium measurement, cells were incubated with biotinylated proteins/antibodies (1 μg/mL CD19-biotin (Accro Biosystems, CD9-H82E9) , 0.5 μg/mL anti-CD28-biotin (Biolegend,302904)) for 5 minutes at 37°. Baseline indo-1AM fluorescence was measured for 30 seconds, before addition of 20μg/mL avidin to crosslink biotinylated proteins. Calcium flux was measured for 5 minutes before addition of 1X cell stimulation cocktail (Invitrogen, 00-4970). Multiplexed populations were deconvoluted and calcium plots generated in FlowJo software (BD), and area under the curve measurements made using Prism software (GraphPad).

Cell stimulation and western blot

Beads for T cell stimulation were prepared as previously described [111]. $2x10^6$ ChTCR and CAR T cells were washed with resuspended in 50ml warm CTL, incubated with either 30mL/10^6 beads or an equal number Nalm-6 cells for specified times, immediately washed with 1mL ice-cold PBS and lysed with NP40 RIPA lysis buffer (20nM TRIS pH8, 150mM NaCl, 1% NP40, 5mM EDTA, 0.1%SDS), supplemented with protease and phosphatase inhibitors (Thermo Scientific, 186093, 78428). Cell lysates were sonicated before centrifuging at 10,000g for 15 minutes at 4°C, when present, beads were removed during the lysate clearing step. Total protein concentration was quantified by Micro BCA assay (Thermo Scientific #23235). Equal masses of protein were loaded on Tris-glycine SDS gels (Bio-Rad, 4561086), and proteins were transferred to PDVF membrane (Bio-Rad, 1704274). Membranes were blocked with blocking buffer (Bio-Rad, 12010020), and incubated overnight with primary antibody diluted (1:2000-1:500) in blocking buffer. Membranes were washed three times for 5 minutes with Tris-Buffer Saline supplemented with 0.1% Tween, then incubated with secondary antibody diluted in blocking buffer (1:10,000). The following antibodies were used: phospho-LAT (Tyr 220) (Cell Signaling, 3584), phospho-LAT (Tyr 171)

(Biolegend, 946602), LAT (E3UCJ) (Cell Signaling, 45533), phospho-Zap 70 (Tyr319) (65E4) (Cell Signaling, 2717), Zap70 (D1C10E) (Cell Signaling, 3165), b-Actin (13E5) (Cell Signaling, 4970). Membranes were incubated with ECL substrate (Bio-Rad, 1705062) and imaged with iBright 1500 Imaging. Band intensities were quantified using ImageJ, normalized to total protein, loading control and control sample as indicated.

Cytokine measurement

T cell cytokine release was determined by measuring cytokine concentration in the supernatant after 18-24 hours of co-culture of ChTCR and CAR T cells with target cells or with plate-bound antigen. For target cell simulation, T cells and target cells were co-cultured at a 1:1 E:T ratio. After antigen stimulation, supernatant was harvested and cytokine concentration was determined by ELISA according to kit manufacture protocol: IL-2 (BioLegend, 431816) IFN-g (BioLegend, 430116). For plate-bound antigen stimulation, 96-well plates were coated with avidin (10μg/mL) overnight and incubated with PBS + 3% BSA to block non-specific protein binding. Avidin-coated plates were then coated with biotinylated extracellular protein domains for one hour at specific concentrations. 50,000 T cells were resuspended in 50μL CTL and transferred to antigen coated plates for incubation. In co-culture experiments against MOLP8 and H929 multiple myeloma cell lines, SLAMF7 antigen was masked to prevent recognition by BCMA/SLAMF7 Bi-ChTCR T cells by pre-incubating targets cells for 1h with Elozotumab antibody (10μg.ml, Selleckchem, A2034) from which the HuLuc63 scFv used to design the Bi-ChTCR is derived.

Cell proliferation assay

ChTCR and CAR T cells were harvested and washed with warm PBS. Cell Trace Violet (CTV) Cell Proliferation dye (Invitrogen, C34557) was resuspended in 200μL DMSO. T cells were resuspended in 1 mL PBS and incubated with 2μL CTV for 10 minutes at 37° C with periodic mixing. 1mL FBS was added to absorbed unbound dye, cells were washed and resuspended in CTL. T cells were co-cultured with Nalm-6 target cells expressing appropriate target antigen at 1:2 E:T ratio for 72 hours. Cells were harvested, washed with PBS, and stained with anti-CD8-APC antibody (Biolegend, 344722) before acquisition by flow cytometry.

Cytotoxicity assay

Target tumor cells were incubated with Cr^{51} overnight, washed, resuspended in culture media, and plated with effector T cells to achieve indicated E:T ratios. Plates were briefly centrifuged (100rpm for 1 minute), then incubated for 4 hours. After incubation, 30μL of supernatant was harvested, transferred to LumaPlates (Revvity, 6006633), and plates were

dried overnight. Plates were read by scintillation counter and percent specific lysis was calculated using the standard formula.

NSG mouse tumor model

6–8-week-old, female NOD/SCID/$gc^{-/-}$ mice were purchased from Jackson Laboratory or bread in-house. For the Raji model, mice were engrafted with 0.5 million Raji/GFP-ffluc intravenously by tail vain injection. For the Nalm-6 models, mice were engrafted with 0.5 million Nalm-6^{WT} GFP-ffluc or 1 million Nalm-6 GFP-ffluc cells that expressed low levels of CD19 antigens by tail vain injection. For experiments with bi-specific receptors, a heterogenous mixture of Nalm-6^{WT} and Nalm-6 cells expressing only a single antigen were engrafted. Antigen expression in all tumor lines was checked by flow cytometry prior to injection. Mice were injected intravenously 7 days (Raji/GFP-ffluc) or 4 days (Nalm-6/GFP-ffluc) after tumor inoculation with ChTCR of CAR modified $CD8^+$ and $CD4^+$ T cells at a 1:1 ratio or with PBS. Cell numbers were normalized based on total number of receptor positive cells in the total cell population, as determined by flow cytometry prior to infusion. Mice were followed by bioluminescence imaging after intraperitoneal injection of luciferin substrate using the Xenogen IVIS Imaging System (Caliper Life Sciences) and for survival. Living Image Software V4.7.3 (Caliper Life Sciences) was used to analyze luciferase activity and photon flux within regions of interest that encompassed the entire body of each individual mouse. Blood was obtained from mice at various timepoints, single-cell suspensions from peripheral blood were prepared by lysing red blood cells using ammonium-chloride-potassium (AKC) lysing buffer (Quality Biological, 118-156-101). Single-cell suspensions were stained with the following antibody panel for flow cytometry analysis; Nalm6-GFP, anti-CD45-PE (Biolegend, 304008), anti-CD8-BUV805 (BD, 612889), anti-CD4-cflour R840 (Cytec, R7-20165), rBCMA-biotin (Accro Biosystems, BCA-H82E4), rSLAMF7-biotin (Accro Biosystems, SL7-H82E0), streptavidin-APC (Invitrogen, 17-4317-82).

Immunoprecipitation of ChTCRs and CARs

HA-tagged ChTCR and CAR lentiviral constructs generated as described in ‘generation of constructs’ in expressed and expressed in primary human CD8 T cells as described. Cells expressing TCR without HA tag were used as a negative control. $30x10^6$ cells were washed 1X in PBS and lysed in 500uL Co-IP lysis buffer (20mM Tris-HCL pH8, 137mM NaCl, 2mM EDTA. 10% glycerol, 1X protease inhibitor, 1X phosphatase inhibitor (Thermo Scientific, 186093, 78428), 0.5% Brij O10 (Sigma, P6136-100g)), for 30 minutes on ice. Lysate was cleared by centrifugation at 10,000g for 15 minutes at 4°C. 10% of lysate was removed for whole cell lysate controls, and equal masses of the remaining lysate were used for anti-HA immunoprecipitation according to manufacturer instructions (ThermoFisher, 8836).

Immunoprecipitated proteins were analyzed by Western Blot as described in "Cell stimulation and Western Blot." Co-immunoprecipitated proteins were detected using the following antibodies. TCR α (H-1) (SCBT, sc-515719), TCR β (E9I1D) (Cell Signaling, 65123), CD247 (BD Pharmingen, 551034), CD3δ (F-1) (SCBT, sc-137137 HRP), CD3γ (EPR4517) (Abcam, ab134096), CD3ε (D7A6E) (85061), HA-tag (C29F4) (Cell Signaling, 3724)

Extended Data

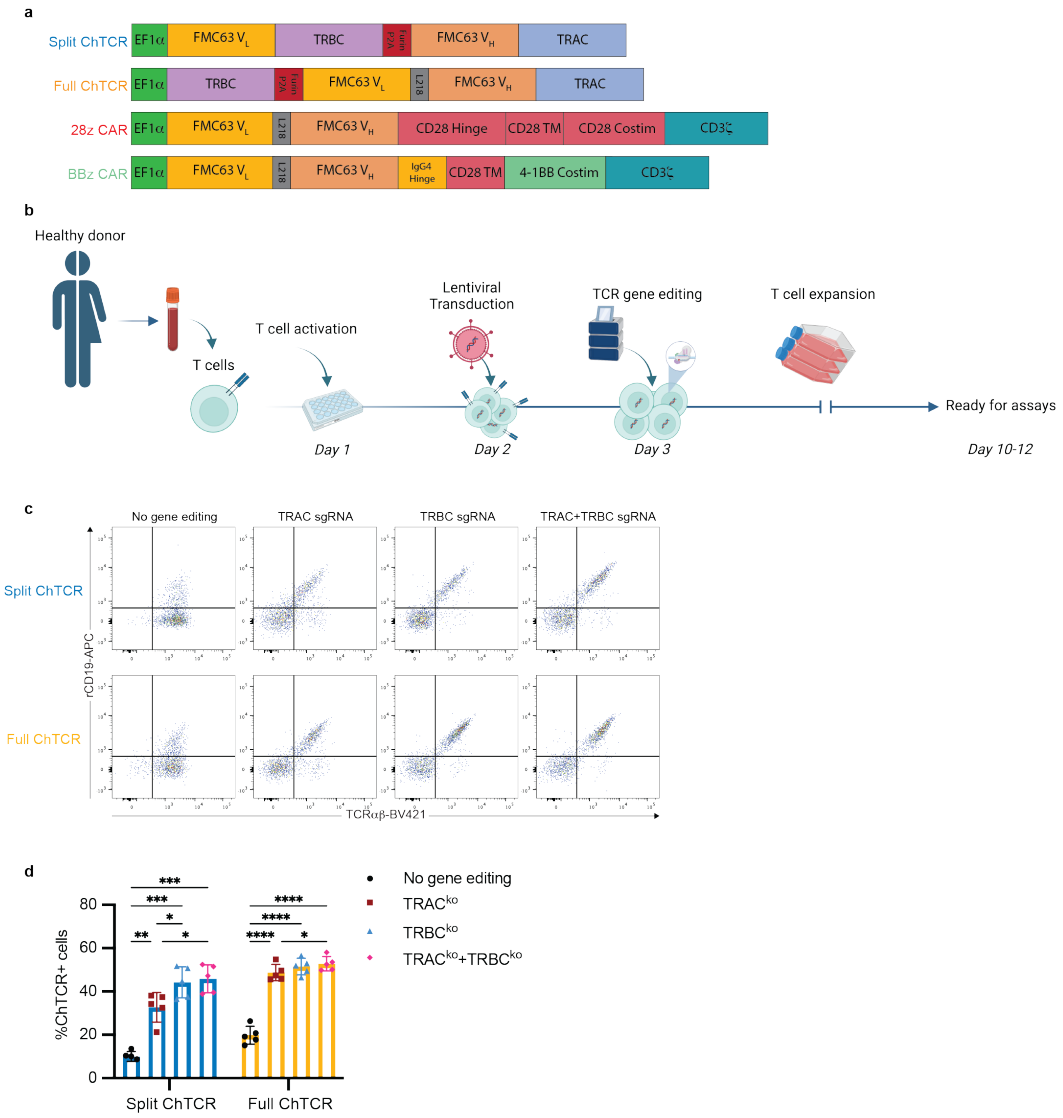

Extended Data Figure 3.1 Receptor constructs, T cell generation and gene editing a. Schematic of CD19-specific ChTCR and CAR receptor constructs. **b.** CAR and ChTCR transduction and cytosine base editing of TCRab genes primary T cells. **c.** Representative flow cytometry plots of ChTCR T cells stained with TCRab-BV421 and recombinant CD19 protein-APC without TCR knockout, after single TRAC KO, single TRBC KO or double TRAC and TRBC KO. **d.** Frequency of ChTCR$^+$ T cells without and with knockout of TRAC, TRBC or both. Data is shown as the mean ± SD for 5 independent experiments. *P<0.05, **P<0.01, ***P<0.001 and ****P<0.0001 by two-way ANOVA.

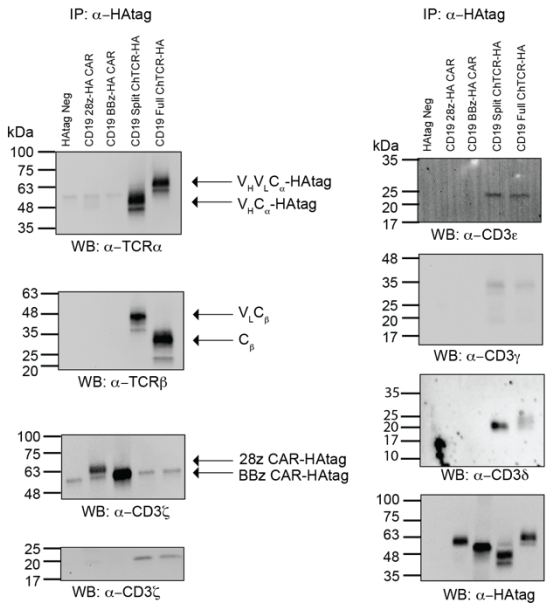

Extended Data Figure 3.2 ChTCRs assemble with all CD3 subunits in primary T cells Western blot analysis of TCRa, TCRb and CD3z, d, e and g subunits following immunoprecipitation of HA-tagged CAR and ChTCR receptors from transduced and gene edited primary T cell using and anti-HA tag antibody. Cell expressing a TCR receptor without an HA tag was used as a negative control. Proteins co-immunoprecipitated with each of the receptors were detected by western blot with antibodies specific to TCRa, TCRb and each of the CD3 subunits. Blotting with anti-HA was performed as a loading/immunoprecipitation control.

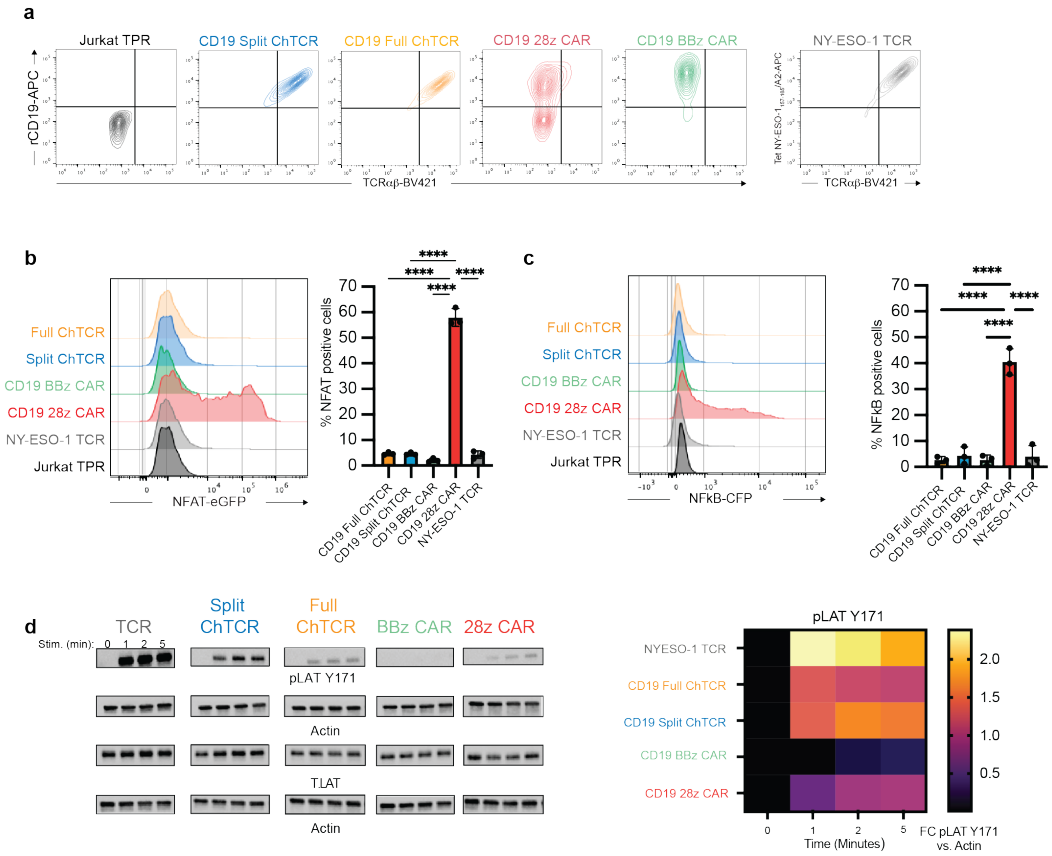

Extended Data Figure 3.3 CD19-specific ChTCRs lack tonic signaling in Jurkat TPR reporter cells a. Representative flow plots showing expression of CD19-specific ChTCRs and CARs (TCRab-BV421 and recombinant CD19-APC) and NY-

ESO-1-specific TCR 1G4 (TCRab-BV421 and NY-ESO-$1_{157-165}$/A2 tetramer-APC) in Jurkat J76 TPR cells. **b.** Left: Representative histogram of NFAT-eGFP reporter expression in J76 TPR Jurkat cells expressing the indicated receptors. Right: Mean frequency ± SD of NFAT-eGFP positive cells (n=3 independent experiments). ****P<0.0001 by two-way ANOVA. **c.** Left: Representative histogram of NFκB-CFP reporter expression in J76 TPR Jurkat cells expressing the indicated receptors. Right: Mean frequency ± SD of NFκB-CFP positive cells (n=3 independent experiments). ****P<0.0001 by two-way ANOVA. **d.** Left: Representative western blot analysis for LAT $pTyr^{171}$, Actin and LAT. Right: Heat map of mean band intensity of LAT $pTyr^{171}$ normalized to actin loading control (n=2 independent experiments).

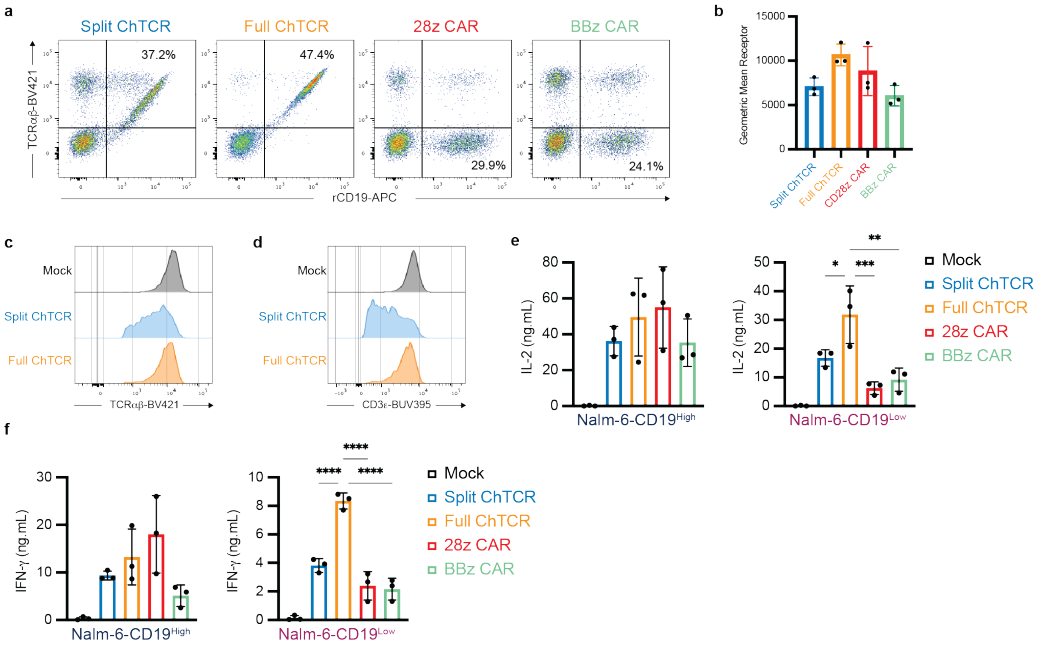

Extended Data Figure 3.4 Full ChTCR+ CD4+ T cells demonstrate superior antigen sensitivity a. Representative flow plots of primary CD4+ T cells stained with anti-TCRab antibody and recombinant CD19 protein 7 days after lentiviral transduction and base editing to knock-out endogenous TCRab expression. **b.** Geometric mean of rCD19-APC binding to primary T cells transduced with CARs or ChTCRs (n=3 biological independent samples). **c.** Representative TCRab expression by mock unedited and TCRab gene edited split and full $ChTCR^+$ T cells. **d.** Representative CD3e expression by mock unedited and TCRab gene edited split and full $ChTCR^+$ T cells. **e. and f**. Right: Concentration of IL-2 (**e**) and IFN-γ (**f**) in culture supernatant after overnight co-culture of T cells expressing each of the indicated receptors with Nalm-6 $CD19^{High}$ (left) of Nalem-6 $CD19^{Low}$ cells (Right) at an effector to target ratio (E:T) of 1:1. Data is shown as the mean ± SD for 3 independent experiments. *P<0.05, **P<0.01, ***P<0.001 by two-way ANOVA.

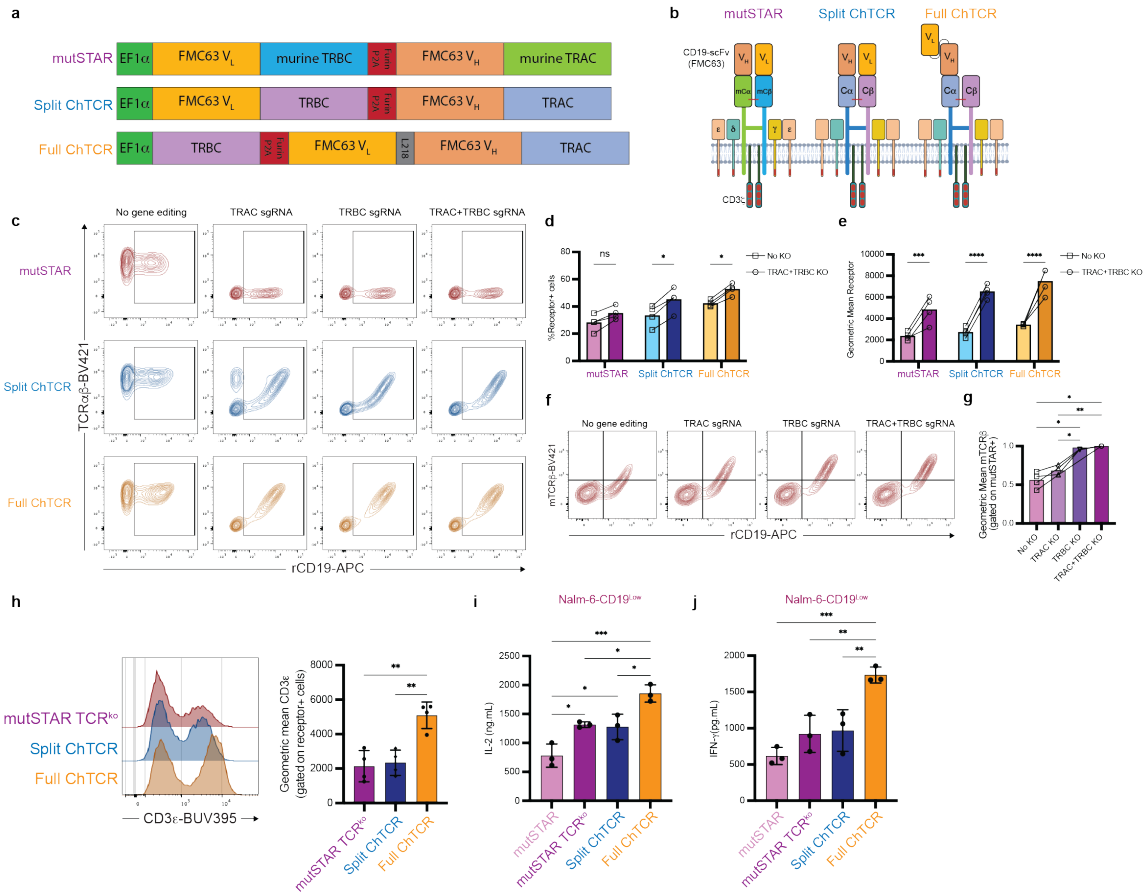

Extended Data Figure 3.5 Endogenous TCR KO improves expression and antigen sensitivity of mutSTAR receptor a. and b. Schematic of CD19-specific mutSTAR, split and full ChTCRs lentiviral constructs (**a**) and receptors assembled at the cell surface (**b**). **c.** Representative flow cytometry plots of mutSTAR and ChTCRs T cells stained with TCRab-BV421 and recombinant CD19 protein-APC without TCR knockout, after single TRAC KO, single TRBC KO or double TRAC and TRBC KO. **d.** Frequency of mutSTAR and ChTCR$^+$ T cells without TCR KO or with knockout of both TRAC and TRBC chains. Data is shown as the mean ± SD for 4 independent experiments. *P<0.05 by two-way ANOVA. **e.** Geometric mean of rCD19-APC binding to primary T cells transduced with mutSTAR or ChTCRs without TCR KO or with knockout of both TRAC and TRBC chains. Data is shown as the mean ± SD for 4 independent experiments. ***P<0.001 and ****P<0.0001 by two-way ANOVA. **f.** Representative flow cytometry plots of mutSTAR T cells stained with mouse TCRb-BV421 and recombinant CD19 protein-APC without TCR knockout, after single TRAC KO, single TRBC KO or double TRAC and TRBC KO. **g.** Geometric mean of mouse TCRb-BV421 in primary T cells transduced with mutSTAR without TCR KO, after single TRAC KO, single TRBC KO or double TRAC and TRBC KO. Data is shown as the mean ± SD for 4 independent experiments. *P<0.05 and **P<0.01 by two-way ANOVA. **h.** Right: Representative flow cytometry histogram of TCR KO T cells expressing mutSTAR, split and full ChTCR receptors stained with CD3e-BUV395 antibody. Left: Geometric mean of CD3e-BUV395 on TCR KO T cells expressing mutSTAR, split and full ChTCR receptors. Data is shown as the mean ± SD for 3 independent experiments. **P<0.01 by two-way ANOVA. **i. and j**. Concentration of IL-2 (**i**) and IFN-γ (**j**) in culture supernatant after overnight co-culture of T cells expressing each of the indicated receptors with Nalm-6 CD19^{Low} target cells at an effector to target ratio (E:T) of 1:1. Data is shown as the mean ± SD for 3 independent experiments. *P<0.05, **P<0.01, ***P<0.001 by two-way ANOVA.

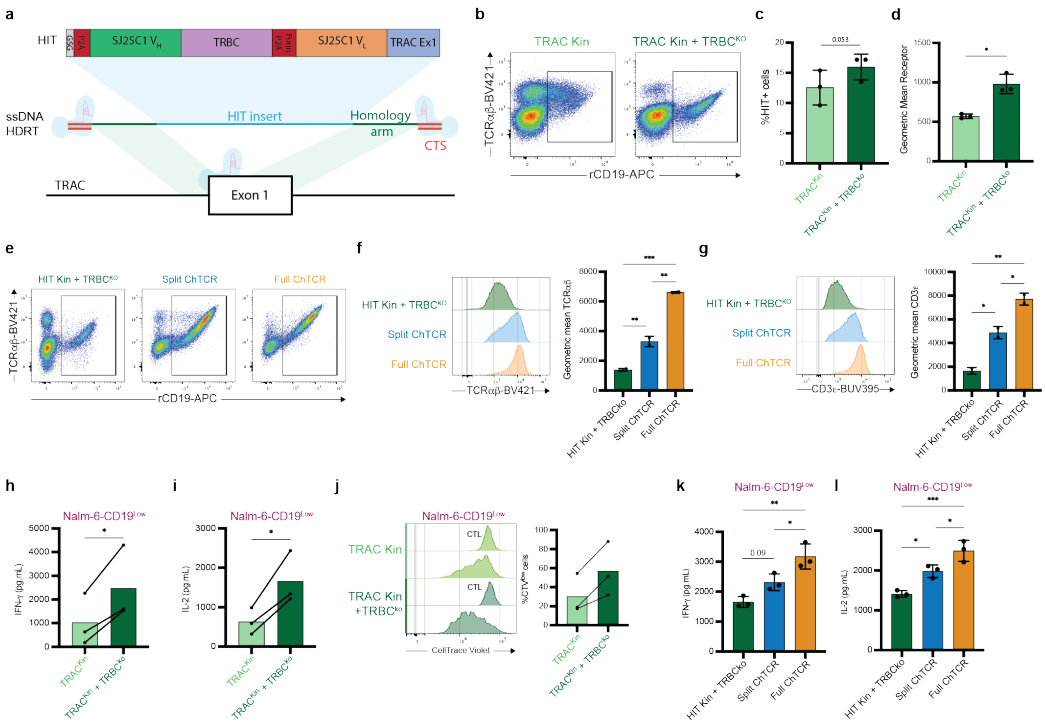

Extended Data Figure 3.6: Endogenous TCR KO improves expression and antigen sensitivity of HIT receptor. a. Schematic of CD19-specific HIT receptor and its targeted knock-in within the TRAC locus. **b.** Representative flow cytometry plots of TRAC-knocked-in HIT T cells stained with TCRab-BV421 and recombinant CD19 protein-APC with or without TRBC KO. **c.** Frequency of HIT$^+$ T cells with or without TRBC KO. Data is shown as the mean ± SD for 3 independent experiments. **d.** Geometric mean of rCD19-APC binding to primary T cells expressing the HIT receptor with or without TRBC KO. Data is shown as the mean ± SD for 3 independent experiments. *P<0.05 by two-way ANOVA. **e.** Representative flow cytometry plots of primary T cells expressing HIT, split or full ChTCR receptors stained with TCRab-BV421 and recombinant CD19 protein-APC with TCR KO. **f.** Geometric mean of TCRab-BV421 in TCR KO T cells expressing HIT, split or full ChTCR receptors. Data is shown as the mean ± SD for 3 independent experiments. **P<0.01, ***P<0.001 by two-way ANOVA. **g.** Geometric mean of CD3ε-BUV395 in TCR KO T cells expressing HIT, split or full ChTCR receptors. Data is shown as the mean ± SD for 3 independent experiments. *P<0.05, **P<0.01 by two-way ANOVA. **h and i.** Concentration of IFN-γ (**h**) and IL-2 (**i**) in culture supernatant after overnight co-culture of T cells expressing the HIT receptor with or without TRBC KO with Nalm-6 CD19^{Low} target cells at an effector to target ratio (E:T) of 1:1. Data is shown as the mean for 3 independent experiments. *P<0.05 by two-way ANOVA. **j.** Left: Representative histograms of CellTrace Violet (CTV) dye dilution in T cells expressing the indicated receptors measured after 3 days of co-culture with Nalm-6 CD19^{Low} tumor cells. Right: Percent of divided cells (mean) for 3 independent experiments. **k and l.** Concentration of IFN-γ (**k**) and IL-2 (**l**) in culture supernatant after overnight co-culture of TCR KO T cells expressing HIT, split or full ChTCR receptors with Nalm-6 CD19^{Low} target cells at an effector to target ratio (E:T) of 1:1. Data is shown as the mean ± SD for 3 independent experiments. *P<0.05, **P<0.01, ***P<0.001 by two-way ANOVA.

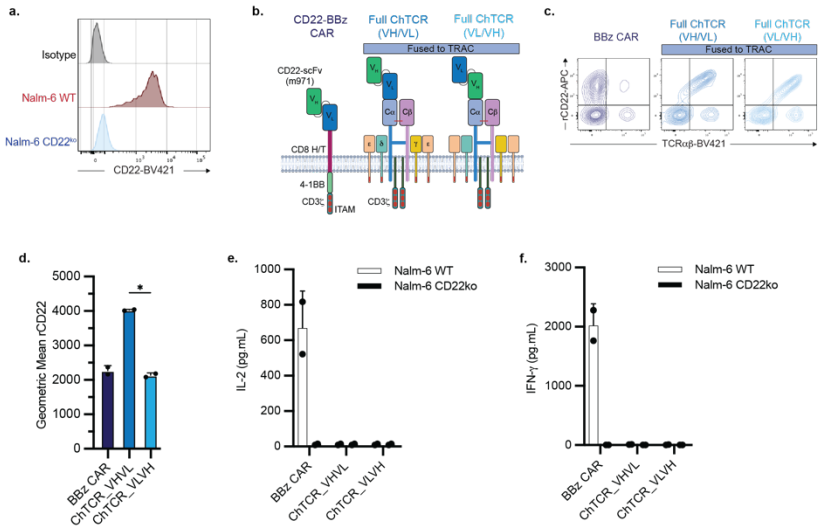

Extended Data Figure 3.7 TRAC usage does not improve m971-based ChTCR T cell functions a. CD22 expression measured by flow cytometry on Nalm-6 WT or CD22^{ko}. **b.** Schematic of anti-CD22 CAR and Full ChTCRs using m971 scFv in VH/VL or VL/VH orientation fused to TRAC. **c.** Representative flow plots showing expression of CD22-specific CAR and Full ChTCRs in primary CD8+ T cells (TCRα/β-BV421 and rCD22-APC). **d.** Geometric mean ± SD of rCD22-protein-APC bound to receptors (n=2 independent experiments). *P<0.05 by two-way ANOVA. **e. and f.** Concentration of IL-2 (**e**) or IFN-γ (**f**) in culture supernatant after overnight co-culture of CAR and ChTCR T cells with the indicated Nalm-6 cells (mean ± SD, n=2 independent experiments).

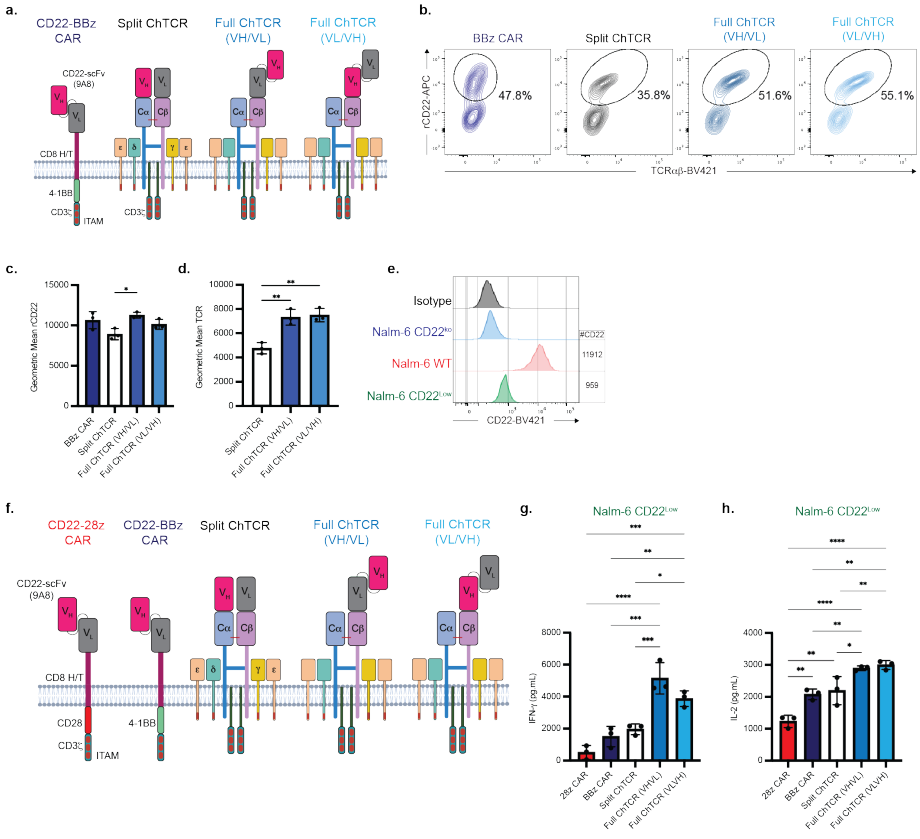

Extended Data Figure 3.8 T cells expressing the CD22-specific Full ChTCR demonstrate superior antigen sensitivity a. Schematic of CD22-specific CAR, Split ChTCR and Full ChTCRs using 9A8 scFv. **b.** Representative flow plots of CAR and ChTCR expression on primary CD8 T cells stained with TCRab-BV421 and recombinant CD22-protein-APC. **c.** Geometric mean ± SD of recombinant CD22-protein-APC bound to CD22-specific receptors (n=3 independent

experiments). *P<0.05 by two-way ANOVA. **d.** Geometric mean ± SD of TCRab-BV421 expression by CD22-specific ChTCRs (n=3 independent experiments). **P<0.01 by two-way ANOVA. **e**. CD22 expression by Nalm-6 WT, CD22^{ko} and CD22^{Low} target cells measured by flow cytometry. **f.** Schematic of CD22-specific 28z and 4-1BBz CARs, Split ChTCR and Full ChTCRs using 9A8 scFv. **g. and h.** Concentration of IFN-γ (**g**) and IL-2 (**h**) in culture supernatant after overnight co-culture of T cells expressing indicated CD22-specific receptors with Nalm-6 CD22^{Low} target cells at an effector to target ratio (E:T) of 1:1. Data is shown as the mean ± SD for 3 independent experiments. *P<0.05, **P<0.01, ***P<0.001, ****P<0.0001 by two-way ANOVA.

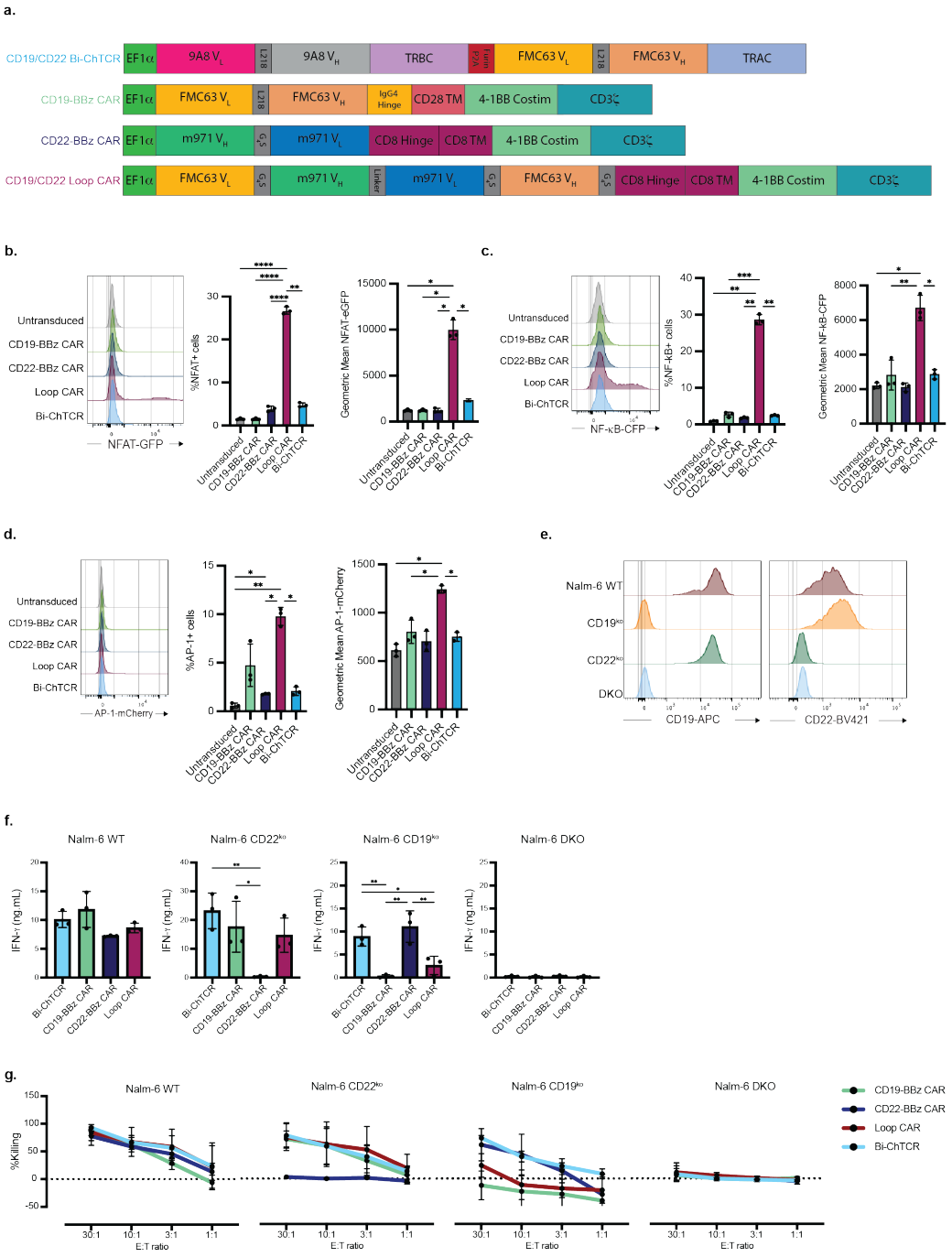

Extended Data Figure 3.9 Design and function of bispecific CD19/CD22 ChTCR a. Schematic of CD19- and CD22-mono- and bispecific receptor constructs. **b-d.** Left: Representative histograms of NFAT-GFP (b), NFκB-CFP (c) and AP-1-mCherry (d) reporter expression in J76 TPR Jurkat cells expressing the indicated receptors. Middle: Frequency of NFAT-

GFP (b), NFκB-CFP (c) and AP-1-mCherry (d) positive cells. Right: Geometric mean ± SD of NFAT-GFP (b), NFκB-CFP (c) and AP-1-mCherry (d) reporter genes (n=3 independent experiments). *P<0.5, **P<0.01, *** P<0.001, ****P<0.0001 by two-way ANOVA. **e.** CD19 and CD22 expression by Nalm-6 WT, $CD19^{+}CD22^{ko}$, $CD19^{ko}CD22^{+}$ and $CD19^{ko}CD22^{ko}$ target cells measured by flow cytometry. **f.** Concentration of IFN-γ in culture supernatant after overnight co-culture of T cells expressing the indicated CARs and Bi-ChTCRs with indicated Nalm-6 cell lines. Data is shown as the mean ± SD for 3 independent experiments. *P<0.05 and **P<0.01 by two-way ANOVA. **g.** Cytotoxicity of the indicated Nalm-6 cell lines by CAR and Bi-ChTCR T cells at varying E:T ratios.

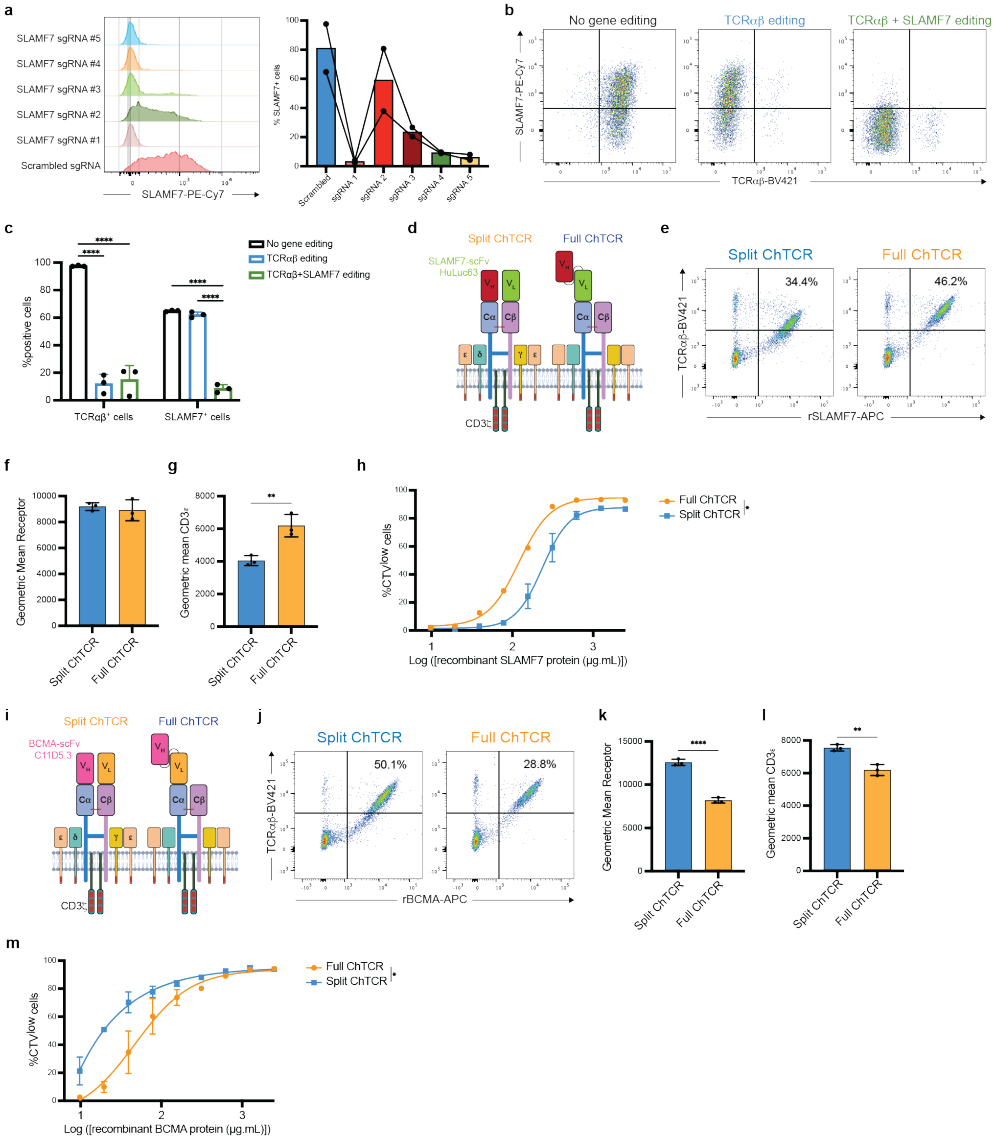

Extended Data Figure 3.10 Comparison of Split and Full ChTCR formats specific for BCMA and SLAMF7 antigens a. Left: Representative flow histograms of SLAMF7 expression on primary CD8 T cells KO for SLAMF7 using CBE and 5 different SLAMF-7 specific sgRNAs. Right: Frequency of SLAMF7+ cells after gene editing (n=2 independent experiments). **b.** Representative flow plots of CD8 primary T cells edited or not for TRAC and TRBC and/or SLAMF7. **c**. Frequency ± SD of TCRab and SLAMF7+ cells after TRAC and TRBC KO with or without concomitant SLAMF7 KO (n=3 independent experiments). ***P<0.001 and ****P<0.0001 by two-way ANOVA. **d.** Schematic of SLAMF7 split and full ChTCRs. **e.** Representative flow cytometry plots of split and full ChTCR T cells stained with TCRab-BV421 and recombinant SLAMF7 protein-APC. **f.** Geometric mean of rSLAMF7-APC binding to primary T cells transduced with split and full ChTCRs. Data is shown as the mean ± SD for 2 independent experiments. **g.** Geometric mean of CD3e-BUV395 in primary T cells transduced with split and full ChTCRs. Data is shown as the mean ± SD for 2 independent experiments. **P<0.01 by two-

way ANOVA. **h.** Percent of divided cells after co-culture of SLAMF7-specific split and full ChTCR T cells on plate-bound antigen for 3 days (mean ± SD for 2 independent experiments). *P<0.05 by two-way ANOVA. **i.** Schematic of BCMA-specific split and full ChTCRs. **j.** Representative flow cytometry plots of split and full ChTCR T cells stained with TCRab-BV421 and recombinant BCMA protein-APC. **k.** Geometric mean of rBCMA-APC binding to primary T cells transduced with split and full ChTCRs. Data is shown as the mean ± SD for 2 independent experiments. ****P<0.0001 by two-way ANOVA. **l.** Geometric mean of CD3e-BUV395 in primary T cells transduced with split and full ChTCRs. Data is shown as the mean ± SD for 2 independent experiments. **P<0.01 by two-way ANOVA. **m.** Percent of divided cells after co-culture of BCMA-specific split and full ChTCR T cells on plate-bound antigen for 3 days (mean ± SD for 2 independent experiments). *P<0.05 by two-way ANOVA.

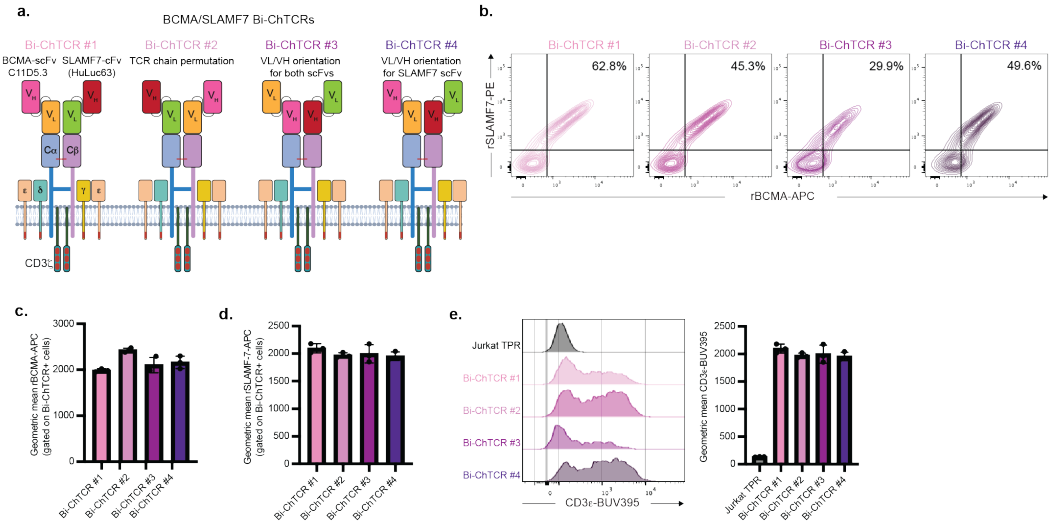

Extended Data Figure 3.11 Optimizing design of BCMA/SLAMF7 Bi-ChTCRs a. Schematic of BCMA/SLAMF7 Bi-ChTCR receptors with different configurations of VH/VL and linkage to TCR chains. **b.** Representative flow plots of Jurkat 76 TPR cells expressing the indicated Bi-ChTCR receptors after staining recombinant SLAMF7 and BCMA protein. **c. and d.** Geometric mean ± SD of rBCMA-PE (c) and rSLAMF7-APC (d) bound to receptors (gated on Bi-ChTCR+ cells; n=3 independent experiments). **e.** Right: Representative histogram of CD3ε expression in Bi-ChTCR+ and Jurkat TPR cells. Right: Geometric mean ± SD of CD3ε expression (gated on Bi-ChTCR+ cells; n=3 independent experiments).

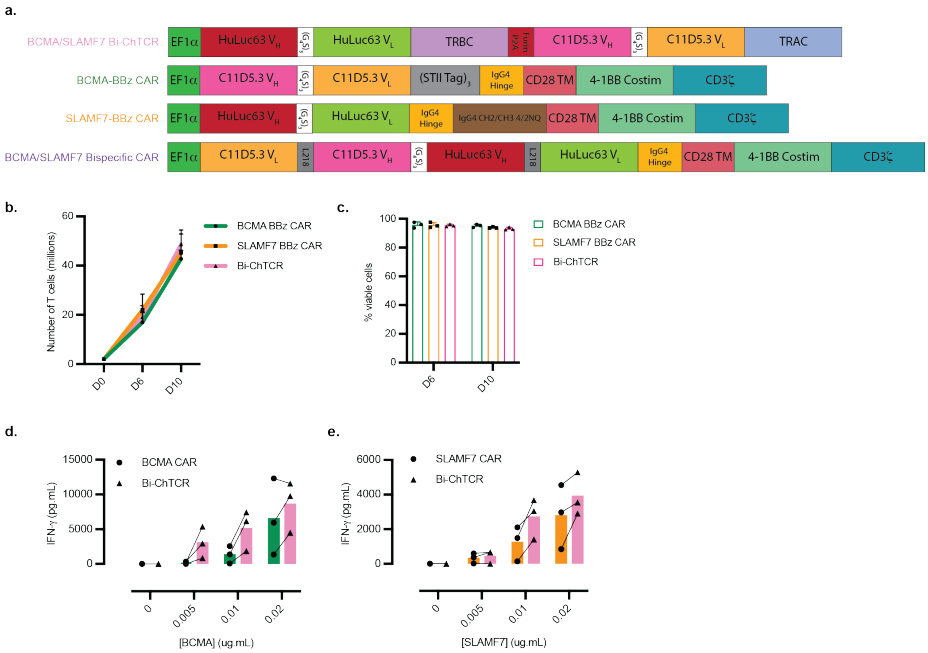

Extended Data Figure 3.12: BCMA/SLAMF7 receptor constructs and antigen sensitivity of BCMA/SLAMF7 Bi-ChTCR

T cells a. Schematic of SLAMF7- and BCMA- mono- and bispecific receptor constructs. **b.** Absolute numbers ± SD of BCMA and SLAMF7 CAR and Bi-ChTCR T cells. **c.** Viability ± SD of BCMA and SLAMF7 CAR and Bi-ChTCR T cells (n=3 independent experiments). **d. and e.** INF-γ production (pg/mL) of CAR and Bi-ChTCR to various concentrations of plate bound recombinant BCMA protein (d) or recombinant SLAMF7 protein (e) (n=3 independent experiments).

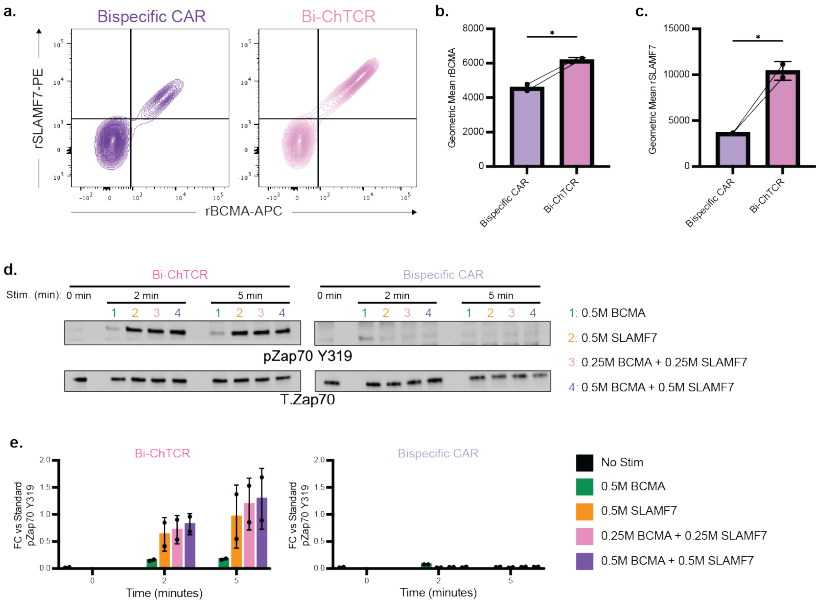

Extended Data Figure 3.13 T cells expressing the BCMA/SLAMF7 Bi-ChTCR are superior to a bispecific CAR for antigen binding and proximal signaling a. Representative flow plots showing binding of recombinant BCMA-APC and SLAMF7-PE to primary CD8 T cells transduced with the BCMA/SLAMF7 bispecific CAR and Bi-ChTCR. **b. and c.** Geometric mean ± SD of rBCMA-APC (b.) and rSLAMF7-PE binding to bispecific CAR and bi-ChTCR T cells (c.) (gated on receptor positive cells; n=2 independent experiments). **d.** Representative western blot analysis for pZap70 pTyr^{319} and Zap70 for Bi-ChTCR or bispecific CAR stimulated with 0.5M of rBCMA (1), 0.5M of rSLAMF7 (2), 0.25M of rBCMA + 0.25M rSLAMF7 (3) or .05M rBCMA + 0.5M rSLAMF7 (4) coated-beads for indicated time. **e.** Mean band intensity ± SD for pZap70 pTyr^{319} normalized to standard (n=2 independent experiments).

Chapter 4: A Mass Cytometry approach to study T cell signaling and function

This chapter presents the preliminary data for the project that will be the focus of my post-doctoral work

Aims

We have developed two novel receptors; the monospecific 'Full ChTCR' and the dual antigen targeting "Bi-ChTCR" that have enhanced sensitivity compared to CARs. The CD19 Full ChTCR showed greater antigen sensitivity than 28ζ and 4-1bbζ CARs and improved sensitivity over receptors with similar architecture; the Split ChTCR, HIT and mutSTAR. The Bi-ChTCR demonstrated improved antigen targeting and sensitivity over bispecific CARs. This novel receptor addresses two main factors limiting CAR T cell function, antigen loss and down regulation. Still, questions remain about how these receptors function so well, and what changes could be made to further improve these receptors.

Despite sharing intracellular signaling domains, the Full ChTCR has improved sensitivity over Split ChTCR, suggesting distinct signaling and cellular outcomes. While Western blot analysis demonstrated differences between ChTCR and CAR signaling, we have not identified differences between the Full and Split receptors that explain their diverging function. A more comprehensive analysis of early signaling events may help to reveal differences between these receptors that explain their different function. Additionally, incorporation of co-stimulatory molecules into HIT and mutSTAR receptors was shown to improve their sensitivity and function [129, 130]. Co-stimulation could similarly benefit Full ChTCR and Bi-ChTCR function. However, incorporation of co-stimulation might risk of driving excess cytokine production and short-lived effector differentiation [69]. A study of the signaling and differentiation of new ChTCR designs that incorporate co-stimulation would aid in the screening and development of new receptors.

We aim to develop a high-parameter mass cytometry panel to address these questions and ultimately inform future chimeric receptor designs.

Introduction

Efforts to improve receptors for adoptive T cell therapies for cancer have focused on improving the receptor-proximal signaling, with the aim to better recapitulate native T cell receptor (TCR) signaling and ultimately improve receptor sensitivity and T cell function. While many new receptors have been proposed, there is still a need to benchmark their functions, relating the signaling improvements of the receptors to the function of the T cells they are expressed in. Assessing synthetic receptors in-vitro remains a key bottle neck in the development of receptors for T cell therapy. Traditional in-vitro 'benchmarks' do not always translate to efficacy in-vivo. There is a need for tools to better assess receptor function, and to identify the origin of deficits or advantages observed from use of these receptors either in pre-clinal mouse models or in patients.

We developed a mass cytometry tool for the analysis of proximal signaling, paired with the ability to track fate and function of T cells over the course of days. This panel integrates the assessment of early signaling events, metabolic changes, the expression of transcription factors, and expression of surface receptors indicative of cell activation and differentiation state. This tool can capture the many changes in a T cell after antigen recognition and will be a valuable tool in the development of novel receptors for use in adoptive T cell therapies.

Design

Improving proximal receptor signaling is a goal of many new Chimeric Antigen Receptor (CAR) designs [123, 124, 129, 130] (Simon and Bugos, *In Press)*. The assessment of these receptor's signaling capabilities has typically used methods including Western blot or Mass Spectrometry that measures changes in phosphorylation states of bulk populations, relative to a base line measurement or other receptors. While these approaches can identify population-level changes, single cell resolution can more detail of early signaling events. TCR-proximal signaling occurs very rapidly, resulting in a heterogenous population of responding cells. Furthermore, genetically engineered cell products are not a homogenous population, they are generated from a mixture of T cell phenotypes. These differences are further driven by the activation, receptor introduction and expansion steps of T cell engineering, which generate additional cell phenotypes that may very between receptor types and impact T cell function [188, 189]. Differences in these starting populations can result in differences in cell signaling and function that are not captured by measurement of bulk population signaling. Additionally, single-cell resolution allows for the detection of co-variating phosphorylation events, providing information about how one signal may influence another [190]. Single-cell methods are well suited to capture these early, rapidly occurring events [191]. Mass cytometry can detect protein phosphorylation state using phospho-site specific antibodies conjugated to metal tags. Metal-labeled antibodies allow for the inclusion of large number of targets because of limited 'spill-over' effects common in fluorescent-based cytometry. Furthermore, metal-tagged antibodies are more resilient than fluorescent-tagged antibodies to the harsh permeabilization methods required for the detection of intracellular phosphorylated proteins, including methanol permeabilization.

To design a receptor proximal signaling panel we included key early signaling intermediates LCK and ZAP70 and CD3ζ. When available, we included multiple phosphorylation sites to capture both activating and inhibitory signaling events. We also included proteins recruited to the LAT signalosome, as deficiencies in LAT signaling has been observed in CAR signaling [111]. In addition to LAT itself, we included the adaptor protein SLP76, the kinase

ITK, and enzyme PLCγ1. To examine signaling downstream of the LAT signalosome we included ERK, pS6, and ATK along with STAT5 to capture MAPK and IL-2 signaling and SHP2 to measure a negative regulator of receptor signaling (**Figure 4.1**)

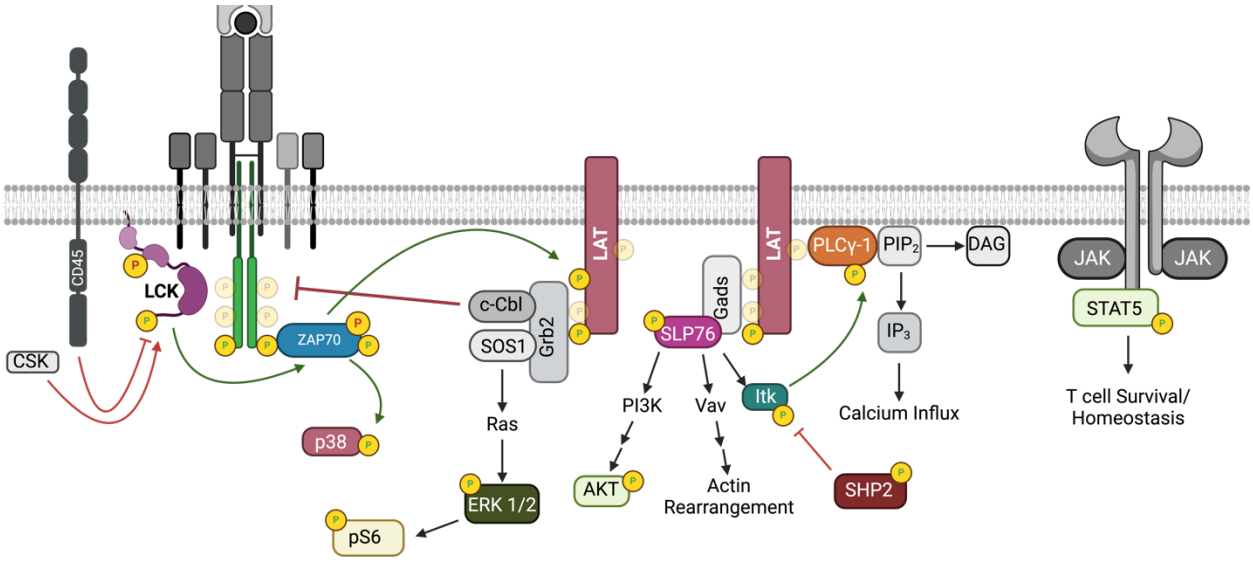

Figure 4.1 Phosphorylated proteins detected by mass cytometry Diagram depiction of proximal T cell signaling, phosphorylation of antibodies indicated with colored cartoon are included in the panel, activating (green) or inhibiting (red) phosphorylation sites are indicated

After a T cell is activated it undergoes metabolic remodeling that influences cell fate and functional capabilities [192]. Early activated T cells generally show simultaneous oxidative and glycolytic activity, while memory cells shift to high oxidative and low glycolytic activity; short lived effectors have the opposite, highly glycolytic and low oxidative activity [193]. Metabolic state similarly correlates with CAR function and persistence. CARs incorporating the 4-1bb costimulatory domain generally show better persistence and central memory differentiation, they also have greater mitochondrial biogenesis and oxidative metabolism compared to CARs with a CD28 costimulatory domain, which favor an effector memory phenotype, lower levels of mitochondrial biogenesis, and increased glycolytic metabolism [69]. These data from both TCR and CAR T cells demonstrate that measuring the metabolic activity of T cells can inform us of their functional potential. We will measure the expression levels of key metabolic regulators, including VDAC – a mitochondrial ion channel that's expression correlates with oxidative phosphorylation activity, HK2 – an enzyme regulating glucose metabolism, ATP5A – a component of the oxidative phosphorylation pathway, CPT1a – a measure of fatty acid oxidation, and CD98 – an amino acid transporter critical for the import of cell nutrients [193, 194]. In additions to measuring expression of proteins directly involved in metabolic pathways we have included an anti-puromycin antibody in the panel to detect protein synthesis. The antibiotic puromycin is incorporated into protein peptides, halting synthesis. The amount to puromycin peptides in

a puromycin-treated cell corresponds to the rate of protein synthesis. These peptides can be detected with an anti-puromycin antibody [195].

The strength of the signal at T cell receives to initiate activation can influence how T cells differentiate into distinct subsets of phenotypic and functional properties. These subsets are associated with different therapeutic efficacy and self-renewal compacity, impacting whether a T cell therapy is initially effective, and whether this efficacy can be sustained [196]. Surface receptor and transcription factor expression are commonly used identifiers of T cell differentiation state and functional potential. Mass cytometry has proven to be an effective tool to identify cell state and functional capacity [197, 198]. To identify T cell phenotypes, we have incorporated canonical markers of T cell differentiation. Markers of T cell activation included in the panel are PD-1, CD137(4-1bb), and CD25. T cell subsets can be identified by first distinguishing $CD8^+$ and $CD4^+$ T cell lineages with additional surface markers and transcription factors to identify T cell naïve, memory, effector, exhausted and regulatory populations (**Table 4.1**).

	T_N	T_{scm}	T_{CM}	T_{EM}	T_{EFF}	T_{EX}	T_{reg}
CCR7	+++	+++	++	-	-	-	-
CD27	+++	+++	++	+/-	-	-	-
CD28	++	+++	+++	+/-	-	+/-	+
CD45RA	+	+	-	+/-	- (+)	-	-
CD95	-	++	+++	+++	+	+++	+
CD127	+++	+++	+	+	+/-	-	-
CD57	-	-	-	-/+	+++	-/+	-
PD-1	-	-	-	-	+/-	+++	-/+
CD39	-	-	-	-	+/-	+	+
CD25	-	-	-	-	+/-	-	+++
FoxP3	-	-	-	-	-	-	+
IRF4	-	-	-	+	+++	+/-	-/+
Tcf1	+++	+++	+	-/+	-/+	-	-
EOMES	+	+	+	++	+++	+/-	-
T-bet	-	+	++	+++	+++	+	-
TOX	-	-	-	+/-	+/-	+++	-

Table 4.1 Markers to distinguish T cell phenotypes Expected expression levels of surface receptors (blue) and transcription factors (green) in indicated cell types. Naïve T cell (T_N), Memory Stem Cell (T_{SCM}), Central Memory (T_{CM}), Effector Memory (T_{EM}), Effector (T_{EFF}), Exhausted (T_{EX}), Regulatory (T_{reg}) T cell populations. Typical expression levels indication: Negative (-), varying or mixed expression (+/- or -/+), low expression (+), intermediate expression (++), high expression (+++). Table modified from [196]

An additional feature of this panel is the ability to track T cell proliferation. While cells can be collected at different timepoints, this does not capture how the T cell has proliferated. Carboxyfluorescein succinimidyl ester (CFSE) dilution, is a tool developed for flow cytometry to track cell divisions. This dye remains in the cytosol for days, when a cell divides the dye is diluted, so lower levels of dye indicate cells that have undergone cell divisions. Dividing cells pass on ~50% of dye to their daughter cell, this relationship allows for the approximation of the number of cell divisions undergone when compared to the intensity of dye in non-divided cells. CFSE labeling has been adapted for mass cytometry

through the use of anti-FITC antibodies, which detects CFSE dye in the cell cytosol [199]. The inclusion of CFSE detection will allow us to follow cell fate over both time and cell division state.

Lastly this panel will include nine anti-CD45 antibodies for use in a combinatorial barcoding scheme. A nine-chose-3 barcode scheme can label up to 84 unique populations, before pooling samples for simultaneous antibody staining and data collection. Sample barcoding reduces the effect of procedural variations in final data analysis, improving our ability to make conclusions about differences between conditions tested [200, 201]. With barcodes, DNA and viability stain, we developed a 56-marker mass cytometry panel for the analysis of signaling and differentiation of engineered T cells (**Table 4.2**).

Marker	Clone	Mass	Element	Utility
CD45	HI30	89	Y	Barcode_1
CD45	HI30	102	Pd	Barcode_7
CD45	HI30	104	Pd	Barcode_8
CD45	HI30	106	Cd	Barcode_2
CD45	HI30	108	Pd	Barcode_9
CD45	HI30	110	Cd	Barcode_3
CD45	HI30	111	Cd	Barcode_4
CD8	RPA-T8	112	Cd	Cell Type
CD137	4B4-1	113	Cd	Activation
Barcode_5	HI30	114	Cd	Barcode_5
CD57	HNK-1	115	In	Differentiation/Exhaustion
Barcode_6	HI30	116	Cd	Barcode_6
Beads		140	Ce	Normalization
FoxP3	QA18A03	141	Pr	TF_Treg
pAKT S473	D9E	142	Nd	TCR/coreceptor signaling
Cleaved Caspase 3	D3E9	143	Nd	Cell Death
CD4	OKT4	144	Nd	Cell Type
CD45RA	HI100	145	Nd	Differentiation
PD1	EH12.2H7	146	Nd	Activation/Exhaustion
Puromycin	12D10	147	Sm	Protein Synthesis
pPLC Y783	A17025A	148	Nd	Proximal TCR signaling
pITK Y511	24a/BTK	149	Sm	Proximal TCR signaling
pSTAT5	47	150	Nd	IL2 receptor JAK/STAT signaling
CD127	QA18A44	151	Eu	Differentiation
IRF4	3E4	152	Sm	TF_Activation
pCD3z Y142	K25-407.69	153	Eu	Proximal TCR signaling
Tcf1	7F11A10	154	Sm	TF_Memory
CD25	BC96	155	Gd	Activation
TOX	Rea473	156	Gd	TF_Exhaustion
pLCK Y394	A18002D	157	Gd	Proximal TCR signaling
CD27	M-T271	158	Gd	Differentiation
VDAC1	20B12AF2	159	Tb	Metabolism/OXPHOS
CD95	EOS9.1	160	Gd	Differentiation
pZap70 Y319	17A/pZap70	161	Dy	Proximal TCR signaling
pLCK Y505	4/LCK-Y505	162	Dy	Proximal TCR signaling/neg
pZAP70 Y292	A160338B	163	Dy	Proximal TCR signaling/neg
EOMES	WD1928	164	Dy	TF_Effector
pLAT Y171_PE	I58-1169	165	Ho	Proximal TCR signaling
T-Bet	4B10	166	Er	TF_Effector
pERK1/2 T202/Y204	D13.14.4E	167	Er	RAS/MAPK singling
CCR7	G043H7	168	Er	Differentiation
HK2	EPR20839	169	Tm	Metabolism/Glucose met.
pSLP76 Y128	J141-668.36.	170	Er	Proximal TCR signaling
anti-FITC (CFSE staining)	polyclonal	171	Yb	Proliferation
CD39	A1	172	Yb	Exhaustion
CD28	CD28.2	173	Yb	Differentiation
ATP5A	15H4C4	174	Yb	Metabolism/OXPHOS
pS6 S235/236	N7-548	175	Lu	mTORC/MAPK signaling
CPT1A	8F6AE9	176	Yb	Metabolism/Fatty Acid Met.
DNA_1	-	191	Ir	Cell
DNA_2	-	193	Ir	Cell
Cyclin B1	GNS-1	194	Pt	Cell Cycle
Cisplatin	-	195	Pt	Viability
p-p38 T180/Y182	D3F9	196	Pt	MAPK signaling
CD98	UM7F8	198	Pt	Metabolism/Amino Acid Transpo
pSHP2 Y580	DD66F1	209	Bi	Proximal TCR signaling/neg

Table 4.2 56-marker Mass Cytometry panel for the characterization of T cell signaling metabolic function and cell differentiation

Results

Panel optimization and testing

ChTCR T cells, which use native TCR machinery, have been shown to have improved sensitivity to target antigen over CARs [Simon and Bugos, *In Review*]. These receptors have improved proximal signaling, and synapse formation compared to CAR. Furthermore, different ChTCR architectures, Full and Split ChTCR, have different functional capacity. Full ChTCR outperform Split ChTCR in pre-clinical mouse models. To better characterized early signaling and T cell differentiation we compared Full ChTCR, Split ChTCR, 28ζ CAR and 4-1bbζ CAR using the 56-marker mass cytometry panel we have developed. We aim to monitor signaling and cell differentiation in a co-culture system, where T cells are stimulated by tumor cells mimic in-vivo T cell tumor cell interactions.

Many assays to study T cell signaling stimulate cells using anti-CD3 and anti-CD28 antibodies that are either crosslinked by soluble avidin, secondary antibody, or immobilized on beads or a plastic surface [190, 202]. This approach has the advantage of a reductionist system, with direct control of which signaling pathways are activated, and simple titration of the amount of stimulation. However, soluble antibody or bead stimulation may not recapitulate the signaling initiated by a cell-cell interaction, particularly due to a lack of synapse formation. Furthermore, the engineered T cell response to tumor cell lines, particularly pre-B acute lymphoblastic leukemia cell line Nalm-6, has been well characterized both in-vitro and in-vivo [123, 130, 203]. Stimulating T cells with Nalm-6 cells in this assay will help to related findings from mass cytometry to the conclusions of others.

Single-cell measurement is well suited to study signaling in co-culture systems because T cells can be identified in a population with target cell. To simplify the identification T cells from Nalm-6 cells, without addition of Nalm-6 specific markers, we took advantage of the CD45 barcode system we have implemented in the panel. Each condition in the co-culture system will get a unique 3-isotope barcode using a combination of anti-CD45 antibodies. To prevent the barcoding of Nalm-6 cells in co-culture we used CRISPR Cas9 to knock out expression of CD45 in Nalm-6 cells (**Figure 4.2a)**. CD45 negative cells were sorted and expanded for use in the co-culture assay. To test that this approach separated Nalm-6 and T cells, we checked expression of CD4 and CD8 in the CD45 negative population, and confirmed most of this population was negative for CD4 or CD8 express (**Figure 4.2b**). Deconvolution of the 9-chose-3 barcode system adds an additional layer of filtering, removing ‘illegal’ barcode combinations that are not designated in the barcode scheme,

this step further isolates properly barcoded T cells, and all 44-barcoded population, plus one 'unassigned' can be distinguished (**Figure 4.2c**). Additional quality controls, including DNA quantity and CD4/CD8 expression will be used to further confirm Nalm-6 cells have been removed from analysis.

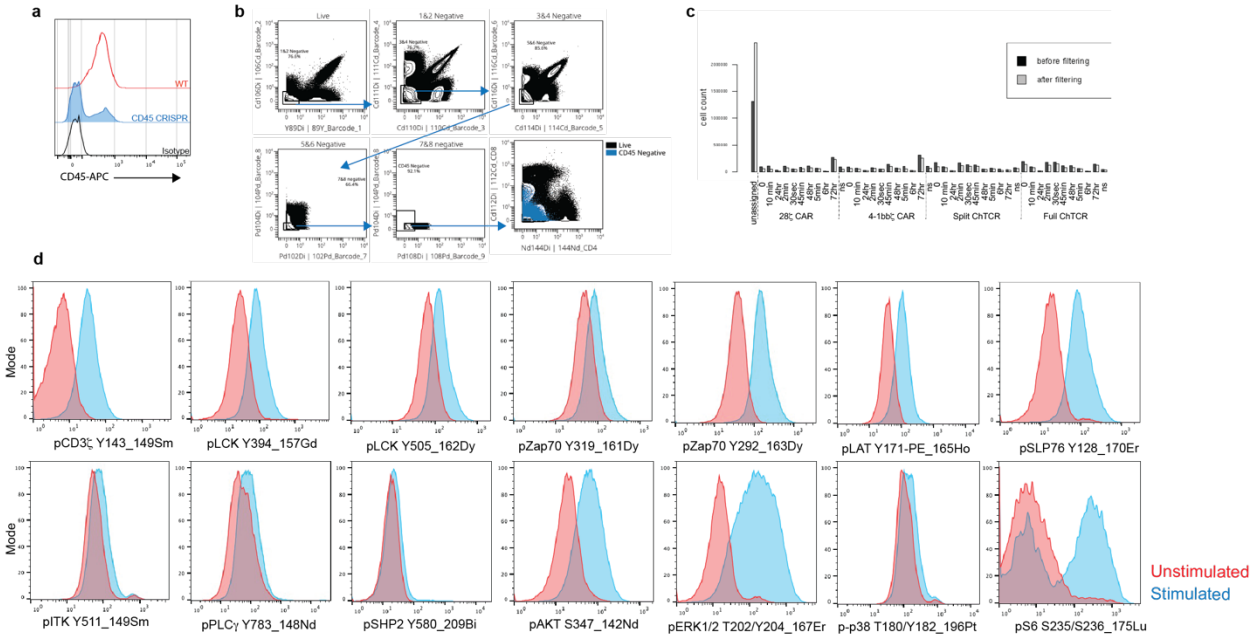

Figure 4.2 Development of a mass cytometry panel to measure proximal receptor signaling a.) Flow cytometry histogram showing CD45-negative population of Nalm-6 cells that were sorted for use in co-culture assay b.) gating scheme to identify Nalm-6 cell negative for all 9 CD45 barcode elements, (bottom right) CD4 and CD8 expression in these cells (blue) overlayed with all live cells c.) distribution of cells in each condition after de-convolution barcoding d.) expression of phosphorylated proteins in unstimulated (Red) and stimulated (Blue) T cells, representative histograms showing expression pattern of antibody clones selected for inclusion in final panel at optimal concentration

The effective detection of phosphorylated signaling molecules is essential to the utility of this panel. We therefore tested the ability of commercially available phosphorylation-site specific antibodies to detect difference in phosphorylation state between baseline and stimulated conditions. Phosphorylation-site specific antibodies were compared between antibody clones, and antibody concentrations were titrated to identify the best concentration to distinguish between baseline and stimulated conditions (**Figure 4.2d**). An antibody clone was selected for each of the targeted proteins, allowing for detection of 14 signaling events that are initiated by receptor activation.

Identification signaling differences between CAR and ChTCR T cells

CD4 and CD8 T cells expressing CD19-Full ChTCR, Split ChTCR, 28ζ CAR or 4-1bbζ CAR were generated and expanded in culture for two weeks. Receptor positive cells were isolated by positive selection of transduction marker 24-hours before beginning co-culture with Nalm-6 cells. For each receptor, CD4 and CD8 cells were combined in a 1:1 ratio, then plated with and equal number of irradiated $CD45^{KO}$ Nalm-6 cells. Target cells were irradiated to prevent outgrowth, reducing number of cells to be measured by mass

cytometry [198]. Prior to co-culture T cells were labeled with CFSE dye, and cells that would be harvest in less than one hour were labeled with Cisplatin-195Pt for viability staining. Co-cultures were collected at 30 seconds, 2, 5, 10, and 45 minutes, 6, 24, 48 and 72 hours. Additionally, cells expressing each receptor were co-cultured with $CD19^{KO}CD45^{KO}$ irradiated Nalm-6 cells for 10 minutes ('0 min') or 6 hours ('NS') to provide a short stimulation and long stimulation baseline conidiations. After viability stain and fixation, cells were stored until the end of the time course, when all co-culture conditions were barcoded with CD45 antibodies, pooled and stained with metal-tagged antibodies, before data collection with mass cytometry (**Figure 4.3**).

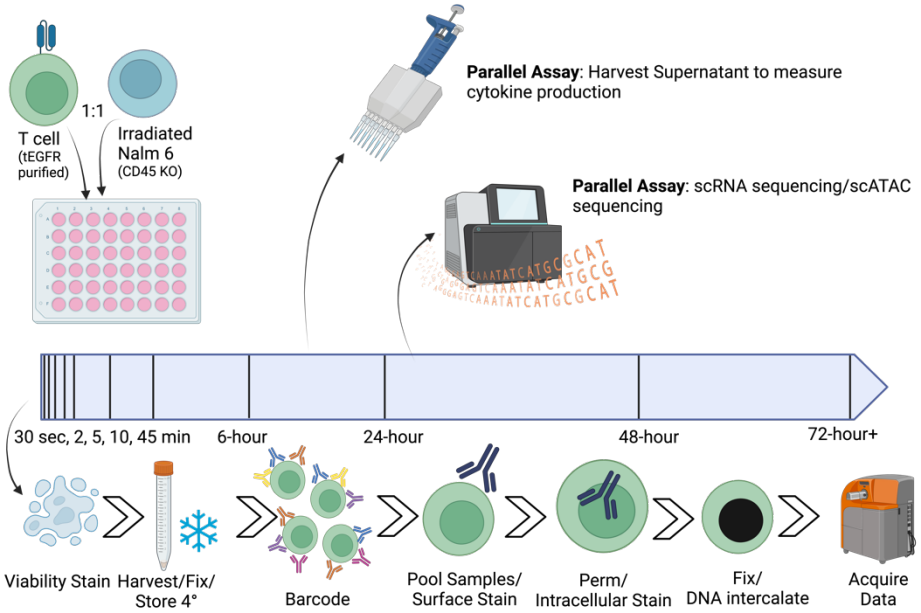

Figure 4.3 Schematic of mass cytometry assay T cells expressing CD19 Full ChTCR, Split ChTCR, 28ζ CAR or 4-11ζ CAR were co-cultured with irradiated CD45 KO cells at a 1:1 ratio. Cells were harvested at the indicated time points, for all time points greater than 45 minutes, supernatant was harvest to measurement of cytokines in supernatant. Cells were stained with a viability stain (cells collect after less than 1 hour were pre-stained with viability stain), fixed with PFA and stored. After all conditions were harvested cells were stained with a 9-chose-3 barcode, then pooled for surface stained, followed by methanal permeabilization, and overnight intracellular stain, cells were incubated with DNA intercalator overnight before data collection. The assay is adaptable to parallel assays to measure features not captured in mass cytometry panel including single-cell RNA sequencing.

Cytokines were collected from co-culture supernatant at 6, 24, 48 and 72 hours. Technical limitations prevented the direct measurement of cytokines intracellularly by mass cytometry, however supernatant cytokine measurement provides a way to monitor T cell function in response to co-culture with antigen positive target cells. Consistent with previously reported data [Simon and Bugos, *In Review*], 28ζ CARs produced the most IL-2, IFNγ and TNF-α at all time points, compared to all other receptors. However, the Full ChTCR produced more cytokines than the 4-1bbζ CAR and the Split ChTCR, this trend particularly apparent comparing IL-2 and TNF-α levels (**Figure 4.4a**). Supernatant cytokine data provided a metric of cell function in response to target recognition. Cytokine production is a consequence of receptor signaling, measuring cytokine production can

served as a read-out of the efficacy of the receptor signaling and a positive control for the assay, indicating T cells are responding to targets cells.

Mass cytometry data was able to distinguish differences in the phosphorylation of proteins that mediate early signaling events in T cell activation between the receptors tested. We used the metric Earth mover's distance (EMD) to quantify the magnitude of change in phosphoproteins abundance in a population of T cell compared to their base line. EMD describes a change in signal strength based on differences in a probability distribution between two populations, baseline and stimulated. This is different that than typical cytometry measurements which collapse data to a mean or median. EMD helps to quantify multiple biological replicates with high consistency, allowing for repeated comparisons between multiple populations and conditions [202]. EMD values indicated a strong induction of CD3ζ Y142 phosphorylation in T cells expressing either CAR construct. Phosphorylation intensity peaked at 5 minutes for T cells expressing the 28ζ CAR and 10 minutes for 4-1bbζ expressing T cells. CD3ζ Y142 phosphorylation intensity was greater in the CAR T cells than either ChTCR T cell population, although the Full ChTCR showed greater CD3ζ phosphorylation than the Split ChTCR (**Figure 4.4b**). However, high CD3ζ phosphorylation did not translate to improved phosphorylation of downstream signaling molecules Zap70 and LAT, particularly for the 28ζ CAR. Despite higher levels of CD3ζ Y142 phosphorylation, the Full ChTCR showed greater Zap70 phosphorylation than the 28ζ CAR, and similar levels of Zap70 phosphorylation to 4-1bbζ , particularly are time points 2 and 5 minutes (**Figure 4.4c**). This trend was mirrored by the measurement of LAT phosphorylation (**Figure 4.4d**). This pattern suggests that initial receptor activation, as measured by CD3ζ phosphorylation, is not the source of signaling deficits observed in CARs. Instead, the 'bottleneck' is the activation of down-stream kinases and adaptors, such as Zap70 and LAT. This model is consistent with other observations, that indicated insufficient recruitment of Zap70 limited CAR sensitivity [42]. The consistency between what was detected by mass cytometry and other methods supports the use of mass cytometry to measure early signaling events in T cells.

In addition to measuring population-level changes in phosphorylation state, the single-cell resolution of mass cytometry allows for the measurement of the co-expression of phosphorylated proteins in a single cell. This resolution allows for a quantification of how changes in the phosphorylation of one protein relates to the change of phosphorylation of another. The degree of influence between two proteins can be quantified with a DREMI score (density resampled estimate of mutual information). DREMI relies on single-cell information, using variations within a population to quantify how much the state of protein X is predictive of the state of protein Y. DREMI uses conditional probability to quantify this relationship, considering how the state of Y varies with different states of X. A high DREMI score indicates indicated a high degree of dependence of Y on X [190]. Information from

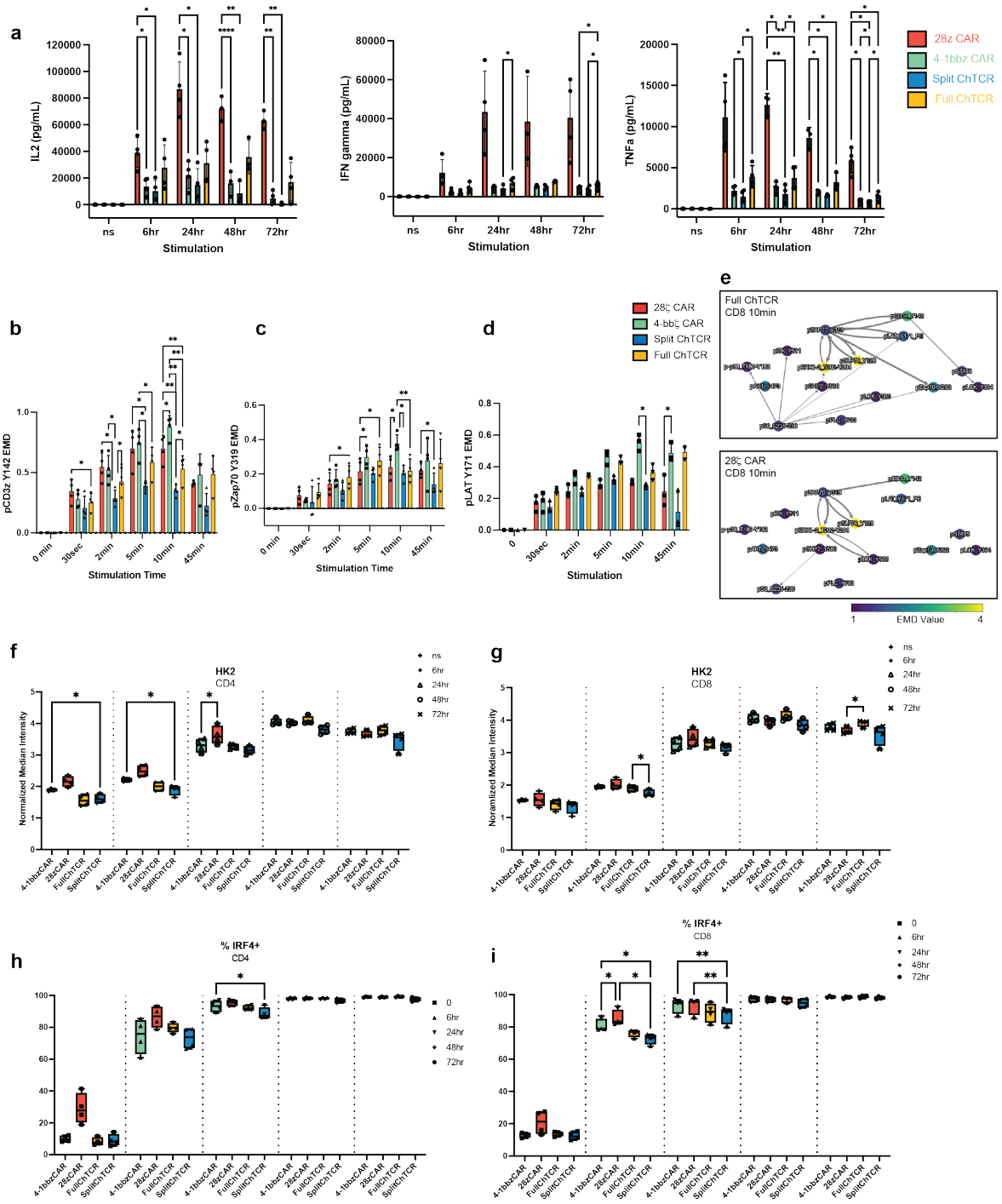

Figure 4.4 Preliminary data shows mass cytometry can differentiation function between engineered T cells a.) IL2 (Left), IFNγ (Center) and TNFα cytokine levels from co-culture of T cells with Nalm-6 cells at indicated timepoints. N = 4 independent T cell donors, independent experiments. Mixed Effect Analysis * P < 0.05, ** P < 0.01, **** P <0.0001 b.) EMD of CD8 T cells expressing indicated receptors, EMD values for pCD3ζ Y142, c) pZap70 Y319 d.) pLAT Y171, all EMD calculation used baseline values measured for each receptor. Two-Way Anova * P < 0.05, ** P < 0.01 e.) Network plot for Full ChTCR (TOP) and 28ζ CAR (BOTTOM), CD8 T cells. Nodes indicate EMD values for indicated protein, edge thickness corresponds to DREMI value. DREMI values are only plotted is significantly different from DREMI value at baseline, baselines calculated individually for each receptor, t-test P<0.05. f.) Normalized median intensity of HK2 expression in

CD4 or g.) CD8 T cells expressing indicated receptors. Two-way ANOVA * P < 0.05 g.) % of CD4, or h.) CD8 cells positive for IRF4 expression. Receptor indicated by color bar, timepoint indicated by point shape. Two-way ANOVA * P < 0.05, ** P < 0.01

both EMD and DREMI calculation can be used to recreate an interaction network, relating the phosphorylation states of individual protein to others, and predicting how information flows through a signaling network [202]. To test the ability of mass cytometry data to reproduce a TCR-like signaling network, were created network plots, where individual nodes represented a phosphorylation site detected by an antibody in the mass cytometry panels. Nodes were colored according to EMD values. Edges between the nodes in the network were drawn according to DREMI values, with thicker lines indicating larger DREMI values, or a strong predicted degree of dependence. Preliminary network plots were able to re-create conical TCR signaling, particularly for the Full ChTCR, with strong interactions between CD3ζ Y142 and Zap70 Y319, Zap70 Y319 and LAT Y171, and Zap70 Y319 and SLP76 Y128 (**Figure 4.4e**). These relationships re-create the known hierarchy of TCR mediated signaling events. Notably, some of these relationships were not significant in 28ζ CAR T cells at the same time point. For example, the DREMI score between Zap70 and LAT, was not different from baseline, neither was the DREMI value between CD3ζ Y142 and LCK Y394 (**Figure 4.4e**).

Mass cytometry recapitulates known metabolic and transcriptional states

In addition to measurement of early signaling events, this mass cytometry panel allowed for the detection of proteins that regulate T cell metabolism. We were able to identify differences in expression of these proteins between receptor types, that is consistent with previously described data. The protein hexokinase 2 (HK2) facilitates the first step of glucose metabolism. The expression levels of HK2 correlates with the levels of glycolysis in a cell. We observed that CD28ζ CAR had the highest levels of HK2 expression at early timepoint, even without stimulation (**Figure 4.4f,g**). This difference was greater in CD4 T cells. In CD4 T cells, ChTCRs generally had lower levels of HK2 expression compared to either CAR (**Figure 4.4f**). High levels of glycolytic activity in CD28ζ CAR is consistent with previously described data that indicated CD28ζ CAR use glycolysis as their main source of energy [69]. The agreement between these two different data sources shows this mass cytometry approach can identify a metabolic phenotype previously observed by different methods.

Similarly, transcription factor data from this mass cytometry panel was able to recapitulate previously observed cell states. The transcription factor IRF4 is expressed in effector T cells, its expression is induced by T cell activation [204]. Our data demonstrated a larger population of CD28ζ CAR positive for IRF4 expression at baseline compared to all other

receptors tested (**Figure 4.4h,i**). This is consistent with the prior observation that CD28ζ CAR tonically signal, that is signal without antigen recognition [68]. IRF4 transcription patterns also demonstrated that at the early timepoints (6 and 24 hours), ChTCRs, in particular the Split ChTCR, have lower proportion of cells positive for IRF4 expression (**Figure 4.4h,i**). However, by 72 hours nearly all cells were positive for IRF4 expression. This data suggests a slower activation or effector response initiation in ChTCR cells compared to CARs.

Preliminary data indicated metabolic and transcriptional differences between T cells expressing each receptor in 'bulk populations.' Further analysis should be done to separate or cluster T cells into phenotypic groups (**Table 4.1**), to determine how different population of T cells respond to stimulation. This would facilitate additional comparisons between receptors to determine if a particular phenotype is more prominent in T cells expressing some receptors compared to others. Phenotypic differences may drive differences seen at bulk population levels. Additionally, proliferation data from CFSE labeling can further refine information that until now has only been annotated by collection point. Division state can be used instead of stimulation time to better inform conclusions about how T cell states change over time.

Conclusions

Preliminary testing of this mass cytometry panel demonstrates its ability to characterize signaling, metabolic and phenotypic profiles, comparing multiple receptors at over ten timepoints. Initial analysis has identified differences in signal transduction, metabolic state and basal 'tonic' activation that has previously been described using different approaches to evaluate T cell function. These finding support this approach as an effective way to integrate the measurement of the many different T cell functions and responses.

This initial experiments successfully characterized differences between ChTCR and CAR T cells against high-antigen targets. Additional analysis will need to be performed to reveal the full extent of these differences. Future experiments will use this panel to evaluate T cell function in response to different conditions. We will compare signaling and T cell differentiation of engineered T cells stimulated with high antigen cells and low antigen cells, looking for how singling changes with different stimulation strength in each of these receptors. Additionally, to mimic multiple antigen encounters or chronic stimulation, we will stimulate engineered T cells multiple times, measuring singling after first stimulation then after two or three stimulations to observe how singling changes after multiple rounds of antigen targeting. In addition to testing existing receptors in different conditions, this tool can be used to compare novel receptors designs, such as the inclusion of different costimulatory domains in the ChTCR architecture, to help determine which design will be

most effective. This tool is highly adaptable to the evaluation of many different engineered T cells and provides the opportunity for the detailed study of engineered T cell signaling and function.

Materials and Methods

Cell Lines

Lenti-X 293T cell line was acquired from Takara Bio USA Nalm-6 (CRL-3273 were acquired from American Type Culture Collection. Lenti-X 293T were maintained in complete culture media (DMEM (Gibco, 11965-092), 10% fetal bovine serum (Corning, 35-011-CV), 2mM L-glutamine (Gibco, 25030-081), 1x penicillin/streptomycin (Gibco, 15140-122), 25mM HEPES (Gibco, 15630080)). NALM-6 were maintained in RPMI 1040 medium (Gibco, 22400-089) supplemented with 10% fetal bovine serum, 2mM L-glutamine, 1x penicillin/streptomycin. Cells were split every 2-3 days and replated at a density of 0.3-0.6x10^6 cells/mL. Tumor cell lines were authenticated in the Fred Hutchinson Cancer Center Genomics Core and all cell lines were routinely checked to ensure they were negative for mycoplasma contamination.

Generation of Nalm-6 lines

Nalm-6 cell lcell negative for expression of CD45 were generated using CRISPR Cas9 gene editing. Briefly, 1x10^6 cells were resuspended in SF buffer (Lonza, V4XC-1032) mixed with 20nM of ribonucleoprotein protein complex formed with CRISPR Cas9 enzyme (Horizon Discovery, CAS12207) and CD45 sgRNAs (Horizon Discovery). NALM-6 cells negative for CD45 were sorted by flow cytometry. Cells were maintained in culture as described and routinely checked for CD45 expression.

Generation of constructs and Lentivirus preparation

Primary human T cells expressing CAR or ChTCRs were generated as previously described (Simon and Bugos, *In Press*). Briefly, ChTCR and CAR lentivirus were synthesized in an Lentivirus vector (HIV-7) for transduction of T cells. CAR and ChTCR sequences were synthesized, followed by a P2A furin cite, then an EGFR extracellular domain tag. Full gene sequences were synthesized commercially (Twist Biosciences). Replication-deficient lentivirus was produced by transient transfection of Lenti-X cells using pPAX2, pVSVG and receptor-encoding lentiviral vector using Xfect polymer transfection reagent (Takara Bio, 631318), according to the manufacture's protocol. Lentiviral supernatant was harvested after 48 hours and filtered using a 0.45-mm PES syringe filter. Virus was further concentrated with Lenti-X Concentrator (Takara Bio, 631232) according to the manufacturer's recommended protocol.

T cell isolation

Peripheral blood was collected from healthy adults enrolled in an IRB approved study at Fred Hutchinson Cancer Center after informed consent. Peripheral blood mononuclear cells (PBMCs) were isolated by density gradient using SepMate-50 (Stem Cell Tech., 85450) and lymphocyte separation media (Corning, 25-072-CV). Bulk CD8+ and CD4+ T cells were isolated using EasySep T cell Isolation kit (Stem Cell Tech, 17953) following manufacturer's instructions. T cells were cryopreserved for later use.

T cell transduction and gene editing

Bulk $CD8^+$ and $CD4^+$ T cells were activated using Dynabeads Human T-Activator CD3/CD28 (Gibco, 11131D) at a 3:1 bead to T cell ratio. T cells were cultured in T cell media (CTL) (RPMI 1040 (Gibco, 22400-089), 10% Human serum (Bloodworks Northwest) 2mM L-glutamine (Gibco, 25030-081), 1x penicillin/streptomycin (Gibco, 15140-122), 0.5mM b-mercaptoethanol) supplemented with IL-2 (50 IU/mL). The next day concentrated lentiviral supernatant was added to activated T cells with LentiBOOST Solution B (100x) (SIRION Biotech SB-P-LV-101-12) and polybrene (Millipore, TR-1003-G) at a final concentration of 4.4mg/mL. T cells were spinoculated at 800g, 32° C for 90 min, after overnight incubation beads removed prior to gene editing. Cytidine base editing was performed to knock-out expression of endogenous TRAC and TRBC. $1x10^6$ T cells were resuspended in P3 buffer (Lonza, V4XP-3032), mixed with 1mg concentration of RNA guide and 1.5mg of CBE BE4max mRNA (Addgene plasmid 112093) (Aldevron), and electroporated using the Lonza 4D device (Lonza) [181]. Sequences for sgRNAs are described in Table S1. T cells were cultured in CTL supplemented with IL-2 (150IU/mL), IL-7 (5ng/ml), IL-15 (5ng/mL) initially, and then maintained in CTL supplemented with IL-2 (50IU/mL) for one week before being used for assays. One day prior to co-cultures EGFR-tag positive cells were isolated using EasySep Human EGFR Positive Selection Kit (Stem Cell #100-1131) according to manufacture protocol.

Metal labeling of Antibodies

Antibodies were conjugated to heavy metal ions with MaxPar (Standard Biotools) reagents using optimized protocols. Briefly, metal chelation was performed by adding 0.05M metal solutions to chelating polymers and incubated at 37° for 60 (Cadmium metals) or 45 (Lanthanide metals) minutes, mixing every 15 minutes. Metal loaded polymers were washed twice using 3-kDa MWCO filter (Milipore), centrifuging 30 min 12,000 g. Antibodies were reduced with 4mM TCEP (Thermo Fisher) for 30 in at 37°. Antibody was washed two times using 50-kDa MWKO filter (Milipore). Partically reduced antibodies and metal-loaded polymers with incubated together for 90 minutes at 37°. Metal conjugated antibodies were

washed four times. Antibody concentration was measured by Nano Drop (Thermo Fisher), antibody stabilizing solution (Candor Bioscience) was added, at least 50%v/v to bring antibodies to final concentration of 100ug/ml or 200ug/mL.

Antibody Titration

Bulk CD8 and CD4 T cells were thawed and activated with CD3/CD28 beads as described. One day before staining, a portion of cells were rested in serum-free media overnight, then activated by incubation with 5ug/ml anti-CD3 biotin (Bioledgend 317319) + 5ug/mL anti-CD28 (Bioledgend 302904) followed by avidin crosslinking (20ug/mL) (Thermo Fisher), and incubation at 37° for 10 minutes followed by immediate fixation in 4% PFA (Thermo Fisher). The remaining activated, but not re-stimulated cells were similarly fixed and populations were pooled for staining. All antibody cocktails were prepared in cell stain media (CSM), PBS, 0.5% BSA, 0.02% Sodium Azide).

CFSE Labeling

CFSE labeling was performed as previously described [199]. Breifly $0.200x10^6$ CD4 and $0.200x10^6$ CD8 T cells per condition (Total 2.2×10^6 CD4s/2.2×10^6 CD8s) were collected and resuspended in 1 mL CTL and transferred to a new 15ml Falcon tube. CFSE dye (Thermo Fisher C34554) was resuspended in 18 uL DMSO. Falcon tubes containing cells were laid on their side, and 118uL of room temperature PBS was pipetted to the side of the tube. 17.6uL of reconstituted CFSE dye was added to PBS, and tubes were inversted and briefly vortex to mixe cells with dye. Cells were incubated for 5 minutes at room temperature followed by 2X wash with 10mL CTL. Cells were resuspended at $0.4 x10^6$ cells/100uL for co-culture assay.

Co-Culture

Approximately 15 hours before co-culture EGFR-purified T cells were collected and resuspended in Serum-free X-Vivo 15 media (Lonza, 02-053Q) at a concentration of $1x10^6$ cells/mL for over-night culture. The morning of co-culture, cells were counted and mixed in a 1:1 ratio of CD4s and CD8s for CFSE labeling and co-culture.

$CD45^{KO}$ and $CD19^{KO}CD45^{KO}$ Nalm-6 cells were harvest, $0.4x10^6$ cells per stimultion condition, were harvested and re-suspended in CTL at a concentration of $4x10^6$ cells/mL. Nalm-6 cells were irradiated 6,000 rads.

CFSE-labeled T cells and irradiated Nalm-6 cells to be co-cultured for greater than 1 hour were plated at 1:1 ration in 0.5mL CTL. T-cells co-cultured for less than 1 hour were resuspended in 240uL PBS, and incubated with 1.6uL of Cell-ID Cisplatin-195PT (Standard BioTools, 201198) and incubated for 5 minutes. Cells were washed with 10mL CTL, and

resuspended in CTL 4x10^6 cells/mL. T cells and Nalm-6 cells were co-cultured in a V-bottom 96-well plate 200uL total volume, and briefly centrifuged 100gx1min. At each timepoint 100uL ice-cold PBS was added to co-culture well, and contents of well were transferred to eppendorph containing 300uL 8% PFA (final concentration 4% PFA), and incubated for 20 minutes. Cells were washed with 1mL CSM, responded in 1.6% PFA in CSM and transferred to new v-bottom plate. Cells were pelleted 1,200gx10min and stored until all time points collected.

For co-cultures greater than 1 hour, 1ug/mL puromycin was added to culture 45 minutes before cell harvest. At time of harvest, 200uL of supernatant was collected for cytokine measurement. Cells were harvest and washed with 1 mL PBS, before Cell-ID Ciplatin-195Pt labeling and fixation as described.

Antibody Staining

44-population 9-chose-3 barcode stain was prepared in 5X volume CSM and divided into 5 96-well plates and stored at -20° for use. After completion of co-culture, v-bottom plate containing cells was centrifuged 1200g x 10 min at 4°, and supernatant removed. Barcode stain was transferred to cells and incubated 1 hour at 4°. Cells were washed 3x with CSM 1200g x 10 min at 4°. All cell populations were transferred to a single flacon tube and resuspend in a single v-bottom plate well for remaining staining steps. Cell surface antibody master mix was prepared in CSM and filtered through a pre-wetted 0.1μm spin column (Millipore, 41104916) to remove aggregates. Cells were incubated with surfac antibody mix for 1 hr at 4° and washed 3X with CSM. Cells were fixed in 4% PFA, RT for 10 min and washed 3X with PBS 4°. Cells were permeabilized in 90% MeOH for 10 minutes on ice, and wash 3X CSM 4° 1,000g x 7 min. Intracellular master mix was prepared in CSM and filtered. Master mix was added to cells and incubated overnight 4° shaking 5,000 rpm. Cells were washed 3X CSM 4° 1,000g x 7 min. Cell were stained with anti-PE antibody prepared in CSM and filtered, hr at 4° and washed 3X with CSM. Cells were resuspened in Cell-ID Ir Intercalator solution (Standard BioTools, 201192B), prepared diluted 1:1000 in 4% PFA, incubated overnight 4° shaking 5,000 rpm. Cells were washed 3X with CAS - Cell Acquisition solution (Standard BioTools , 201244) 4° 1,000g x 7 min. Cells were filters, and resuspended with 1X 4-element calibration beads (Standard BioTools, 201078) and data acquired on mass cytometer (Fluidigm, Helios).

Mass Cytometry Data processing

Raw mass cytometry data was bead-normalized and barcoded cells were assigned to their original populations using the CAYALYST R package [205]. Normalized data was imported to FlowJo (BD), and manual gating was applied to remove debris, and gate on live, single

cells, and gate CD4 and CD8 positive cells. Gated populations were exported as individual FCS files. Pre-processed FCS files were inputs for the CyGNAL analysis pipeline [206], to make EMD and DREMI measurements as described. Network interaction plots were generated using custom in-house python code. Individual analyte expression levels were measured by gating in FlowJo 10.10.0 or OMIQ (Dotmatics) cytometry software. Graph generated with Prism 10 (GraphPad)

Luminex Cytokine Measurement

Cytokine production was measured by Luminex according to standard protocol.

Chapter 5: Concluding Remarks

CAR T cell therapies have been a breakthrough in cancer therapy. In the last decade thousands of patients have received CAR T cell therapies, achieving unprecedented responses [70]. However, the loss of CAR T cell efficacy due to reduced or lost antigen expression remains a major hurdle to the efficacy of CAR therapies. There is a currently unmet need for new receptors that have improved antigen sensitivity over CARs and an ability to overcome antigen loss with dual antigen targeting. In this thesis I have presented a promising new approach that addressed both these limitations of CAR therapy. These data present a novel and adaptable approach for the sensitive and potent recognition of two antigens in a single engineered T cell product. Bi-ChTCRs show promise for combating antigen escape and relapse in both B cell malignancies and multiple myeloma and have a high potential for clinical translation.

It could be considered remarkable that CARs are able to activate T cells and respond to tumor cells as effectively as they do. A CARs is a synthetic receptor that is a fusion of multiple signaling domains of proteins that natively function as independent molecules. While they have limitations, their value cannot be denied. Fundamental knowledge of TCR signaling pathways allowed for the creation of these synthetic molecules. It informed the initial design by identifying the critical signaling domain required for TCR activation [106, 207], and directed the modification of CARs to improve persistence and in-vivo efficacy with the incorporation of co-stimulatory domains [77, 208]. We and others have demonstrated TCR signaling-informed receptors design can improve chimeric antigen receptor design and function even further [110, 123, 124, 126, 129, 130][Simon and Bugos, *In Press*]. Furthermore, detailed study of synthetic receptor signaling is critical to identify what ways these receptors recapitulate TCR signaling and in which ways they come short. These studies have proven to be fruitful in the identification of specific signal deficiencies of CARs [42, 111] that were then directly addressed in the design of novel receptors. We aim to continue this cycle in the design and testing of new receptors for T cell therapies. In addition to demonstrating the potency of sensitivity of Full ChTCRs and Bi-ChTCRs we have performed signaling analysis, directly measuring if these receptors are able to make up known deficiencies in CAR signaling. We used co-immunoprecipitation to show that ChTCRs associate efficiently with all TCR/CD3 subunits. We have also demonstrated that knockout of endogenous TCR improves ChTCR expression and sensitivity, likely due to improved availability to the endogenous pool of CD3 subunits [Simon and Bugos, *In Press*]. Furthermore, we were the first group to definitively demonstrate the ChTCRs and Bi-ChTCRs form a canonical TCR synapse, a known deficiency of CARs. Finally, we directly assessed the phosphorylation of signaling molecules that are not well engaged by CARs, showing improved LAT and Zap70 phosphorylation with activation of ChTCR or Bi-ChTCR

compared to CARs [Simon and Bugos, *In Press*]. These signaling studies compliment and inform in-vitro and in-vivo tests of receptor function, providing mechanistic explanations for improved function and identifies TCR signaling elements critical to T cell sensitivity.

Bi-ChTCRs presented in our manuscript are a promising new advance for engineered T cell therapies. Still, additional study and modification of these receptors could further improve their efficacy. Our findings present new questions about the signaling and function of synthetic receptors. One question of great interest to us is a mechanistic understanding of why the Full ChTCR has improved sensitivity over the Split ChTCR, and other Split ChTCR architectures (HIT and mutSTART), despite having the same available signaling domains. We have observed that Full ChTCR has improved expression levels over the Split ChTCR, but the signaling consequences of this observation are not yet characterized. An additional remaining question is whether co-stimulation will be required for optimal function of Bi-ChTCRs. Incorporation of co-stimulation has improved CAR functionality, and the function of HIT and mutSTAR receptors [78, 80, 129, 130]. However, the Full ChTCR and Bi-ChTCR performed better than CAR T cells, which have engineered co-stimulation, in pre-clinical mouse models. Similarly, while HIT and mutSTAR T cells required co-stimulation in most models to improve function over CARs, the Full ChTCR outperformed the Split ChTCR in in-vitro sensitivity assays and in mouse models [Simon and Bugos, *In Press*]. These findings suggest the Bi-ChTCRs and Full ChTCR may drive a sufficiently potent response without co-stimulation.

These questions will be the basis of my future research. To this end I have developed a mass cytometry assay to directly assess receptor proximal signaling, metabolic state and differentiation in multiple T cell populations simultaneously. Initial data generated using this assay shows that it efficiently identifies difference between cell populations and is capable of recapitulating observations made using alternate techniques. This assay will be the basis of understanding differences between Full and Split ChTCRs and inform the design and testing of approaches to incorporate co-stimulation in ChTCR designs. This approach will build on the proven approach of using the study of TCR signaling to inform improved receptor design.

It has become to a scientific cliché to reference the Issac Newton-attributed quote “If I have seen further, it is by standing on the shoulders of giants.” However, this is still true. The identification and description of TCR signaling proteins, including CD3 subunits, LCK Zap70, LAT, CD28 and 4-1bb, were necessary for the development and then further improvement of CAR T cell therapies. The continued study of TCR signaling, and the signaling of synthetic receptors will be critical for improving receptor function, and ultimately their ability to be effective cancer therapeutics.

References

1. Murphy, K. and C. Weaver, *Janeway's Immmunobiology*. 2016, Boca Raton, FL: CRC Press.
2. Shah, K., et al., *T cell receptor (TCR) signaling in health and disease.* Signal Transduction and Targeted Therapy, 2021. **6**(1).
3. Krangel, M.S., *Mechanics of T cell receptor gene rearrangement.* Current Opinion in Immunology, 2009. **21**(2): p. 133-139.
4. Dong, D., et al., *Structural basis of assembly of the human T cell receptor–CD3 complex.* Nature, 2019. **573**(7775): p. 546-552.
5. Love, P.E. and S.M. Hayes, *ITAM-mediated Signaling by the T-Cell Antigen Receptor.* Cold Spring Harbor Perspectives in Biology, 2010. **2**(6): p. a002485-a002485.
6. Bettini, M.L., et al., *Cutting Edge: CD3 ITAM Diversity Is Required for Optimal TCR Signaling and Thymocyte Development.* The Journal of Immunology, 2017. **199**(5): p. 1555-1560.
7. Willcox, B.E., et al., *TCR Binding to Peptide-MHC Stabilizes a Flexible Recognition Interface.* Immunity, 1999. **10**(3): p. 357-365.
8. Van Der Merwe, P.A. and O. Dushek, *Mechanisms for T cell receptor triggering.* Nature Reviews Immunology, 2011. **11**(1): p. 47-55.
9. Courtney, A.H., W.-L. Lo, and A. Weiss, *TCR Signaling: Mechanisms of Initiation and Propagation.* Trends in Biochemical Sciences, 2018. **43**(2): p. 108-123.
10. Mariuzza, R.A., P. Agnihotri, and J. Orban, *The structural basis of T-cell receptor (TCR) activation: An enduring enigma.* Journal of Biological Chemistry, 2020. **295**(4): p. 914-925.
11. Wei, Q.R., et al., *Lck bound to coreceptor is less active than free Lck.* Proceedings of the National Academy of Sciences of the United States of America, 2020. **117**(27): p. 15809-15817.
12. Casas, J., et al., *Ligand-engaged TCR is triggered by Lck not associated with CD8 coreceptor.* Nature Communications, 2014. **5**(1): p. 5624.
13. Hartl, F.A., et al., *Noncanonical binding of Lck to CD3ε promotes TCR signaling and CAR function.* Nature Immunology, 2020. **21**(8): p. 902-913.
14. Brdicka, T., et al., *Intramolecular Regulatory Switch in ZAP-70: Analogy with Receptor Tyrosine Kinases.* Molecular and Cellular Biology, 2005. **25**(12): p. 4924-4933.
15. Deindl, S., et al., *Structural Basis for the Inhibition of Tyrosine Kinase Activity of ZAP-70.* Cell, 2007. **129**(4): p. 735-746.
16. Sjölin-Goodfellow, H., et al., *The catalytic activity of the kinase ZAP-70 mediates basal signaling and negative feedback of the T cell receptor pathway.* Science Signaling, 2015. **8**(377): p. ra49-ra49.
17. Balagopalan, L., et al., *The LAT Story: A Tale of Cooperativity, Coordination, and Choreography.* Cold Spring Harbor Perspectives in Biology, 2010. **2**(8): p. a005512-a005512.

18. Bartelt, R.R. and J.C.D. Houtman, *The adaptor protein LAT serves as an integration node for signaling pathways that drive T cell activation*. WIREs Systems Biology and Medicine, 2013. **5**(1): p. 101-110.
19. Blank, C.U., et al., *Defining 'T cell exhaustion'*. Nature Reviews Immunology, 2019. **19**(11): p. 665-674.
20. Houtman, J.C.D., et al., *Oligomerization of signaling complexes by the multipoint binding of GRB2 to both LAT and SOS1*. Nature Structural & Molecular Biology, 2006. **13**(9): p. 798-805.
21. Chen, L. and D.B. Flies, *Molecular mechanisms of T cell co-stimulation and co-inhibition*. Nat Rev Immunol, 2013. **13**(4): p. 227-42.
22. Jaeger-Ruckstuhl, C.A., et al., *Signaling via a CD27-TRAF2-SHP-1 axis during naive T cell activation promotes memory-associated gene regulatory networks*. Immunity, 2024. **57**(2): p. 287-302.e12.
23. Green, J.M., et al., *Coordinate Regulation of T Cell Activation by CD2 and CD28*. The Journal of Immunology, 2000. **164**(7): p. 3591-3595.
24. Honikel, M.M. and S.H. Olejniczak, *Co-Stimulatory Receptor Signaling in CAR-T Cells*. Biomolecules, 2022. **12**(9): p. 1303.
25. Stanford, S.M., N. Rapini, and N. Bottini, *Regulation of TCR signalling by tyrosine phosphatases: from immune homeostasis to autoimmunity*. Immunology, 2012. **137**(1): p. 1-19.
26. Shakiba, M., et al., *TCR signal strength defines distinct mechanisms of T cell dysfunction and cancer evasion*. Journal of Experimental Medicine, 2022. **219**(2).
27. Gaud, G., R. Lesourne, and P.E. Love, *Regulatory mechanisms in T cell receptor signalling*. Nature Reviews Immunology, 2018. **18**(8): p. 485-497.
28. Dustin, M.L., *The Immunological Synapse*. Cancer Immunology Research, 2014. **2**(11): p. 1023-1033.
29. Wherry, E.J. and M. Kurachi, *Molecular and cellular insights into T cell exhaustion*. Nature Reviews Immunology, 2015. **15**(8): p. 486-499.
30. Pauken, K.E. and E.J. Wherry, *Overcoming T cell exhaustion in infection and cancer*. Trends in Immunology, 2015. **36**(4): p. 265-276.
31. Dustin, M.L., *T-cell activation through immunological synapses and kinapses*. Immunol Rev, 2008. **221**: p. 77-89.
32. Dustin, M.L., *Recent advances in understanding TCR signaling: a synaptic perspective*. Faculty Reviews, 2023. **12**.
33. Yokosuka, T., et al., *Newly generated T cell receptor microclusters initiate and sustain T cell activation by recruitment of Zap70 and SLP-76*. Nature Immunology, 2005. **6**(12): p. 1253-1262.
34. Dustin, M.L., A.K. Chakraborty, and A.S. Shaw, *Understanding the Structure and Function of the Immunological Synapse*. Cold Spring Harbor Perspectives in Biology, 2010. **2**(10): p. a002311-a002311.
35. Balagopalan, L., K. Raychaudhuri, and L.E. Samelson, *Microclusters as T Cell Signaling Hubs: Structure, Kinetics, and Regulation*. Frontiers in Cell and Developmental Biology, 2021. **8**.

36. Demetriou, P., et al., *A dynamic CD2-rich compartment at the outer edge of the immunological synapse boosts and integrates signals*. Nature Immunology, 2020. **21**(10): p. 1232-1243.
37. Siokis, A., et al., *Characterization of mechanisms positioning costimulatory complexes in immune synapses*. iScience, 2021. **24**(10): p. 103100.
38. Ashby, K.M. and K.A. Hogquist, *A guide to thymic selection of T cells*. Nature Reviews Immunology, 2024. **24**(2): p. 103-117.
39. Appleman, L.J. and V.A. Boussiotis, *T cell anergy and costimulation*. Immunological Reviews, 2003. **192**(1): p. 161-180.
40. Gaud, G., et al., *CD3ζ ITAMs enable ligand discrimination and antagonism by inhibiting TCR signaling in response to low-affinity peptides*. Nature Immunology, 2023.
41. Thill, P.A., A. Weiss, and A.K. Chakraborty, *Phosphorylation of a Tyrosine Residue on Zap70 by Lck and Its Subsequent Binding via an SH2 Domain May Be a Key Gatekeeper of T Cell Receptor Signaling In Vivo*. Molecular and Cellular Biology, 2016. **36**(18): p. 2396-2402.
42. Gudipati, V., et al., *Inefficient CAR-proximal signaling blunts antigen sensitivity*. Nature Immunology, 2020. **21**(8): p. 848-856.
43. Lo, W.-L., et al., *Slow phosphorylation of a tyrosine residue in LAT optimizes T cell ligand discrimination*. Nature Immunology, 2019. **20**(11): p. 1481-1493.
44. Huseby, E.S. and E. Teixeiro, *The perception and response of T cells to a changing environment are based on the law of initial value*. Sci Signal, 2022. **15**(736): p. eabj9842.
45. Li, K.-P., et al., *T-cell receptor signal strength and epigenetic control of Bim predict memory CD8+ T-cell fate*. Cell Death & Differentiation, 2020. **27**(4): p. 1214-1224.
46. Töpfer, K., et al., *Tumor Evasion from T Cell Surveillance*. BioMed Research International, 2011. **2011**(1): p. 1-19.
47. Dunn, G.P., L.J. Old, and R.D. Schreiber, *The Immunobiology of Cancer Immunosurveillance and Immunoediting*. Immunity, 2004. **21**(2): p. 137-148.
48. Chen, S., Daniel and I. Mellman, *Oncology Meets Immunology: The Cancer-Immunity Cycle*. Immunity, 2013. **39**(1): p. 1-10.
49. Mellman, I., et al., *The cancer-immunity cycle: Indication, genotype, and immunotype*. Immunity, 2023. **56**(10): p. 2188-2205.
50. Sharma, P., et al., *Immune checkpoint therapy-current perspectives and future directions*. Cell, 2023. **186**(8): p. 1652-1669.
51. Hossen, M.M., et al., *Current understanding of CTLA-4: from mechanism to autoimmune diseases*. Frontiers in Immunology, 2023. **14**.
52. Lee, D., et al., *PD-L1: From cancer immunotherapy to therapeutic implications in multiple disorders*. Mol Ther, 2024.
53. Sadelain, M., I. Rivière, and S. Riddell, *Therapeutic T cell engineering*. 2017.
54. Zaretsky, J.M., et al., *Mutations Associated with Acquired Resistance to PD-1 Blockade in Melanoma*. New England Journal of Medicine, 2016. **375**(9): p. 819-829.

55. Rosenberg, S.A., P. Spiess, and R. Lafreniere, *A New Approach to the Adoptive Immunotherapy of Cancer with Tumor-Infiltrating Lymphocytes*. Science, 1986. **233**(4770): p. 1318-1321.
56. Sarnaik, A.A., et al., *Tumor-infiltrating lymphocytes: A new hope.* Cancer Cell, 2024. **42**(8): p. 1315-1318.
57. Kumar, A., R. Watkins, and A.E. Vilgelm, *Cell Therapy With TILs: Training and Taming T Cells to Fight Cancer.* Front Immunol, 2021. **12**: p. 690499.
58. Matsueda, S., et al., *Recent clinical researches and technological development in TIL therapy.* Cancer Immunology, Immunotherapy, 2024. **73**(11).
59. Goebeler, M.-E. and R.C. Bargou, *T cell-engaging therapies — BiTEs and beyond.* Nature Reviews Clinical Oncology, 2020. **17**(7): p. 418-434.
60. Tian, Z., et al., *Bispecific T cell engagers: an emerging therapy for management of hematologic malignancies.* Journal of Hematology & Oncology, 2021. **14**(1).
61. Kassner, J., et al., *Current landscape of CD3 bispecific antibodies in hematologic malignancies.* Trends Cancer, 2024. **10**(8): p. 708-732.
62. Palecki, J., et al., *T-Cell redirecting bispecific antibodies: a review of a novel class of immuno-oncology for advanced prostate cancer.* Cancer Biology & Therapy, 2024. **25**(1).
63. Nicolai, C.J., et al., *In vivo CAR T-cell generation in nonhuman primates using lentiviral vectors displaying a multidomain fusion ligand.* Blood, 2024. **144**(9): p. 977-987.
64. Simoni, Y., et al., *Bystander CD8+ T cells are abundant and phenotypically distinct in human tumour infiltrates.* Nature, 2018. **557**(7706): p. 575-579.
65. Bradley, P., *Structure-based prediction of T cell receptor:peptide-MHC interactions.* Elife, 2023. **12**.
66. Foldvari, Z., et al., *A systematic safety pipeline for selection of T-cell receptors to enter clinical use.* npj Vaccines, 2023. **8**(1).
67. D'Angelo, S.P., et al., *Afamitresgene autoleucel for advanced synovial sarcoma and myxoid round cell liposarcoma (SPEARHEAD-1): an international, open-label, phase 2 trial.* Lancet, 2024. **403**(10435): p. 1460-1471.
68. Long, A.H., et al., *4-1BB costimulation ameliorates T cell exhaustion induced by tonic signaling of chimeric antigen receptors.* Nat Med, 2015. **21**(6): p. 581-90.
69. Kawalekar, O.U., et al., *Distinct Signaling of Coreceptors Regulates Specific Metabolism Pathways and Impacts Memory Development in CAR T Cells.* Immunity, 2016. **44**(2): p. 380-390.
70. Mitra, A., et al., *From bench to bedside: the history and progress of CAR T cell therapy.* Frontiers in Immunology, 2023. **14**.
71. Majzner, R.G., et al., *GD2-CAR T cell therapy for H3K27M-mutated diffuse midline gliomas.* Nature, 2022. **603**(7903): p. 934-941.
72. Kuwana, Y., et al., *Expression of chimeric receptor composed of immunoglobulin-derived V regions and T-cell receptor-derived C regions.* Biochem Biophys Res Commun, 1987. **149**(3): p. 960-8.

73. Gross, G., T. Waks, and Z. Eshhar, *Expression of immunoglobulin-T-cell receptor chimeric molecules as functional receptors with antibody-type specificity.* Proceedings of the National Academy of Sciences, 1989. **86**(24): p. 10024-10028.
74. Eshhar, Z., et al., *Specific activation and targeting of cytotoxic lymphocytes through chimeric single chains consisting of antibody-binding domains and the gamma or zeta subunits of the immunoglobulin and T-cell receptors.* Proceedings of the National Academy of Sciences, 1993. **90**(2): p. 720-724.
75. Kershaw, M.H., et al., *A Phase I Study on Adoptive Immunotherapy Using Gene-Modified T Cells for Ovarian Cancer.* Clinical Cancer Research, 2006. **12**(20): p. 6106-6115.
76. Lamers, C.H.J., et al., *Treatment of Metastatic Renal Cell Carcinoma With Autologous T-Lymphocytes Genetically Retargeted Against Carbonic Anhydrase IX: First Clinical Experience.* Journal of Clinical Oncology, 2006. **24**(13): p. e20-e22.
77. Krause, A., et al., *Antigen-dependent CD28 Signaling Selectively Enhances Survival and Proliferation in Genetically Modified Activated Human Primary T Lymphocytes.* The Journal of Experimental Medicine, 1998. **188**(4): p. 619-626.
78. Maher, J., et al., *Human T-lymphocyte cytotoxicity and proliferation directed by a single chimeric TCRζ /CD28 receptor.* Nature Biotechnology, 2002. **20**(1): p. 70-75.
79. Savoldo, B., et al., *CD28 costimulation improves expansion and persistence of chimeric antigen receptor–modified T cells in lymphoma patients.* Journal of Clinical Investigation, 2011. **121**(5): p. 1822-1826.
80. Imai, C., et al., *Chimeric receptors with 4-1BB signaling capacity provoke potent cytotoxicity against acute lymphoblastic leukemia.* Leukemia, 2004. **18**(4): p. 676-684.
81. Cappell, K.M. and J.N. Kochenderfer, *Long-term outcomes following CAR T cell therapy: what we know so far.* Nature Reviews Clinical Oncology, 2023. **20**(6): p. 359-371.
82. Locke, F.L., et al., *Long-term safety and activity of axicabtagene ciloleucel in refractory large B-cell lymphoma (ZUMA-1): a single-arm, multicentre, phase 1–2 trial.* The Lancet Oncology, 2019. **20**(1): p. 31-42.
83. Abramson, J.S., et al., *Lisocabtagene maraleucel for patients with relapsed or refractory large B-cell lymphomas (TRANSCEND NHL 001): a multicentre seamless design study.* The Lancet, 2020. **396**(10254): p. 839-852.
84. Wang, M., et al., *KTE-X19 CAR T-Cell Therapy in Relapsed or Refractory Mantle-Cell Lymphoma.* New England Journal of Medicine, 2020. **382**(14): p. 1331-1342.
85. Fowler, N.H., et al., *Tisagenlecleucel in adult relapsed or refractory follicular lymphoma: the phase 2 ELARA trial.* Nature Medicine, 2022. **28**(2): p. 325-332.
86. Jacobson, C.A., et al., *Axicabtagene ciloleucel in relapsed or refractory indolent non-Hodgkin lymphoma (ZUMA-5): a single-arm, multicentre, phase 2 trial.* Lancet Oncol, 2022. **23**(1): p. 91-103.
87. Maude, S.L., et al., *Tisagenlecleucel in Children and Young Adults with B-Cell Lymphoblastic Leukemia.* New England Journal of Medicine, 2018. **378**(5): p. 439-448.

88. Shah, B.D., et al., *KTE-X19 for relapsed or refractory adult B-cell acute lymphoblastic leukaemia: phase 2 results of the single-arm, open-label, multicentre ZUMA-3 study.* The Lancet, 2021. **398**(10299): p. 491-502.
89. Raje, N., et al., *Anti-BCMA CAR T-Cell Therapy bb2121 in Relapsed or Refractory Multiple Myeloma.* New England Journal of Medicine, 2019. **380**(18): p. 1726-1737.
90. Martin, T., et al., *Ciltacabtagene Autoleucel, an Anti–B-cell Maturation Antigen Chimeric Antigen Receptor T-Cell Therapy, for Relapsed/Refractory Multiple Myeloma: CARTITUDE-1 2-Year Follow-Up.* Journal of Clinical Oncology, 2023. **41**(6): p. 1265-1274.
91. Munshi, N.C., et al., *Idecabtagene Vicleucel in Relapsed and Refractory Multiple Myeloma.* New England Journal of Medicine, 2021. **384**(8): p. 705-716.
92. Jain, M.D., et al., *Five-Year Follow-Up of Standard-of-Care Axicabtagene Ciloleucel for Large B-Cell Lymphoma: Results From the US Lymphoma CAR T Consortium.* Journal of Clinical Oncology, 2024. **42**(30): p. 3581-3592.
93. Braig, F., et al., *Resistance to anti-CD19/CD3 BiTE in acute lymphoblastic leukemia may be mediated by disrupted CD19 membrane trafficking.* Blood, 2017. **129**(1): p. 100-104.
94. Sotillo, E., et al., *Convergence of Acquired Mutations and Alternative Splicing of CD19 Enables Resistance to CART-19 Immunotherapy.* Cancer Discovery, 2015. **5**(12): p. 1282-1295.
95. Fischer, J., et al., *CD19 Isoforms Enabling Resistance to CART-19 Immunotherapy Are Expressed in B-ALL Patients at Initial Diagnosis.* Journal of Immunotherapy, 2017. **40**(5): p. 187-195.
96. Lee, H., et al., *Mechanisms of antigen escape from BCMA- or GPRC5D-targeted immunotherapies in multiple myeloma.* Nat Med, 2023. **29**(9): p. 2295-2306.
97. Samur, M.K., et al., *Biallelic loss of BCMA as a resistance mechanism to CAR T cell therapy in a patient with multiple myeloma.* Nature Communications, 2021. **12**(1).
98. Locke, F.L., et al., *Impact of tumor microenvironment on efficacy of anti-CD19 CAR T cell therapy or chemotherapy and transplant in large B cell lymphoma.* Nature Medicine, 2024. **30**(2): p. 507-518.
99. Fry, T.J., et al., *CD22-targeted CAR T cells induce remission in B-ALL that is naive or resistant to CD19-targeted CAR immunotherapy.* Nature Medicine, 2018. **24**(1): p. 20-28.
100. Green, D.J., et al., *Response to BCMA CAR-T Cells Correlates with Pretreatment Target Antigen Density and Is Improved By Small Molecule Inhibition of Gamma Secretase.* Blood, 2019. **134**.
101. Watanabe, K., et al., *Target antigen density governs the efficacy of anti-CD20-CD28-CD3 zeta chimeric antigen receptor-modified effector CD8+ T cells.* J Immunol, 2015. **194**(3): p. 911-20.
102. Walker, A.J., et al., *Tumor Antigen and Receptor Densities Regulate Efficacy of a Chimeric Antigen Receptor Targeting Anaplastic Lymphoma Kinase.* Molecular Therapy, 2017. **25**(9): p. 2189-2201.

103. Caruso, H.G., et al., *Tuning Sensitivity of CAR to EGFR Density Limits Recognition of Normal Tissue While Maintaining Potent Antitumor Activity.* Cancer Research, 2015. **75**(17): p. 3505-3518.
104. Shabaneh, T.B., et al., *Systemically administered low-affinity HER2 CAR T cells mediate antitumor efficacy without toxicity.* Journal for ImmunoTherapy of Cancer, 2024. **12**(2): p. e008566.
105. Siller-Farfán, J.A. and O. Dushek, *Molecular mechanisms of T cell sensitivity to antigen*. Immunological Reviews, 2018. **285**(1): p. 194-205.
106. Irving, B.A. and A. Weiss, *The cytoplasmic domain of the T cell receptor zeta chain is sufficient to couple to receptor-associated signal transduction pathways.* Cell, 1991. **64**(5): p. 891-901.
107. Ardouin, L., et al., *Crippling of CD3-ζ ITAMs Does Not Impair T Cell Receptor Signaling*. Immunity, 1999. **10**(4): p. 409-420.
108. Irving, B.A., A.C. Chan, and A. Weiss, *Functional characterization of a signal transducing motif present in the T cell antigen receptor zeta chain*. The Journal of experimental medicine, 1993. **177**(4): p. 1093-1103.
109. Letourneur, F. and R.D. Klausner, *Activation of T Cells by a Tyrosine Kinase Activation Domain in the Cytoplasmic Tail of CD3 ε*. Science, 1992. **255**(5040): p. 79-82.
110. Wu, W., et al., *Multiple Signaling Roles of CD3epsilon and Its Application in CAR-T Cell Therapy.* Cell, 2020. **182**(4): p. 855-871 e23.
111. Salter, A.I., et al., *Comparative analysis of TCR and CAR signaling informs CAR designs with superior antigen sensitivity and in vivo function*. Sci Signal, 2021. **14**(697).
112. Lindner, S.E., et al., *Chimeric antigen receptor signaling: Functional consequences and design implications*. Science Advances, 2020. **6**(21): p. eaaz3223.
113. Chen, J., et al., *Tuning charge density of chimeric antigen receptor optimizes tonic signaling and CAR-T cell fitness.* Cell Research, 2023. **33**(5): p. 341-354.
114. Ajina, A. and J. Maher, *Strategies to Address Chimeric Antigen Receptor Tonic Signaling*. Mol Cancer Ther, 2018. **17**(9): p. 1795-1815.
115. Eyquem, J., et al., *Targeting a CAR to the TRAC locus with CRISPR/Cas9 enhances tumour rejection*. Nature, 2017. **543**(7643): p. 113-117.
116. Asmamaw Dejenie, T., et al., *Current updates on generations, approvals, and clinical trials of CAR T-cell therapy.* Human Vaccines & Immunotherapeutics, 2022. **18**(6).
117. Guedan, S., et al., *ICOS-based chimeric antigen receptors program bipolar TH17/TH1 cells*. Blood, 2014. **124**(7): p. 1070-1080.
118. Goodman, D.B., et al., *Pooled screening of CAR T cells identifies diverse immune signaling domains for next-generation immunotherapies*. Science Translational Medicine, 2022. **14**(670).
119. James, J.R., *Tuning ITAM multiplicity on T cell receptors can control potency and selectivity to ligand density.* Science Signaling, 2018. **11**(531): p. eaan1088.
120. Velasco Cárdenas, R.M.-H., et al., *Harnessing CD3 diversity to optimize CAR T cells*. Nature Immunology, 2023.

121. Fitzer-Attas, C.J., et al., *Harnessing Syk family tyrosine kinases as signaling domains for chimeric single chain of the variable domain receptors: optimal design for T cell activation*. J Immunol, 1998. **160**(1): p. 145-54.
122. Minguet, S., M.V. Maus, and W.W. Schamel, *From TCR fundamental research to innovative chimeric antigen receptor design*. Nature Reviews Immunology, 2024.
123. Tousley, A.M., et al., *Co-opting signalling molecules enables logic-gated control of CAR T cells*. Nature, 2023. **615**(7952): p. 507-516.
124. Balagopalan, L., et al., *Generation of antitumor chimeric antigen receptors incorporating T cell signaling motifs*. Science Signaling, 2024. **17**(846).
125. Minguet, S., et al., *Full Activation of the T Cell Receptor Requires Both Clustering and Conformational Changes at CD3*. Immunity, 2007. **26**(1): p. 43-54.
126. Baeuerle, P.A., et al., *Synthetic TRuC receptors engaging the complete T cell receptor for potent anti-tumor response*. Nat Commun, 2019. **10**(1): p. 2087.
127. Burton, J., et al., *Inefficient exploitation of accessory receptors reduces the sensitivity of chimeric antigen receptors*. Proceedings of the National Academy of Sciences, 2023. **120**(2).
128. Hassan, R., et al., *Mesothelin-targeting T cell receptor fusion construct cell therapy in refractory solid tumors: phase 1/2 trial interim results*. Nature Medicine, 2023. **29**(8): p. 2099-2109.
129. Liu, Y., et al., *Chimeric STAR receptors using TCR machinery mediate robust responses against solid tumors*. Sci Transl Med, 2021. **13**(586).
130. Mansilla-Soto, J., et al., *HLA-independent T cell receptors for targeting tumors with low antigen density*. Nature Medicine, 2022.
131. Wang, J., et al., *A novel adoptive synthetic TCR and antigen receptor (STAR) T-Cell therapy for B-Cell acute lymphoblastic leukemia*. American Journal of Hematology, 2022. **97**(8): p. 992-1004.
132. Spiegel, J.Y., et al., *CAR T cells with dual targeting of CD19 and CD22 in adult patients with recurrent or refractory B cell malignancies: a phase 1 trial*. Nature Medicine, 2021. **27**(8): p. 1419-1431.
133. Dai, H., et al., *Bispecific CAR-T cells targeting both CD19 and CD22 for therapy of adults with relapsed or refractory B cell acute lymphoblastic leukemia*. Journal of Hematology & Oncology, 2020. **13**(1).
134. Cordoba, S., et al., *CAR T cells with dual targeting of CD19 and CD22 in pediatric and young adult patients with relapsed or refractory B cell acute lymphoblastic leukemia: a phase 1 trial*. Nature Medicine, 2021. **27**(10): p. 1797-1805.
135. Shah, N.N., et al., *Bispecific anti-CD20, anti-CD19 CAR T cells for relapsed B cell malignancies: a phase 1 dose escalation and expansion trial*. Nature Medicine, 2020. **26**(10): p. 1569-1575.
136. Larson, S.M., et al., *CD19/CD20 Bispecific Chimeric Antigen Receptor (CAR) in Naive/Memory T Cells for the Treatment of Relapsed or Refractory Non-Hodgkin Lymphoma*. Cancer Discovery, 2023. **13**(3): p. 580-597.
137. Mei, H., et al., *A bispecific CAR-T cell therapy targeting BCMA and CD38 in relapsed or refractory multiple myeloma*. Journal of Hematology & Oncology, 2021. **14**(1).

138. Shi, M., et al., *Bispecific CAR T cell therapy targeting BCMA and CD19 in relapsed/refractory multiple myeloma: a phase I/II trial*. Nature Communications, 2024. **15**(1).
139. Leung, I., et al., *Compromised antigen binding and signaling interfere with bispecific CD19 and CD79a chimeric antigen receptor function*. Blood Advances, 2023. **7**(12): p. 2718-2730.
140. Wang, N., et al., *Efficacy and safety of CAR19/22 T-cell cocktail therapy in patients with refractory/relapsed B-cell malignancies*. Blood, 2020. **135**(1): p. 17-27.
141. Boyiadzis, M.M., et al., *Chimeric antigen receptor (CAR) T therapies for the treatment of hematologic malignancies: clinical perspective and significance*. Journal for ImmunoTherapy of Cancer, 2018. **6**(1).
142. Schuster, S.J., et al., *Chimeric Antigen Receptor T Cells in Refractory B-Cell Lymphomas*. New England Journal of Medicine, 2017. **377**(26): p. 2545-2554.
143. Neelapu, S.S., et al., *Axicabtagene Ciloleucel CAR T-Cell Therapy in Refractory Large B-Cell Lymphoma*. New England Journal of Medicine, 2017. **377**(26): p. 2531-2544.
144. Derrien, J., et al., *Acquired resistance to a GPRC5D-directed T-cell engager in multiple myeloma is mediated by genetic or epigenetic target inactivation*. Nat Cancer, 2023. **4**(11): p. 1536-1543.
145. Isakov, N., et al., *ZAP-70 binding specificity to T cell receptor tyrosine-based activation motifs: the tandem SH2 domains of ZAP-70 bind distinct tyrosine-based activation motifs with varying affinity*. Journal of Experimental Medicine, 1995. **181**(1): p. 375-380.
146. Wang, J., et al., *Optimizing adoptive polyclonal T cell immunotherapy of lymphomas, using a chimeric T cell receptor possessing CD28 and CD137 costimulatory domains*. Hum Gene Ther, 2007. **18**(8): p. 712-25.
147. Salter, A.I., et al., *Phosphoproteomic analysis of chimeric antigen receptor signaling reveals kinetic and quantitative differences that affect cell function*. Sci Signal, 2018. **11**(544).
148. Mukhopadhyay, H., et al., *Systems Model of T Cell Receptor Proximal Signaling Reveals Emergent Ultrasensitivity*. PLoS Computational Biology, 2013. **9**(3): p. e1003004.
149. Sykulev, Y., et al., *Evidence that a Single Peptide–MHC Complex on a Target Cell Can Elicit a Cytolytic T Cell Response*. Immunity, 1996. **4**(6): p. 565-571.
150. Watanabe, K., et al., *Expanding the Therapeutic Window for CAR T Cell Therapy in Solid Tumors: The Knowns and Unknowns of CAR T Cell Biology*. Front Immunol, 2018. **9**: p. 2486.
151. Xu, Y., et al., *A novel antibody-TCR (AbTCR) platform combines Fab-based antigen recognition with gamma/delta-TCR signaling to facilitate T-cell cytotoxicity with low cytokine release*. Cell Discov, 2018. **4**: p. 62.
152. Huppa, J.B. and M.M. Davis, *T-cell-antigen recognition and the immunological synapse*. Nature Reviews Immunology, 2003. **3**(12): p. 973-983.
153. Weber, E.W., et al., *Transient rest restores functionality in exhausted CAR-T cells through epigenetic remodeling*. Science, 2021. **372**(6537).

154. Kokalaki, E., et al., *Dual targeting of CD19 and CD22 against B-ALL using a novel high-sensitivity aCD22 CAR*. Mol Ther, 2023. **31**(7): p. 2089-2104.
155. Majzner, R.G., et al., *Tuning the Antigen Density Requirement for CAR T-cell Activity.* Cancer Discovery, 2020. **10**(5): p. 702-723.
156. Feucht, J. and M. Sadelain, *Function and evolution of the prototypic CD28zeta and 4-1BBzeta chimeric antigen receptors*. Immunooncol Technol, 2020. **8**: p. 2-11.
157. Roddie, C., et al., *Dual targeting of CD19 and CD22 with Bicistronic CAR-T cells in Patients with Relapsed/Refractory Large B Cell Lymphoma*. Blood, 2023.
158. Gogishvili, T., et al., *SLAMF7-CAR T cells eliminate myeloma and confer selective fratricide of SLAMF7+ normal lymphocytes*. Blood, 2017. **130**(26): p. 2838-2847.
159. Zah, E., et al., *Systematically optimized BCMA/CS1 bispecific CAR-T cells robustly control heterogeneous multiple myeloma*. Nature Communications, 2020. **11**(1).
160. Abramson, J.S., et al., *Two-year follow-up of lisocabtagene maraleucel in relapsed or refractory large B-cell lymphoma in TRANSCEND NHL 001*. Blood, 2024. **143**(5): p. 404-416.
161. Cowan, A.J., et al., *gamma-Secretase inhibitor in combination with BCMA chimeric antigen receptor T-cell immunotherapy for individuals with relapsed or refractory multiple myeloma: a phase 1, first-in-human trial*. Lancet Oncol, 2023. **24**(7): p. 811-822.
162. Leung, I., et al., *Compromised antigen binding and signaling interfere with bispecific CD19 and CD79a chimeric antigen receptor function*. Blood Adv, 2023. **7**(12): p. 2718-2730.
163. Tsuchida, C.A., et al., *Mitigation of chromosome loss in clinical CRISPR-Cas9-engineered T cells*. Cell, 2023. **186**(21): p. 4567-4582.e20.
164. Webber, B.R., et al., *Highly efficient multiplex human T cell engineering without double-strand breaks using Cas9 base editors*. Nature Communications, 2019. **10**(1).
165. Chiesa, R., et al., *Base-Edited CAR7 T Cells for Relapsed T-Cell Acute Lymphoblastic Leukemia*. New England Journal of Medicine, 2023. **389**(10): p. 899-910.
166. Chang, J.-F., et al., *Rational protein engineering to enhance MHC-independent T cell receptors*. Cancer Discovery, 2024.
167. Davenport, A.J., et al., *Chimeric antigen receptor T cells form nonclassical and potent immune synapses driving rapid cytotoxicity*. Proceedings of the National Academy of Sciences, 2018. **115**(9): p. E2068-E2076.
168. Hay, K.A., et al., *Kinetics and biomarkers of severe cytokine release syndrome after CD19 chimeric antigen receptor–modified T-cell therapy*. Blood, 2017. **130**(21): p. 2295-2306.
169. Patel, A., et al., *Using CombiCells, a platform for titration and combinatorial display of cell surface ligands, to study T-cell antigen sensitivity modulation by accessory receptors*. The EMBO Journal, 2023. **43**(1): p. 132-150.
170. Dobrin, A., et al., *Synthetic dual co-stimulation increases the potency of HIT and TCR-targeted cell therapies*. Nature Cancer, 2024.

171. Ereño-Orbea, J., et al., *Structural details of monoclonal antibody m971 recognition of the membrane-proximal domain of CD22*. Journal of Biological Chemistry, 2021. **297**(2): p. 100966.
172. Haso, W., et al., *Anti-CD22-chimeric antigen receptors targeting B-cell precursor acute lymphoblastic leukemia*. Blood, 2013. **121**(7): p. 1165-74.
173. Xiao, Q., et al., *Size-dependent activation of CAR-T cells*. Sci Immunol, 2022. **7**(74): p. eabl3995.
174. Fernández De Larrea, C., et al., *Defining an Optimal Dual-Targeted CAR T-cell Therapy Approach Simultaneously Targeting BCMA and GPRC5D to Prevent BCMA Escape–Driven Relapse in Multiple Myeloma*. Blood Cancer Discovery, 2020. **1**(2): p. 146-154.
175. Stenger, D., et al., *Endogenous TCR promotes in vivo persistence of CD19-CAR-T cells compared to a CRISPR/Cas9-mediated TCR knockout CAR*. Blood, 2020. **136**(12): p. 1407-1418.
176. Majzner, R.G. and C.L. Mackall, *Clinical lessons learned from the first leg of the CAR T cell journey*. Nature Medicine, 2019. **25**(9): p. 1341-1355.
177. Rosskopf, S., et al., *A Jurkat 76 based triple parameter reporter system to evaluate TCR functions and adoptive T cell strategies*. Oncotarget, 2018. **9**(25): p. 17608-17619.
178. Sommermeyer, D., et al., *Fully human CD19-specific chimeric antigen receptors for T-cell therapy*. Leukemia, 2017. **31**(10): p. 2191-2199.
179. Pont, M.J., et al., *γ-Secretase inhibition increases efficacy of BCMA-specific chimeric antigen receptor T cells in multiple myeloma*. Blood, 2019. **134**(19): p. 1585-1597.
180. Kuball, J., et al., *Facilitating matched pairing and expression of TCR chains introduced into human T cells*. Blood, 2007. **109**(6): p. 2331-8.
181. Kluesner, M.G., et al., *CRISPR-Cas9 cytidine and adenosine base editing of splice-sites mediates highly-efficient disruption of proteins in primary and immortalized cells*. Nature Communications, 2021. **12**(1).
182. Shy, B.R., et al., *High-yield genome engineering in primary cells using a hybrid ssDNA repair template and small-molecule cocktails*. Nature Biotechnology, 2023. **41**(4): p. 521-531.
183. Wakimoto, Y., J. Jiang, and H. Wakimoto, *Isolation of single-stranded DNA*. Curr Protoc Mol Biol, 2014. **107**: p. 2 15 1-2 15 9.
184. Nguyen, D.N., et al., *Polymer-stabilized Cas9 nanoparticles and modified repair templates increase genome editing efficiency*. Nature Biotechnology, 2020. **38**(1): p. 44-49.
185. Bandaranayake, A.D., et al., *Daedalus: a robust, turnkey platform for rapid production of decigram quantities of active recombinant proteins in human cell lines using novel lentiviral vectors*. Nucleic Acids Res, 2011. **39**(21): p. e143.
186. Su, X., et al., *Reconstitution of TCR Signaling Using Supported Lipid Bilayers*, in *The Immune Synapse*. 2017, Springer New York. p. 65-76.

187. Felce, J.H., et al., *Single-Molecule, Super-Resolution, and Functional Analysis of G Protein-Coupled Receptor Behavior Within the T Cell Immunological Synapse*. Frontiers in Cell and Developmental Biology, 2021. **8**.
188. Sommermeyer, D., et al., *Chimeric antigen receptor-modified T cells derived from defined CD8+ and CD4+ subsets confer superior antitumor reactivity in vivo*. Leukemia, 2016. **30**(2): p. 492-500.
189. Singh, N., et al., *Early memory phenotypes drive T cell proliferation in patients with pediatric malignancies*. Science Translational Medicine, 2016. **8**(320): p. 320ra3-320ra3.
190. Krishnaswamy, S., et al., *Conditional density-based analysis of T cell signaling in single-cell data*. Science, 2014. **346**(6213): p. 1250689.
191. Ma, C.Y., et al., *Stimulation strength controls the rate of initiation but not the molecular organisation of TCR-induced signalling*. eLife, 2020. **9**.
192. Verbist, K.C., et al., *Metabolic maintenance of cell asymmetry following division in activated T lymphocytes*. Nature, 2016. **532**(7599): p. 389-393.
193. Levine, L.S., et al., *Single-cell analysis by mass cytometry reveals metabolic states of early-activated CD8+ T cells during the primary immune response*. Immunity, 2021. **54**(4): p. 829-844.e5.
194. Hartmann, F.J., et al., *Single-cell metabolic profiling of human cytotoxic T cells*. Nature Biotechnology, 2021. **39**(2): p. 186-197.
195. Arguello, R.J., et al., *SCENITH: A Flow Cytometry-Based Method to Functionally Profile Energy Metabolism with Single-Cell Resolution*. Cell Metab, 2020. **32**(6): p. 1063-1075 e7.
196. Gattinoni, L., C.A. Klebanoff, and N.P. Restifo, *Paths to stemness: building the ultimate antitumour T cell*. Nature Reviews Cancer, 2012. **12**(10): p. 671-684.
197. Newell, W., Evan, et al., *Cytometry by Time-of-Flight Shows Combinatorial Cytokine Expression and Virus-Specific Cell Niches within a Continuum of CD8+ T Cell Phenotypes*. Immunity, 2012. **36**(1): p. 142-152.
198. Michelozzi, I.M., et al., *High-dimensional functional phenotyping of preclinical human CAR T cells using mass cytometry*. STAR Protoc, 2022. **3**(1): p. 101174.
199. Good, Z., et al., *Proliferation tracing with single-cell mass cytometry optimizes generation of stem cell memory-like T cells*. Nature Biotechnology, 2019. **37**(3): p. 259-266.
200. Muftuoglu, M., et al., *Extended live-cell barcoding approach for multiplexed mass cytometry*. Scientific Reports, 2021. **11**(1).
201. Zunder, E.R., et al., *Palladium-based mass tag cell barcoding with a doublet-filtering scheme and single-cell deconvolution algorithm*. Nature Protocols, 2015. **10**(2): p. 316-333.
202. Fisher, J., et al., *Engineering gammadeltaT cells limits tonic signaling associated with chimeric antigen receptors*. Sci Signal, 2019. **12**(598).
203. Feucht, J., et al., *Calibration of CAR activation potential directs alternative T cell fates and therapeutic potency*. Nature Medicine, 2019. **25**(1): p. 82-88.

204. Krishnamoorthy, V., et al., *The IRF4 Gene Regulatory Module Functions as a Read-Write Integrator to Dynamically Coordinate T Helper Cell Fate*. Immunity, 2017. **47**(3): p. 481-497.e7.
205. Crowell, H.L., et al., *An R-based reproducible and user-friendly preprocessing pipeline for CyTOF data*. F1000Research, 2022. **9**: p. 1263.
206. Sufi, J., et al., *Multiplexed single-cell analysis of organoid signaling networks*. Nature Protocols, 2021. **16**(10): p. 4897-4918.
207. Weissman, A.M., et al., *Molecular cloning and chromosomal localization of the human T-cell receptor zeta chain: distinction from the molecular CD3 complex*. Proceedings of the National Academy of Sciences, 1988. **85**(24): p. 9709-9713.
208. Prasad, K.V., et al., *T-cell antigen CD28 interacts with the lipid kinase phosphatidylinositol 3-kinase by a cytoplasmic Tyr(P)-Met-Xaa-Met motif*. Proceedings of the National Academy of Sciences, 1994. **91**(7): p. 2834-2838.